Master Thesis in Geosciences

Assessment and modelling of two lahars caused by "Hurricane Stan" at Atitlan, Guatemala, October 2005

Byron Quan Luna

Disaster in Atitlan (Painting by Rodriguez P.)

UNIVERSITY OF OSLO

FACULTY OF MATHEMATICS AND NATURAL SCIENCES

Assessment and modelling of two lahars caused by “Hurricane Stan” at Atitlan, Guatemala, October 2005

Byron Quan Luna

Master Thesis in Geosciences

Discipline: Environmental Geology and Geohazards

Department of Geosciences

Faculty of Mathematics and Natural Sciences

UNIVERSITY OF OSLO

June 2007

To the victims of the Hurricane Stan in Guatemala.

List of contents

Acknowledgements

Very special thanks to my supervisor and teacher, Kaare Høeg. His lectures and his guidance was reason I decided to choose this interesting topic. I am grateful for his support, patience and help all through my master studies. I have learned many things from him. I am much honored to be one of his students.

Thanks to my other supervisor, Ulrik Domaas. His help and support were fundamental for making this thesis. Thanks for facilitating the RAMMS program and all the Guatemala information. He made this thesis an exciting and enjoyable challenge. I am thankful for his advices and his guidance all through the elaboration of this thesis.

Thanks to Jose Cepeda and Graziella Devoli for their patience to my questions and their help all through this thesis. Both of them were always eager to help and assist me in the nicest way.

I would also like to thank:

Farrokh Nadim and Bjørn Kalsnes for giving me the chance to make my thesis at ICG and giving me a place to work there. I am very grateful for their collaboration and for making a nice working environment for me. I know that soon both of them will learn to speak spanish after all the times I asked Jose and Graziella.

All the NGI and ICG staff that was always willing to help me. Thanks to Karl Harbitz, Peter Gauer, Fabio DeBlasio, Dieter Issler, Frode Sandersen, Oddvar Kjestad and to all the personnel that in one way or another contributed with me during the elaboration of this thesis.

WSL/SLF in Switzerland that made the RAMMS program available for my thesis. A special thanks to Marc Christen and Christoph Graf for their help in the use of the program.

The University of Oslo and the Department of Geosciences for giving me the opportunity to make my master studies there.

My family for their support in every moment of my life and during this thesis.

God for all the blessings in my life, for giving me choices and the freedom to decide.

Abstract

In October 2005, massive slope failures were triggered all around Guatemala by the heavy rainfall that accompanied Hurricane Stan and unchained a series of landslides, debris flows and lahars. Two communities called Panabaj and San Juan La Laguna located inside the Atitlan caldera in the highlands of Guatemala were seriously affected by these events. Panabaj located in the aprons of the Toliman volcano was completely destroyed and more than 1,200 people were killed by a slope failure that created a lahar. San Juan La Laguna is located at the border of an alluvial fan that is a natural channel for discharge of the San Pedro volcano, a whole neighborhood of the community was destroyed by a lahar created by a small slope failure in the southwestern part of the volcano and by a series of landslides and contributive flows from the steep side of the basin that added material to the lahar. The volcanic lahars happened almost at the same time. A peak of precipitation of nearly 300 mm in 24 hours (54.4 mm three hours before the lahars occurred), a volcanic setting and steep slopes near the borders of the craters was the scenario where the 2005 events took place.

This study gives a background of the two lahar events and simulates them by using two computer programs. Although very close in location, the flows had different types of origin and post failure behavior. A description of the geology, past lahar events and climate of the area is done to give an insight of the context where the events occurred.

An important objective of this thesis is also to study the capabilities and use of the two computer programs RAMMS and FLO 2D, for possible future applications at NGI (Norges Geotekniske Institutt) and ICG (International Centre for Geohazards).

The Panabaj lahar was simulated with the RAMMS computer program and the San Juan La Laguna lahar was simulated with the FLO 2D computer program. Different computer programs were selected for this study because of the differences in the nature and behavior of the two lahars. The two computer programs are described with their numerical models. The results of these simulations are analyzed and compared with the field observations.

The behavior and processes of the flow during its trajectory were well simulated by the RAMMS and FLO 2D program, respectively. Using a back analysis, a calibration of the parameters that best fitted the event in Panabaj was made with the RAMMS program. A selection of the best suited input parameters and a discharge hydrograph based on the accumulated rainfall was built to produce a simulation of the San Juan La Laguna slide. The simulations gave reasonable results in terms of run out distances, velocities and the spreading of the material in the deposition area

In the Appendix A, the chronology of Hurricane Stan in Guatemala is described. In the Appendix B, a simulation of a tsunami that took place in the Lake Atitlan one hour after the Panabaj lahar happened, was done combining the RAMMS and the FLO 2D program. The tsunami was generated by a lahar from the San Pedro Volcano and affected the shores of Santiago and Panabaj communities.

1. Introduction and scope

1.1 Background

"When the skies are dark for days and the volcano cries and shout, a big danger is around, but we stop listening to the nature feelings", this are the words of Ramiro, a 77 years old habitant of Panabaj that survive the Panabaj lahar that destroyed almost entirely the community and left more than 1,200 people dead.. Ramiro still remembers how around 50 years ago a similar event happened, "a big wave of mud came from the mouth of the volcano but my father knew beforehand and warned my family to go to a safe place". (Prensa Libre, 0october 2005)

In October 2005, Hurricane Stan caused intense precipitation throughout much of the territory of Guatemala. This continuous rainfall resulted in landslides, debris flows, and mudflows. In the communities of Panabaj a landslide of pyroclastic material that created a lahar originated on the flanks of the Toliman volcano and destroyed most of the community. Almost at the same time, in the San Juan La Laguna community, a whole neighborhood was destroyed by a lahar that originated by a landslide in the San Pedro Volcano and other small slope failures in the steep part of the basin that contributed to the flow.

Volcanic lahars are frequently associated with volcanic activity or collapse of steep slopes due to water saturation or prolonged periods of erosion. They represent significant threats to the population living on and around volcanoes. As population grows, the need for available land grows, and this has resulted in an increase in the number of people living on or close to places with high risk potential.

Hazard zoning around volcanoes has involved identifying and interpreting deposits from previous landslides activity. This task can become very time consuming and requires a large amount of field work. The results of this are maps based on the subjective experience of the investigator and may be difficult to be interpreted. The development of numerical simulation models have increasingly been used for developing hazard maps. Although, field

work is essential, computer models can reduce the time and effort and has the potential to reproduce the phenomenon with consistency.

The task of modeling landslides and debris flow events by computer simulations is only beginning to be understood. The correct use of these tools can benefit the public authorities when making decisions about communities with potential hazards. The goals of computer modeling should be to assess potential activity in advance with a range of potential scenarios associated with slope failures and debris flows and to inform local populations of these natural hazards so they can respond to these potential hazards in deliberate and reasonable ways. It is important to evaluate the efficiency and reliability of these simulation tools that integrate the physical models of such events, the numerical methodology and geographical information systems.

A variety of models exist for simulating mass-flows and for identifying the hazards the different phenomena present. In this thesis, I will asses and model the lahar that occurred in San Juan La Laguna (Atitlan, Guatemala) with the FLO 2D program (two dimensional flood routing model) and the lahar flow that occurred in Panabaj (Atitlan, Guatemala) with a two-dimensional model called RAMMS. The programs are used to compare the run-out distances, thicknesses of the deposits in the deposition area and velocities of the flows to measurements observed in the field.

1.2 Objectives

- To give an assessment and background of the two landslide events that occurred at Atitlan, Guatemala in 2005 due to the Hurricane Stan. They are known as “The San Juan La Laguna lahar” and “The Panabaj lahar”. Both flows occurred during the same rainstorm event and are very close in location to each other, but their failure and post failure behavior were different.

- Describe the geological settings of the Atitlan area and its features; make a review of the registered past lahars and assess the climatic conditions of the area before and during the Hurricane Stan event.

- Describe the characteristics, numerical models and capabilities of the computer programs used to simulate the lahar events. FLO 2D program for “The San Juan La Laguna lahar” and RAMMS program for the “The Panabaj lahar”.

- Explain the methodology used for simulating the events with the computer programs and compare the results with the field observations.

2. Regional context

2.1 Central America

Central America is a narrow isthmus (~538,000 km^2) connecting North and South America and bordered by the Caribbean Sea to the east and the Pacific Ocean to the west. It includes seven small countries: Guatemala, Belize, Honduras, El Salvador, Nicaragua, Costa Rica and Panama (Fig.2.1). Although differences exist among these countries, common features can be observed with respect to seismic and volcanic hazard, climate and geology.

Figure 2.1 Map of Central America

A common feature is the Central American Volcanic Chain that runs parallel to the Pacific coast from the Guatemala-Mexico border to Panama, superposed on the older structures and formed after the two blocks had been sutured. The volcanic chain is composed of active and dormant volcanoes of Quaternary age. It is a product of the north-east-directed subduction of the Cocos plate beneath the Caribbean plate that occurs in the Middle American Trench situated in the Pacific Ocean (Newhall, 1987). The largest earthquakes in the region are produced by the convergence of these two plates, but the seismic activity is also influenced by the interaction of other major plates (North American, South American, and Nazca).

Landslides occur on slopes of active and dormant volcanoes composed of Quaternary volcanic rocks, which are frequently hydro-thermally altered, and on the mountain ranges of the interior on steep slopes composed of highly weathered soils and rocks (Vallance et.al.,2005). Landslides take place primarily during the wet season and are triggered by intensive rainfalls sometimes associated with tropical cyclones. They may also be triggered during the dry season by earthquakes and volcanic eruptions.

2.2 The Republic of Guatemala

Guatemala with an area of 108,889 m² is a country in Central America bordered by Mexico to the Northwest, the Pacific Ocean to the Southwest, Belize and the Caribbean Sea to the Northeast, and Honduras and El Salvador to the Southeast. Guatemala is the most populous nation in Central America (12 million habitants). Geographically, Guatemala is a mountainous country except for the south coastal area and the northern vast lowlands. Two mountain chains enter Guatemala from the West to East, dividing the country into three major regions: highlands (where the mountains are located), the Pacific Coast (south of the mountains) and the Petén region (north of the mountains). All major cities are located in the highlands and the Pacific coast regions. These three regions vary in climate, elevation and landscape, providing big contrasts between hot and humid tropical lowlands and colder and drier highlands peaks.

Guatemala experiences a rainy season that begins in May and extends to October. Because of its geographic position and geological setting, the country is subject to a large variety of natural phenomena such as tropical cyclones, droughts, floods, landslides, earthquakes, volcanic eruptions, and tsunamis.

Guatemala's highlands lie in the boundary between the Caribbean and North American tectonic plates, this situation creates frequent earthquakes and volcanic activity. Guatemala has 37 volcanoes, four of them active: Pacaya, Santiaguito, Fuego and Tacana.

Solola is a one of the 22 departments of the Republic of Guatemala and is located in the Guatemala higlands. Inside the Solola department lies the Atitlan Caldera that features the Lake Atitlan and three stratovolcanoes: San Pedro, Toliman and Atitlan (Fig.2.2). The Atitlan caldera is located along the West-Northewest trending chain of volcanoes parallel to the mid-American trench.

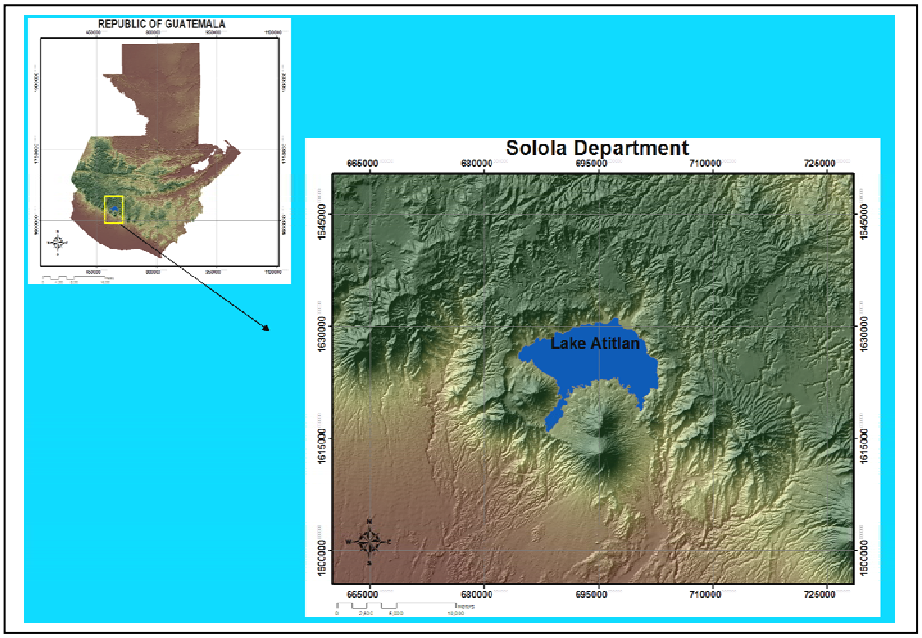

Figure 2.2. Location of Solola Department in the Republic of Guatemala.

3. Definitions and terminology

3.1 Lahars and debris flows on volcanoes

Volcanic debris flows are commonly known as lahars, they behave similarly to debris flows in other settings, but can differ very much in origin and size. Small-volume lahars typically travel only a few kilometers from their source, but large-volume debris flows can travel many kilometers from a volcano. They destroy everything in their paths and even small debris avalanches can leave deposits up to 10 m thick. Larger debris flows commonly leave deposits that are more than 100 m thick on valley floors. The size difference can be explained by the abundance of loose debris on the steep slopes and skirts of volcanoes, the presence of weakened hydro-thermally altered rock, rainfall that washes over slopes and the potential for releasing both water and sediment during and immediately after eruptions (Vallance et.al., 1988). Because of their large sizes and propensity for long distance transport, volcanic debris flows show downstream evolution less commonly observed in debris flows from other environments. A rheologically specific definition for lahars causes confusion, because some sediment-water flows from volcanoes transform from water flood, to hyperconcentrated flow, to debris flow, and back again to more dilute phase during a single event (Pierson, 1987). A lahar event can vary in character with time and distance downstream. It may comprise one or more flow phases, which include a debris-flow phase, transitional or hyperconcentrated-flow phase, and streamflow phase. A “debris-flow phase” is one in which the solid and liquid fractions are approximately equal volumetrically and in which the two fractions in a vertical section move downstream approximately in unison. A “streamflow phase” is one in which fine-grained sediment moves in suspension with the fluid (suspended load) and coarse-grained sediment moves along the bed at discrete intervals (bedload). It is useful to define a “transitional flow phase”, commonly known as “hyperconcentrated flow”, intermediate between that of debris flow and streamflow. Unlike streamflow, this transitional phase carries very high sediment loads, and unlike the debris flow phase coarse-grained solids tend to separate vertically from the liquid-and-fine solids mixture (Fig.3.1 a, b and c).

Transitions are gradational and dependent on factors as sediment size distribution and energy of the flow (Vallance, 1998).

Fig. 3.1 a) Picture of the debris flow phase (top left), b) Picture of the streamflow phase (top right), c) Picture of the hyperconcentrated phase.

Lahars cause erosion by undercutting steep slopes and terrace scarps and by scouring their beds. Water-rich hyperconcentrated-flow phases are typically more erosive than sediment-rich debris-flow phases but local erosion can occur during any flow phase. Undercutting of steep slopes, fluvial terraces scarps, channel bed erosion and active stream banks is probably the most important way in which lahars erode and incorporate sediment. With continued entrainment, lahars become richer in exotic sediment, like alluvium and colluviums because the flow front and following peak stages of the flow are the most erosive (Pitman et.al. 2003).

Lahars initiate when a failure occurs on high slopes terrains, often near the crater of the volcano (Tilling, 1989). The flows gather volume and momentum as they descend the slopes of the volcano, often reaching speeds of tens of meters per second. Such flows reach areas at the base of the volcano in a matter of minutes. They spread out very rapidly in low terrain, inundating the area with thick and viscous mixtures of sand, gravel, mud, and blocks of rock up to several meters in diameter (Iverson, 2001). Lahars strip the landscape of vegetation, and therefore often incorporate large trees and related debris. Lahars primarily follow river valleys and like floods inundate floodplains and can bury structures in low areas. These flows are often so strong and viscous that even flows of only a few tens of centimeters thick can completely destroy houses. People trapped within such flows rarely survive.

Once a lahar deposit fills a stream channel with sediment, the stream begins to erode a new path. These new channels can be very unstable and shift quickly as sediment is eroded and carried farther down the valley (Legros, 2002). In some instances, lahars clog channels or block tributaries forcing water to collect behind the blockage. The impounded water can spill over the blockage, draining the water and generating a flood that moves down the valley. Breaching of such blockages may occur within hours or even months after impoundment (Hayashi and Self, 1992).

3.2 Description of a Hurricane

A hurricane is born in warm tropical waters and is the most severe category of the meteorological phenomenon known as the "tropical cyclone." Tropical cyclones are low pressure systems that have thunderstorm activity and rotate counterclockwise. A tropical cyclone that has winds of 38 mph or less is called a tropical depression. When the tropical cyclone's winds reach 39-73 mph, it is called a tropical storm. When the winds exceed 74 mph, the storm is considered to be a Hurricane. The Saffir-Simpson Hurricane Scale defines hurricane strength by categories. A Category 1 storm is the weakest hurricane (winds 74-95 mph); a Category 5 hurricane is the strongest (winds greater than 155 mph). These are relative terms, because lower category storms can sometimes cause greater damage than higher category storms, depending on where they strike and the hazards they bring. The main

hazards associated with tropical cyclones and especially hurricanes are storm surges, high winds, heavy rain, and flooding.

The process by which a tropical cyclone forms and strengthens into a hurricane depends on at least three conditions: 1) A pre-existing disturbance with thunderstorms; 2) Warm ocean temperatures to a depth of about 45 meters; 3) Light upper level winds that do not change much in direction and speed in almost all the depth of the atmosphere (low wind shear).

Heat and energy for the storm are taken by the disturbance through contact with warm ocean waters. The winds near the ocean surface spiral into the disturbance's low pressure area. The warm ocean waters add moisture and heat to the air which rises. As the moisture condenses into drops, more heat is released, contributing additional energy to power the storm. Bands of thunderstorms form, and the storm's cloud rise higher into the atmosphere. During their life span, hurricanes can last for more than two weeks over the ocean and can travel up the entire Atlantic Coast. Just as many factors contribute to the birth of a hurricane, there are many reasons why a hurricane begins to decay. Wind shear can tear the hurricane apart. Moving over cooler water or drier areas can lead to weakening also. The contact with the land typically shuts off the hurricane's main moisture source, and the surface circulation can be reduced by friction when it passes over. Generally, a weakening hurricane or tropical cyclone can reintensify if it moves into a more favorable region.

Typical hurricanes are about 300 miles wide although they can vary considerably in size. The eye at a hurricane's center is a relatively calm, clear area approximately 20-40 miles across. The eyewall surrounding the eye is composed of dense clouds that contain the highest winds in the storm. The storm's outer rainbands (often with hurricane or tropical storm-force winds) are made up of dense bands of thunderstorms ranging from a few miles to tens of miles wide and 50 to 300 miles long. Hurricane-force winds can extend outward to about 25 miles in a small hurricane and to more than 150 miles for a large one. Tropical storm-force winds can stretch out as far as 300 miles from the center of a large hurricane (NOAA, 1999).

4. Local Context

4.1 Study area

For this thesis, an area located to the Southwest of the Atitlan caldera that contains the three volcanoes and the two communities (Panabaj and San Juan La Laguna) affected by the lahars was chosen for study (Fig.4.1). This area is located inside the geographical coordinates between 14.557° and 14.736° North latitude and -91.347° and -91.132° West longitude.

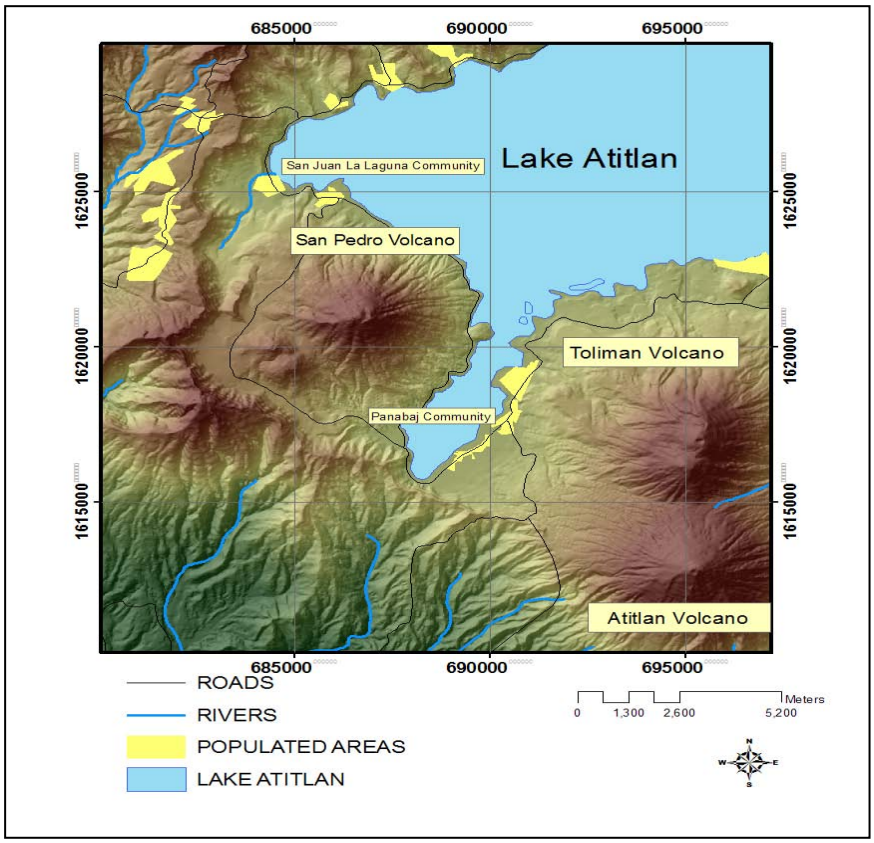

Fig.4.1. Map of the study area inside the Atitlan caldera.

4.2 History of lahars in the Atitlan study area

The slopes of a volcano can be unstable in times of heavy rain and seismic activity. In the past decade, a few small-scale lahars have occurred on the flanks of the Toliman, Atitlan and San Pedro volcanoes because of nearby tectonic earthquakes. Lahar flows are extremely dangerous because they travel farther from a volcano than any other phenomenon, except tephra, and affect stream valleys where population is settled (Malin, 1982)

The first recorded lahar in Guatemala occurred on the Agua Volcano on September 11, 1541. Heavy rains caused a debris flow that inundated Cuidad Vieja, killed more than 600 people including the wife (Beatriz de la Cueva de Ubeda) of the Spanish conqueror of Guatemala (Pedro de Alvarado) and destroyed the town. Cuidad Vieja was the capital city of Guatemala in 1541. The following eyewitness accounts record this event:

“This has been a year of much rain, and having been raining Thursday, Friday and Saturday, with strong winds and not much water, the mentioned "lavada" (wash) happened two hours into the night. A great storm of water came from atop the volcano (Agua) which is above the city, it was so sudden that [we] did not ...prevent the deaths and damages that happened; the stone storm (debris flow) was so huge that it swallowed the water in front of it, and much wood and trees, those who saw it were impressed, it entered through the house of the "Adelantado " don Pedro Alvarado, and it took away all the walls and the roof (Marroquín). The well remembered [event] of September 11th, 1541, that totally destroyed old Guatemala City (this first capital is now named Cuidad Vieja) lasting many days. Were it not for the noisy uproar underneath the earth that the earthquakes caused, many more deaths would have taken place than those that happened there, a number greater than six hundred people (Vázquez 1937:1:154).”

Some history books suggest that the 1541 debris flow was originated from the breaking of a crater-lake, but the accounts clearly shows that the lahar flow at the Agua volcano was similar to the 2005 debris flow at the Atitlan basin. In each case, the event occurred in the latter half of the rainy season, when the ground was water saturated. In each case, several days of heavy rain triggered a landslide, which in turn generated a lahar. In each

case, survivors reported that the ground shook immediately prior to the arrival of the lahar. In each case, the lahar destroyed population centers on the skirts of the volcano.

Based on interviews with elderly people of the affected communities, historic references, hydro-meteorological analysis and the soil profile of the area (Fig.4.2); the history of the debris flow events in the Atitlan area during the last century can be deduced. Although this area is prone to landslides and debris flows, there are few registered events in this area. A reason for this can be because the habitants of the place are used to this kind of events and do not inform the authorities until a major damage has occurred. The events are usually related to the latter half of the rainy season (October and beginning of November) with intense precipitations caused by storms and hurricanes.

- The first event occurred during the years 1910 and 1920. There is a lack of information for this event because of the isolation and difficult access to the area in that period of time, but it is estimated that the debris flow from the beginning of the century was half of the size of the 2005 event.

- During the intense rainfall in 1949 that happened at the end of October, known as the "1949 storm", slope failures occurred from the flanks of the Atitlan, San Pedro and Toliman volcano. This event is still remembered by some people from the area and according to their stories, the 1949 debris flows were not as destructive as the debris flows caused but Hurricane Stan in 2005. To have an idea of the size of the "1949 storm" event, the habitants of San Juan La Laguna tells a story of a catholic priest that was sleeping inside the church. The church was lifted from the ground and was carried to the middle of the lake by the debris flow. The church was floating in the lake for some time and the fishermen went to rescue the priest in the middle of the storm while the priest was still sleeping. After the priest was rescued, the church sank immediately in the lake. Ever since that day, according to the fishermen, the lake has been blessed with many fish; relating this to the story of the bible of the multiplication of fishes and bread that Jesus made.

- On Sunday 15th September 2002 at least 42 people were killed and many were missing after a landslide triggered by heavy rains struck a coffee-farming village. A torrent of mud, rocks and tree trunks poured down the slopes of the nearby Toliman volcano late on Thursday, burying much of the village of El Porvenir. Villagers fled in panic to seek higher ground as more than 20 houses were engulfed. El Porvenir lies in a narrow valley at the skirts of the Toliman volcano. Most residents work on nearby coffee plantation (BBC News).

- A landslide on the outer flanks of Tolimán volcano passed through and buried portions of a mountain village at 04:18 on 23 April, 2003. Regional authorities blamed steep slopes, wet soils, and minor tremors. The disaster struck the village of Chichicaste, which lies along the volcanic front. As of the afternoon of 23 April, the Guatemalan agency CONRED reported 200 people evacuated, 20 missing, and 6 confirmed dead. Known damage to infrastructure included 40 homes at risk, another 12 with severe damage, and 6 destroyed.

- The Hurricane Stan in 2005, according to the elderly people living in the area, caused the most destructive event that has happened in the area. This event destroyed almost entirely the Panabaj community (1400 dead) and caused great damage to many communities around the Lake Atitlan shores.

It is difficult to compare debris flows by their destructive power. Small volume debris flows can be as destructive as big volume ones. The increase of population in the surroundings of the Lake Atitlan and in marginal areas (skirts of the volcanoes), the flourishment of tourism in the area and the economic pressure that has pushed agricultural activity higher up the slopes, has increased dramatically the risk of the population.

During interviews with the habitants of the place, the most destructive events have been the ones that occurred approximately every 50 years (1910-1920 debris flow, “1949 storm”, Hurricane Stan 2005). This 50 year pattern between each very large debris flow event makes the population feel relatively safe again. Inhabitants think the next event will not come again for 50 years. During the field work made in the area, the San Juan La Laguna habitants that

were affected were returning and rebuilding their homes in the same place as before (alluvial fan), the almost destroyed school was just cleaned and is in activity again in the same location, and the farmers are growing corn plants in the channel where the debris flow ran through (they say it is a very good soil to crop in). Almost the same feeling of security is sensed in Panabaj, many affected families have been relocated in temporary shelters located within 100-300 m of the debris flow deposits of October 2005. This temporary housing is located on a gently sloping alluvial fan, but people are already settling down. This perception of safety can be very dangerous in this area.

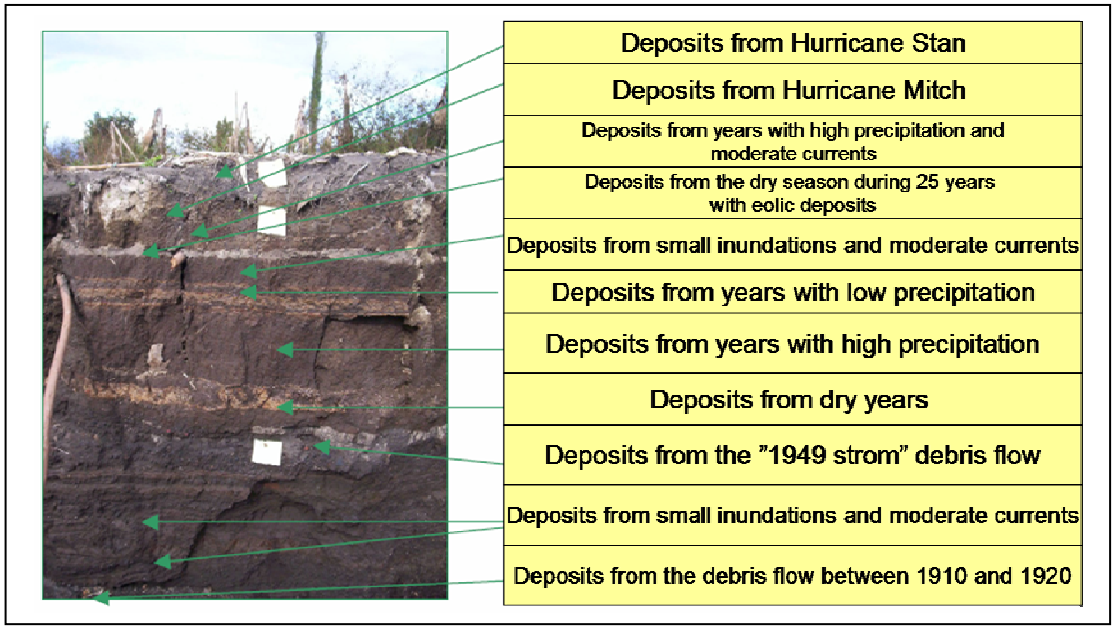

Fig.4.2. The soil profile from Panabaj community shows the deposits from some of the major lahar events in the area (Giron, 2006).

4.3 Geology and geomorphology of the Atitlan area

The Atitlan caldera is a collapse caldera, volcanic activity began in the Lake Atitlan area in the late Pleistocene (about 11-12 million years ago) (Newhall, 1987). Three cycles of growth of stratovolcanoes have been recorded. The first cycle (14-11 million years ago) ends up with eruption of ash flows denominated by the name of “Maria Tecun” and the formation

of the great “Caldera Atitlan I” that is located north of the present basin of the lake (Fig.4.3a). The second cycle (10-8 million years ago) ends up with the eruption of ash flows denominated by the name of “San Jorge”, a collapse event that forms the “Caldera Atitlan II” and a late stage of ring dike injections. The reason for the existence and southwestern migration of the Atitlan caldera complex are not well understood (Newhall, 1987). The third cycle (around 1.8 million years ago) includes the growth of the Early Quaternary stratovolcanoes, voluminous eruptions of Los Chocoyos (eruption that formed the caldera) and less quantities of silicilic eruptions formed the present day “Caldera Atitlan III” and the growth of the modern stratovolcanoes San Pedro, Toliman and Atitlan (Fig.4.3b). A large explosive eruption about 84,000 years ago formed the most recent Atitlan caldera that is filled now by the Lake Atitlan. This caldera event erupted a large volume of tephra (300 km^3) that has been identified from Florida's coast to Ecuador and formed a voluminous ignimbrite whose deposits occur throughout much of the Guatemalan Highlands and Pacific Coastal Plain. The Atitlan caldera has erupted at least five times in the last 84,000 years. The high heat fluxes measured, the geologic register of post-caldera eruptions and the inexplicable fluctuations of the level of the lake, suggest that remainders of magma are still in the bottom of the lake and that future eruptions are possible. The caldera has more than 3,000 km of depth and it has a relatively flat bottom as was observed by the bathymetry built based on seismic reflection profiles (Newhall, 1987).

Three cones (San Pedro, Toliman and Atitlan volcanoes) have grown on the southern edge of the previously existing Atitlan caldera. Lavas exposed on the flanks of these cones are generally calc-alkaline andesites, but their chemical compositions vary widely. The Atitlan volcano borders the southern rim of the Atitlan caldera. It is the largest and the most southerly of the three cones. The Atitlan volcano erupts more explosively to form pyroclastic flows and widespread tehpras of basaltic-andesitic composition. The Toliman and San Pedro volcanoes are situated within the caldera. Their flanks are mantled by more silicic lava flows. Recent dacitic lavas from vents south of the San Pedro volcano and silicic pyroclastic rocks which mantle the slopes of the San Pedro may reflect residual post-caldera rhyolitic volcanism. The activity at Toliman and San Pedro produces thick lava flows or lava domes and some tephra (ash and scoria) layers.

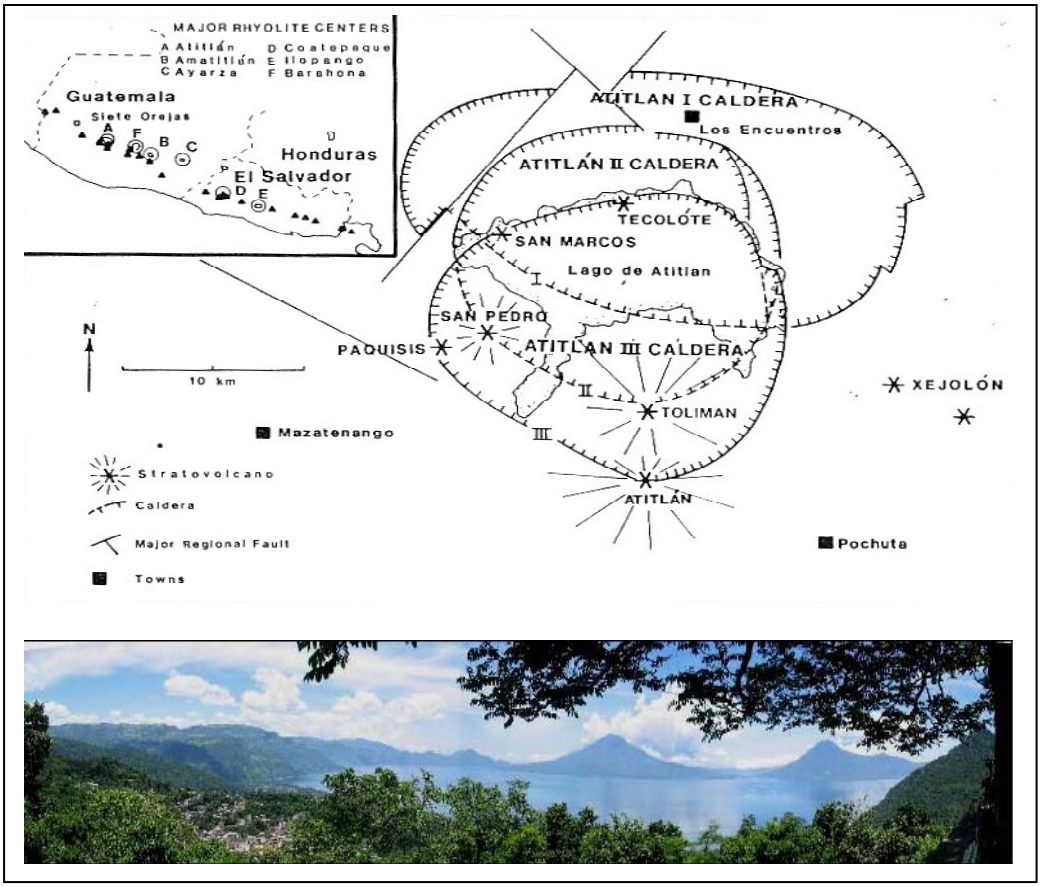

Fig.4.3.a) Southwestern migration of Atitlan caldera during the three cycles of formation (Newhall, 1987) (top), b) View of the overall Atitlan III caldera walls. Toliman volcano to the far left and San Pedro volcano to the far right (bottom).

The geologic evidence indicates that lahars and debris flows have been recurrent processes that affected the area during the last 35,000 years (Newhall, 1987). Historically, the Tolimán volcano has been the most active with lahars of the three volcanoes in the caldera possibly because slopes of 52 ° can be found in the high parts near the crater. The debris flow that happened in October of 2005 represents just one event of this recent activity. Another evidence of the occurrence of debris flows in the past is the existence of fluvial paleochannels that cross old alluvial fans (Fig.4.4). In addition the bathymetry of the lake shows topographic irregularities composed by sediments with 10 to 15 m of thickness that could correspond to a big landslide that happened 1,000 years ago. Studies of recent sediments of the lake through seismic reflection profiles shows a period of active sedimentation (17,500-35,000 years).

Some samples taken from different drill holes in the lake reveals the environmental impact of the deforestation in the area caused by the Mayas and the 2,000 years of fast and unusual sedimentation (near 0.5 cm/year).

The Toliman and San Pedro volcanoes are considered dormant while the Atitlan volcano has registered some activity. According to their eruptive history, the highest threat in the area is the one concerning landslides and debris flows. All of the three volcanoes have had this kind of events before.

Fig.4.4 Evidence of a paleochannel in the area.

The most important features of the Atitlan caldera are the Lake Atitlan and the three volcanoes located at the southern edge of the caldera (San Pedro, Toliman and Atitlan).

The Lake Atitlan has an altitude of 1562 m.a.s.l. and is the largest lake in the Guatemala Highlands with an area of 127 km² (19 km long and 10 km wide). It is recognized to be the deepest lake in Central Amercia, its bottom has not been completely sounded. Estimates of its maximum depth range up tp 340 m. The lake is shaped by deep escarpments which surround it and by the three volcanoes on its southern flank. It is mentioned as one of the most beautiful lakes in the world by Aldous Huxley (English writer).

The San Pedro Volcano has an altitude of 3,020 m.a.s.l. (1470 m above the Lake Atitlan level) and has a base of 6.43 km in diameter (16.67 km³ of volume). The mean slope angle of the San Pedro Volcano is 45° and diminishes at the base with 22°. It is located in the geographic coordinates 14.656° North latitude and -91.266° West longitude. It has a composite cone and is an extinct volcano. The San Pedro Volcano is almost symmetrical except in the Southwest part where it comes across the chain of mountains that limits the caldera. The San Juan La Laguna and San Pedro La Laguna are located to the north of the San Pedro Volcano skirts.

The Atitlan volcano has an altitude of 3547 m.a.s.l.. Its geographic coordinates are 14.581° North latitude and -91.187° West longitude. The Atitlan is the youngest and most active of the three volcanoes. The Atitlan Volcano is a composite volcano, with a steep-sided, symmetrical cone comprising alternating layers of lava flows, volcanic ash, cinders, blocks, and bombs. Since the arrival of the Spanish in the mid-1400, eruptions have occurred in six eruptive clusters (1469, 1505, 1579, 1663, 1717, 1826–1856) (Vallance 2005).

The Toliman Volcano has an altitude of 3540 m.a.s.l.. Its geographical coordinates are 14.619° North latitude and -91.186° West longitude and is a large stratovolcano that rises above the south shore of Lake Atitlán, near the inferred southern margin of the Atitlán caldera. A shallow elliptical crater truncates the summit (250 by 150 m crater), and a minor subsidiary peak to the SSW also has a shallow crater. In contrast to the tephra-covered surface of its twin volcano to the south, Volcán Atitlán, the surface of Tolimán is draped by prominent thick lava flows. Many of the flows were erupted from vents on the volcano's flanks and form an irregular shoreline on the south side of Lake Atitlán. No historical eruptions are known from Tolimán. However, a lava flow that entered Lake Atitlán from the parasitic lava dome of Cerro de Oro on the northern flank was estimated to be less than a few thousand years old.

The geomorphology of the Atitlan caldera is related to the volcano activity of the area. The geomorphology units can be divided in 7 units according to the eruptive stages of the volcanoes and the dynamics of the sediments: - Volcanic lacustrian plains, - Old alluvial fans, - Stratovolcanoes cones, - Craters, - Intervolcanic plains, - Superimposed volcanic plateaus, - Long hills system.

4.4 Slopes and land use

The angle of the slope, the degree of inclination of the terrain and the land use are essential factors for the stability of the soil. Most of the debris flows happen for slope angles of 30º – 50º. In the Southwest area of the Atitlan basin, slope angles of 50° to 87° cause frequent rock falls in the area. The most critical zone in the area can be found where the alluvial fans are formed and debris flows sedimentary charge is deposited. These areas can be found when the slope angle is lower than 15º and is where most of the communities surrounding the lake are located (Fig. 4.5).

Other important factor for slope stability is the land use and the vegetative cover. In many cases, human activity and the influence of the vegetation does not have a direct influence in the generation and activity of lahars. The saturation of the loose volcanic soil and the steepness of the slopes in the region are the main factors that influence the formation of lahars. The vegetative cover does not provide a significant contribution to the slope stability.

Because of the steepness of the topography, the land use in the Atitlan basin is divided in three main activities: 1) The highlands are used for forest (conipher and latifolia forest); 2) The midlands are used for coffee plantations (combined with species of fast growing trees to shadow the coffee plant); 3) The lowlands are cropped mainly with corn and black beans (mainly a subsistence agriculture practice since most of the diet is based on corn).

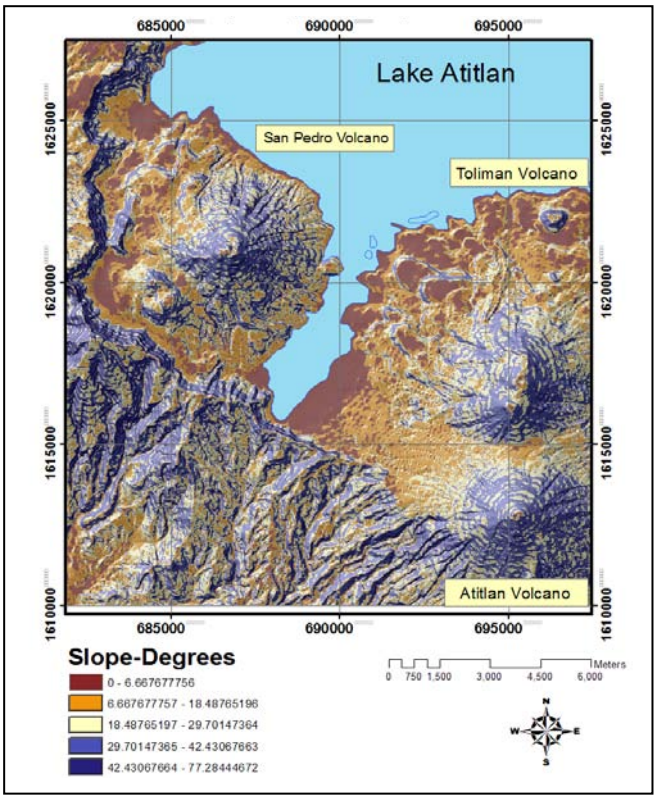

Fig.4.5 Map of slopes angles in the Atitlan study area.

4.5 Climate

Two meteorological stations owned by INSIVUMEH (Guatemala Institute of Seismology, Vulcanology, Meteorology and Hydrology) are located in the studied basin area (San Pedro La Laguna station and Santiago Station). Because of the lack of records and control in the San Pedro La Laguna station, all the meteorological information stems from the Santiago station (Fig.4.6a). The recorded mean temperatures fluctuate between 12.5 ºC min. to 26.0 ºC max. and the mean annual precipitation is 1010 mm (figure4.6b). The rainy season lasts 5.5 to 6.5 months between the months of May and October. The wind velocities oscillate from 70 to 100 km/h (INSIVUMEH, 2005).

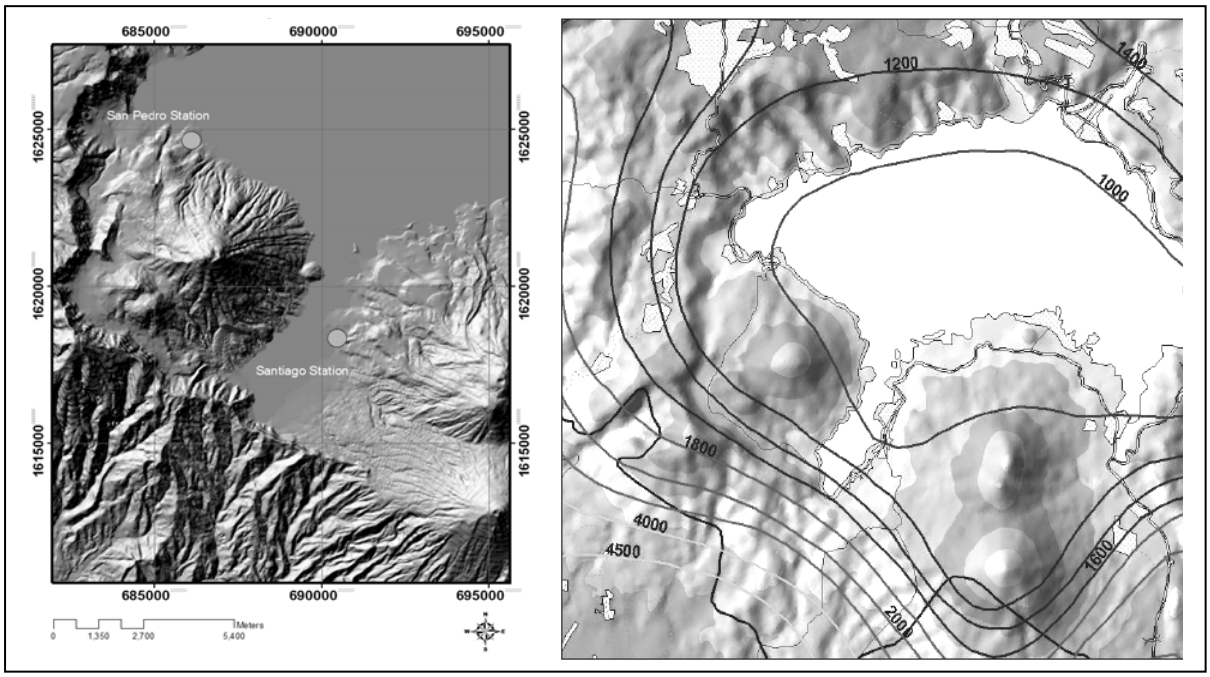

Fig.4.6. a) Location of the meteorological stations in the Atitlan study area (right), b) Map of the precipitation isolines (mm) for the Atitlan study area (Giron, 2007).

Four events with high precipitation have been recorded during the last 36 years in this area. The first event occurred during the year 1973 when the Category 5 Pacific hurricane called “Ava” hit the coasts of Guatemala. The second event happened in 1995 when Tropical storm “Gil” caused heavy precipitation in all the lowlands of Guatemala. The third event was during 1998 (year of the Hurricane Mitch). The fourth event happened in the year 2005 during Hurricane Stan.

Figure 4.7b shows the precipitation during the different months of the year. It can be observed that the months with the highest intensity of rain are June and September with values near 210 mm and the driest ones are January and February. Although the months of July and August are inside the rainy season, they have lower precipitation than June and September because of a phenomenon called “canicula” (two or three weeks with no precipitation).

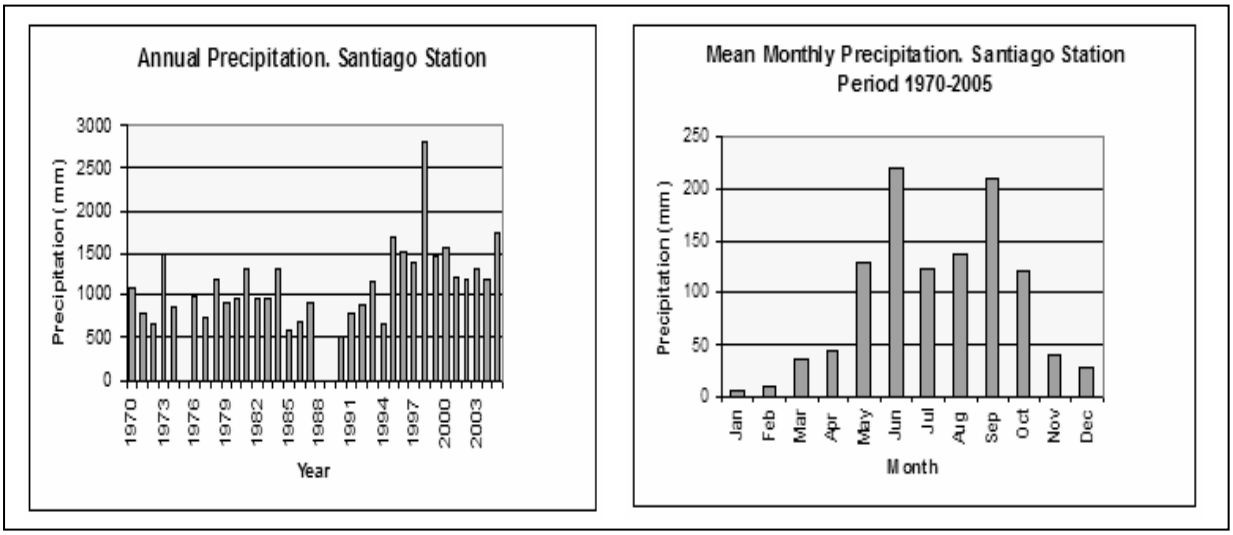

Fig.4.7. a) Graph of annual precipitation for the Atitlan area, Santiago meteorological station (left). b) Graph of the mean monthly precipitation for the Atitlan area. Santiago station. Period 1970-2005.

The Hurricane Stan event occurred during the period of 1st to 10th of October. The mean monthly precipitation for the period 1970-2004 for October is 139.8 mm. Because of the Hurricane event in 2005, the mean monthly value for October in the area reached 496.1 mm. A statistical approach to calculate the return period using the monthly maximum values of the Santiago Area during the period 1970-2005 was done with the statistical computer program called the “R program”. The distribution that best fitted the data was the Generalized Extreme Value distribution (GEV). The monthly rainfall precipitation with 50 year return period is of the order of 475 mm (Fig 4.8).

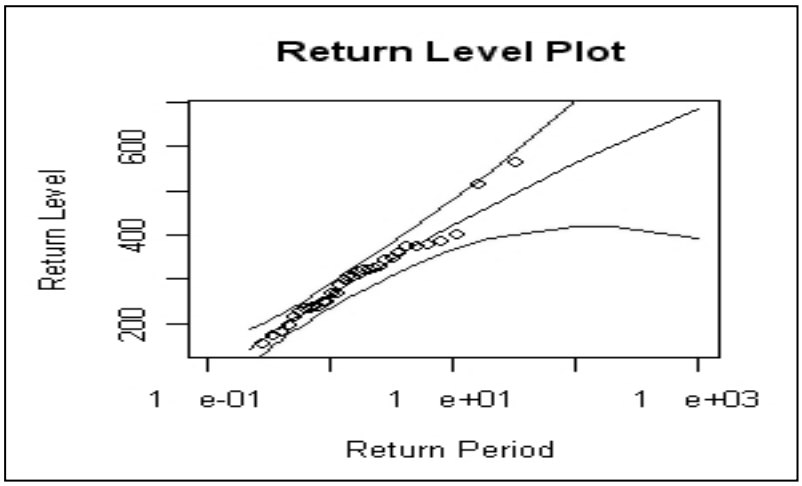

Fig 4.8. Plot obtained by the statistical computer program "R" of the monthly return period for the Santiago station for the period 1970-2005. The x axis is return period in years and the y axis is return level in mm.

4.6 Hurricane Stan in Guatemala

The fast increase in precipitation that happened at the beginning of October 2005, was created by the interaction of various meteorological systems: the formation and evolution of the Hurricane Stan in the Atlantic Ocean (Fig.4.9), the high position in latitude of the Intertropical Convergence Zone (belt of low pressure girdling Earth at the equator) associated with a low pressure system in the Pacific Ocean and the persistence in low atmosphere of the flows of the south and southwest wind penetrating from the Pacific Ocean. When these events interacted with the Guatemalan relief, they created an intermittent rainfall that lasted from the 30th of September until the 10th of October.

The chronology of the Hurricane Stan as it reached Guatemala and the precipitation values for the Atitlan area is shown in Appendix A.

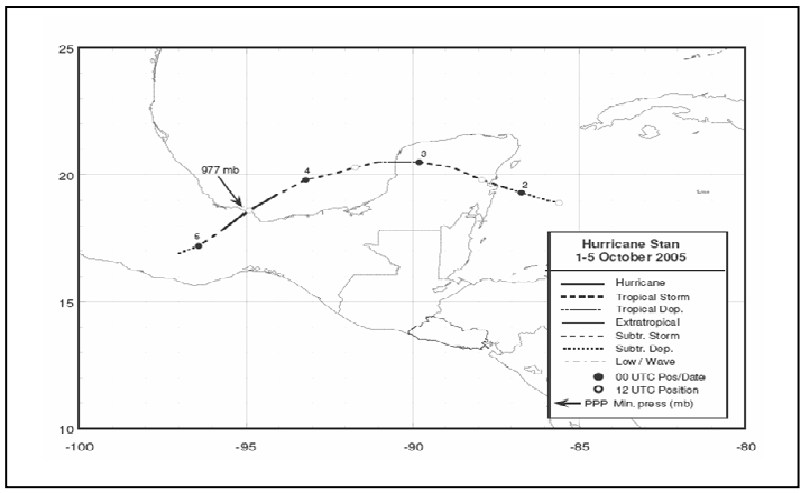

Fig.4.9 Path of the tropical cyclone that turned into the Hurricane Stan and its stages of evolution (NOAA, 2005).

The accumulated rainfall during the 2nd and the 9th of October recorded in the Santiago Station was 562.3 mm. The day with the highest accumulated rainfall was the 4 of October with 297.5 mm that coincides with the debris flow in Panabaj and San Juan La Laguna. The increase in intensity of the rainfall happened very suddenly, in a 24 hour lapse the accumulated rainfall go went from 78.6 mm (3 of October) to 376.1 mm. (4 of October) and for the next 24 hours values of accumulated rainfall were 520.1 mm. (5 of October) making the rescue efforts for the victims very difficult. Three hours before the failure collapse that produced the lahars, a precipitation of 54.4 mm was measured. These precipitation results were obtained from reading and interpreting the pluviograph measurements from the Santiago station for the period of time when the Hurricane Stan happened and may not agree with other published values.

The debris flow events in Panabaj and San Juan La Laguna happened after 5 months of the rainy season (May to September) and for this reason the critical rainfall intensity was lower because the soil was already saturated. Although the slope material has adjusted to the climate conditions during its lifetime, the abnormal rainfall situation triggered the event. The intensity of rain falling within a short period of time (70.3 mm in 4 hours) was critical for the slide to occur. Figure 4.10 shows the distribution of the rainfall during the storm period.

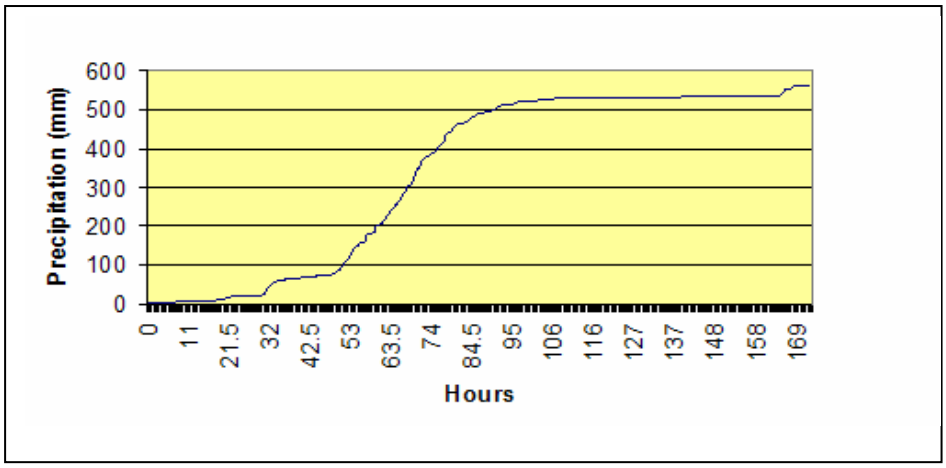

Fig.4.10 Accumulated Rainfall (mm) measured in hours during the Hurricane Stan event. Santiago meteorological station.

To have a point of reference of the magnitude of the event, the Hurricane Stan precipitation values were compared with the Hurricane Mitch (1998) precipitation values in the Atitlan area. Hurricane Mitch had a period of intense rains of 6 days, with a maximum daily accumulated precipitation of 95.2 mm (Buckman, 2001). Hurricane Stan had a period of intense rains of 3 days with a maximum daily accumulation of 297.5 mm.

During Hurricane Mitch, maximum values of accumulated precipitation reached 326.7 mm and were reached in a more gradual way, staying constant during 3 days. During Hurricane Stan maximum values of accumulated precipitation reached 562.3 mm and were reached in a fast way, with a variation of 26 mm in 3 days. Figure 4.11 shows that the rainfalls during Hurricane Stan happened in a shorter period of time and were more intense than the ones with the Hurricane Mitch.

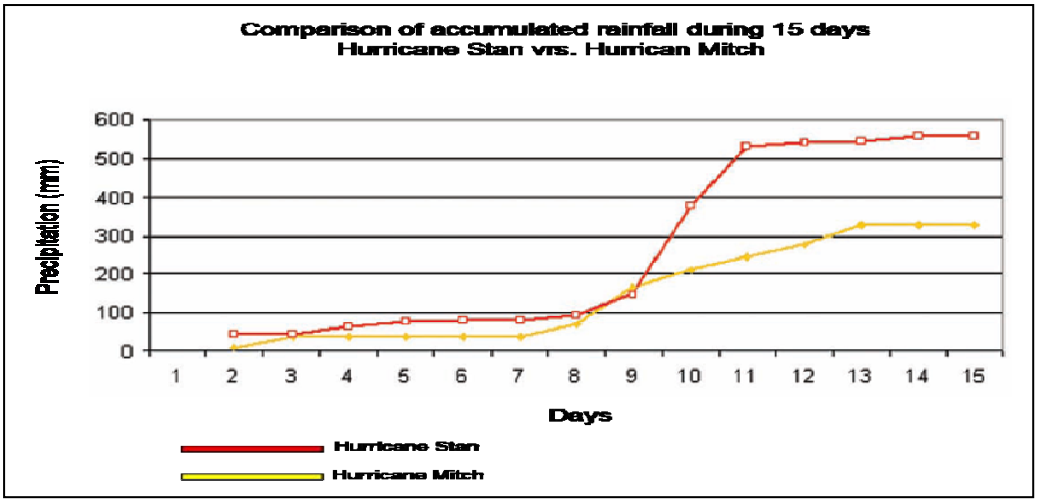

Fig.4.11 Comparison graph of accumulated precipitation (mm) during Hurricane Stan and Hurricane Mitch.

4.7 Hydric balance

The temperature recorded by the INSIVUMEH in the Santiago station for the period of 1970 to 2005 was used to calculate the mean monthly value. Figure 4.12 shows the graphic behavior of the mean monthly temperatures. February is the month with lowest temperatures with values of 15.9 ºC and August is the warmest month with mean values of 19.4 ºC.

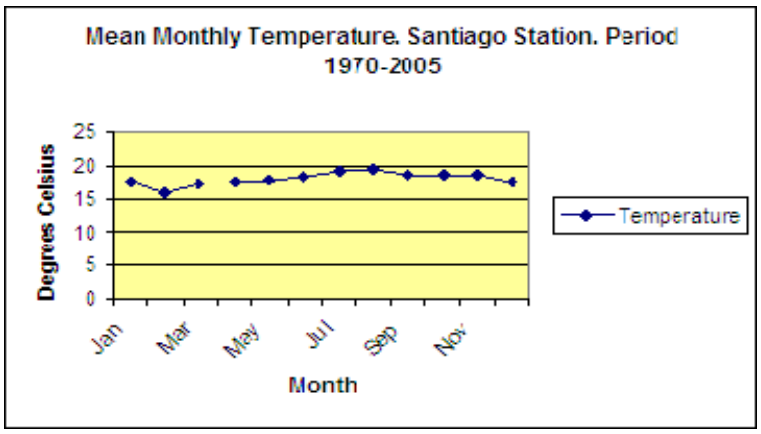

Fig.4.12. Mean monthly temperatures values during the period 1970-2005 in Santiago station.

Table 4.1 shows the calculated mean monthly values from the period of 1970 to 2005 for precipitation, potential and real evapotranspiration, run-out and infiltration in the Santiago station. The calculated mean annual evapotranspiration is 68.0 mm per year. The calculated mean annual infiltration is 582.92 mm per year. The mean monthly infiltration values were obtained with the formula: Infiltration = Precipitation – Evapotranspiration. The months with highest values for infiltration are June and October with 115.9 and 116.1 mm and the months with lowest infiltration are January and February.

The run-out was obtained with the formula: Run-out = Precipitation x Coefficient for run-out. The used value of coefficient for run-out for the Atitlan area is 0.3 (value used by INSIVUMEH for the Atitlan area). This coefficient is related to the different land covers and hydrologic soil group. The months of January and February have low values of run-out (1.11 and 4.32 mm) whereas the highest run-out is during the months of June and September (63.24 and 63.3 mm) (Fig.4.13).

	Precipitation (mm)	Potential evapo-transpiration (mm)	Real evapo-transpiration (mm)	Run-out (mm)	Infiltration (mm)
Jan	3.7	57.47	18.7	1.11	2
Feb	9.6	44.72	24.6	4.32	9.4
Mar	29.8	59.67	33.8	8.94	16.4
Apr	46.7	62.31	47.7	14.01	25.7
May	122.9	68.132	68.13	36.87	67.6
Jun	210.8	72.02	72.03	63.24	115.9
Jul	115.5	80.5	80.5	34.5	63.5
Aug	130.1	79.86	79.86	39.03	71.6
Sep	211	69.56	69.56	63.3	116.1
Oct	119.8	68.2	68.2	35.94	65.9
Nov	39.7	64.11	58.7	11.91	21.8
Dec	18.3	57.52	24.3	5.49	10.1

Table 4.1 Hydric Balance calculated for the Atitlan area.

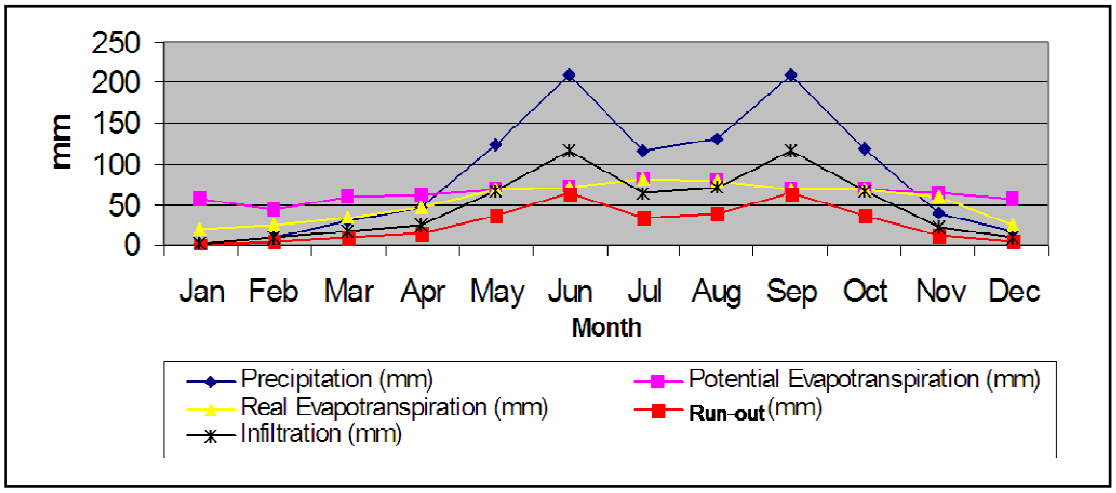

Fig.4.13. Graph of the Hydric Balance for the Atitlan area. Santiago Station. Period 1970-2005. Mean monthly values.

5. The Panabaj lahar

Fig.5.1. The Toliman volcano and the channel were the lahar flowed to the Panabaj community (left). Destruction left by the lahar in the Panabaj community (top right and bottom right).

The Panabaj community is located on the skirts of the Toliman volcano at the shores of the Southwest part of the Lake Atitlan. Its geographical coordinates are 14.624° North latitude and -91.231° West longitude. The name Panabaj is derived from the Tzutujil dialect (Prw´a´ch´ba´k) meaning “Head of Mud” because of the mud flow events that are common in the area. The Panabaj community is located between the slopes of two volcanoes making it a very susceptible area for mud and debris flows. During the Hurricane Stan event, the population of the Panabaj community was on the alert for debris flows but there was no local organized emergency plan to deal with such a hazard and potential consequences. The night before the lahar event, the municipality and the fire brigade were informed by the INSIVUMEH of the unfavorable weather conditions and they made a warning to the population. Hours later, a failure in the flank of the Toliman volcano produced a lahar that consisted of soil, water, rocks and trees (Giron and Garavito, 2006). The velocity of the flow eroded parts of the channel making the debris flow grow and gain more momentum (Fig.5.1).

The flow reached the alluvial fan (where the Panabaj community is located) and destroyed the community almost entirely. More than 1200 people died. They were buried or were dragged with the flow to the Atitlan lake. The precipitation that kept falling during the next day made the rescuing effort very difficult. In addition to the high death toll, the debris flows at Panabaj resulted in extreme hardship in many parts of the community that survived the debris flows themselves. Nearly all of the community is comprised of farmers cultivating small plots of land and living in poverty. Since the debris flows, many individuals in this community have been reduced to extreme poverty, as the heavy rains and debris flows devastated houses and destroyed the crop land that constitutes a major source of income. The Panabaj area has been declared a “mass grave” by the Guatemala authorities.

The slope failure that occurred on the Tolimán volcano resulted in the generation of a moderate size debris flow that descended the volcano rapidly and split into two stream valleys high on the flanks of the volcano. The flows continued to descend both channels until they reached the alluvial fan near the shores of Lake Atitlan. Once reaching the alluvial fan, the flows spread over the relatively flat surface very rapidly. The steep and narrow shape of the channels and the splitting of the flow in the high part of the volcano made the lahar arrive the alluvial fan in 4 different waves.

The lahar that affected the Panabaj community was relatively small in volume. Because the lahar split into two different river valleys high on the flanks of the volcano, two separate flows inundated Panabaj (the western and eastern debris flows) (Sheridan 2006). The deposits were composed mostly of coarse sand-sized (1 mm in diameter or coarser) material. Common moderate volume flows like the one that happened in Panabaj tend to occur during extreme rainfall events while large debris flows occur during seismic or volcanic events. In Panabaj, the volumes of the eastern and western debris flows were calculated by field observations to outline the boundaries of the debris flows and to estimate variation in flow thicknesses. Figure 5.2a shows a map that delimitates the inundated areas by the eastern and western debris flows. The area inundated by the Western flow is approximately 180,000 m^2 and the area inundated by the Eastern debris flow is 76,000 m^2. On average these flows are 1.6 m thick throughout most of their area, although their thickness exceeds 2 meters in some of the main channels. Based on observations of high water marks preserved on buildings and

trees, up to 40% of the flow by volume consisted of water and fine grained sediments that have been dewatered from the deposit during and since deposition. The flow volume of the two flows combined does not exceed 400,000 m³. Thus the combined volume of the two flows is a relatively small volume.

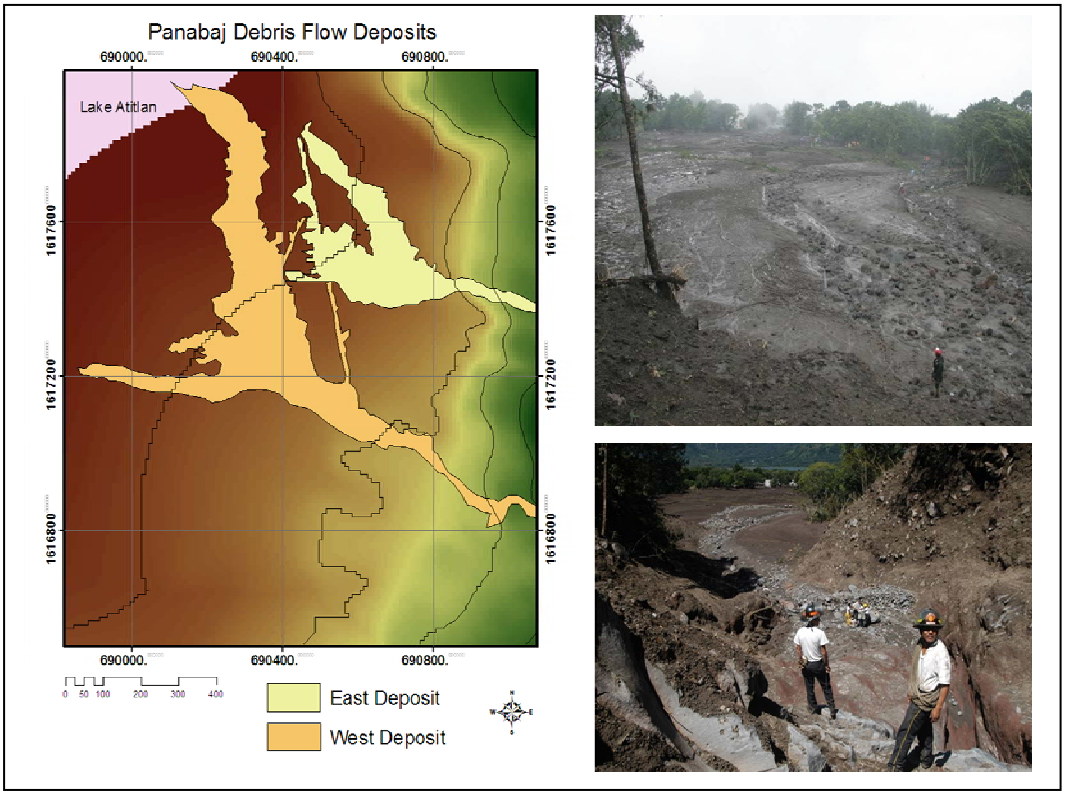

Fig 5.2. a) Map of the deposition area in the Panabaj community (left) (Sheridan, 2006), b) Hyperconcentrated deposits left by the lahar (right top and bottom).

Hyperconcentrated flow inundated a larger area down-slope from these deposits. These flows consisted mostly of water with fine-grained clay and sand-sized particles suspended. As the lahar came to rest, it became separated into fine-grained and coarse-grained fractions. As the coarse grained fraction lost momentum and came to rest, the fine-grained fraction of the flow separated and continued down-slope. A hyperconcetrated flow is less turbulent and less destructive than the thicker, coarse grained part of the flow, but nonetheless

is capable of causing damage and may leave deposits of fine-grained mud and sand up to 10-20 cm thick (Fig.5.2b) (Vallance, 1998). Because these hyperconcentrated flows were rich in suspended clay and sand sized particles, damage in areas located down-slope from the main deposits was substantial in some cases. These hyperconcentrated flows reached Lake Atitlan and were sufficiently strong to sweep some large debris into the lake and also some people.

The way the lahar wrapped around trees that remained standing and the damage patterns observed on trees themselves were used to make a map of directions of the flow. In many cases tree bark was stripped and the trees impacted on their up-stream sides (Sheridan, 2006). These flow indicators are more common at the edges of the flow, and give a sense of mass movement.

Figure 5.3a, shows the direction on the flow surface. Most of the flow reveals a fanning pattern, converging on the channels that fed the two debris flows. Visual observations in the field were made of the damage to structures such as road cuts, fences, soccer fields, average height of houses and wire fences to estimate the thickness of the deposited flow. The thickest part of the deposit was approximately 2.5 m. Close to the end of the flow, thicknesses of 1.6 – 1.8 m, were observed. In some areas, the impact of the hyperconcentrated flow against buildings resulted in the accumulation of up to 80 cm of fine-grained sediment (Fig.5.3b).

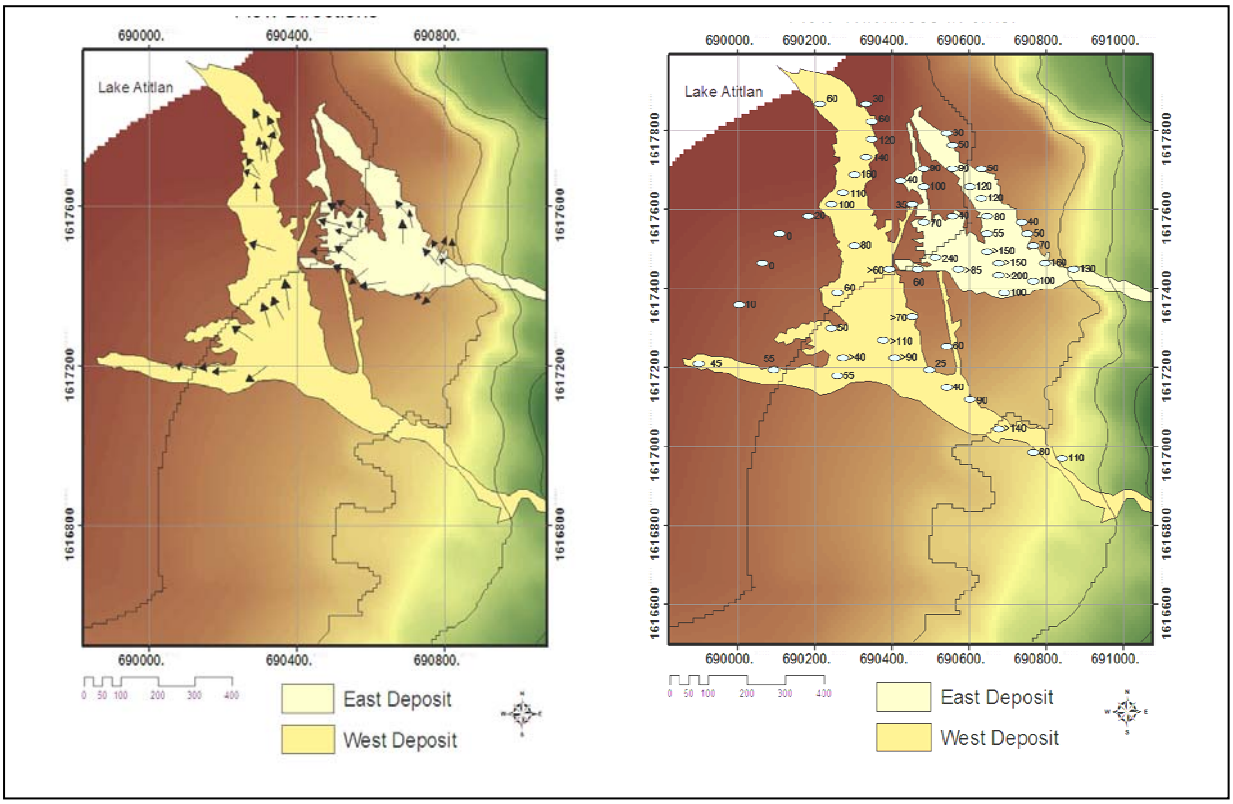

Fig.5.3. a) Flow directions of the Panabaj lahar (left) b) Thickness of the deposits left by the lahar in the alluvial fan (right) (Sheridan,2006).

The longitudinal profiles of the flow shows the topographic variation on the flow surface from points on the alluvial fan to points up the channels above the fan (Figures 5.4 and 5.5). In the channels, these longitudinal profiles show the change in elevation of the center of the channel slope, as it descends. After the split into two flows high up on the flanks of the volcano, about 65% of the flow (by volume) descended the western channel, forming the western flow. This western channel normally captures much of the stream flow on this part of the volcano. The longitudinal profile shows a gradually decreasing slope as the channel approaches the alluvial fan. Approximately one kilometer above the alluvial fan, this channel descends steep topography, with a slope of 11.5°. This average slope gradually decreases down the channel, reaching only 5.3° just above the alluvial fan. The Eastern channel is not a normal drainage on the volcano. A debris flow moved into this channel only because the capacity of the western channel was exceeded. The Eastern channel is not mature,

in the sense that the longitudinal profile shows step grades and varying steepness along the profile, rather than the gradual change in slope observed along the western channel. Average slopes on the Eastern channel are up to 16.7°. The eastern channel slope bed steepens dramatically to 12.8° just above the alluvial fan. This increase in slope increased the debris flow velocity just before it reached the populated alluvial fan.

To estimate mean flow velocity and peak discharge in the two channels a method that uses the superelevation of the flow as it turns bends in the flow channel during descent. As material flows in a channel, centrifugal forces cause the mass of debris to rise up the outside of bends. The superelevation (the height to which material rises as it banks through a curve), that is the difference between the height of the flow on the inside of the channel bend and the outside of the channel bend, provides an indication of mean flow velocity in the channel. In order to determine flow velocities using this method, the average channel bed slope, elevation, and the radius of curvature of the bend must be determined. Measurements collected around channel bends along the channel bed slope and on the margins of the channel, tracing the high water mark where vegetation has been stripped from the channel banks. It is possible to calculate the mean velocity during peak discharge from the following relationship:

$$v = \sqrt{\frac{gdr}{b}} \qquad (5.1)$$

where g = gravitational acceleration, d = superelevation, r = centerline radius of curvature and b = channel width. Along the eastern flow channel, measurements on two bends give results of mean flow velocities of 11 m/s and 13 m/s, respectively. Channel cross-sectional area in the two areas was 154 and 160 m^2 during peak discharge. The peak discharge (flux) along the Eastern flow was approximately 1690-2000 m^3/s. According to these flow velocities, the debris flow would descend from its entire flow path from the landslide area high on the volcano to the community of Panabaj in less than five minutes. The total duration of the flow was between 2 and 3 minutes. This suggests that insufficient time is available to actually evacuate the alluvial fan after a debris flow has been initiated.

The coefficient of friction is a measure of the resistance to flow generated by the avalanches at the contact with the underlying topography. In its simplest form, it can be estimated by the tangent of the mean slope from the top of the source area to the most distal part of the flow, otherwise known as the Heim Coefficient.

$$\frac{H\,\max}{L\,\max} = \tan\alpha \qquad (5.2)$$

where H_{max} is the fall height from the top of the source region to the toe of the deposit, L_{max} is the horizontal distance traveled from the source to the toe of the deposit, and tan α is the Heim Coefficient. For the Panabaj lahar, the H/L relationship for this debris flow was estimated as L = 4910 m and H = 1440 m giving a coefficient of 0.29 (16.3°)

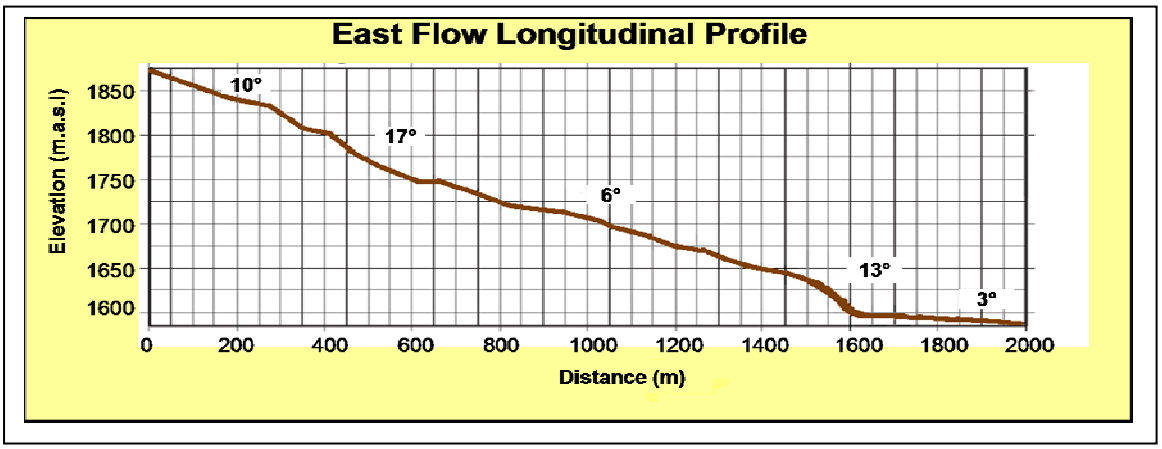

Fig.5.4. Longitudinal profile of the channel followed by the East flow.

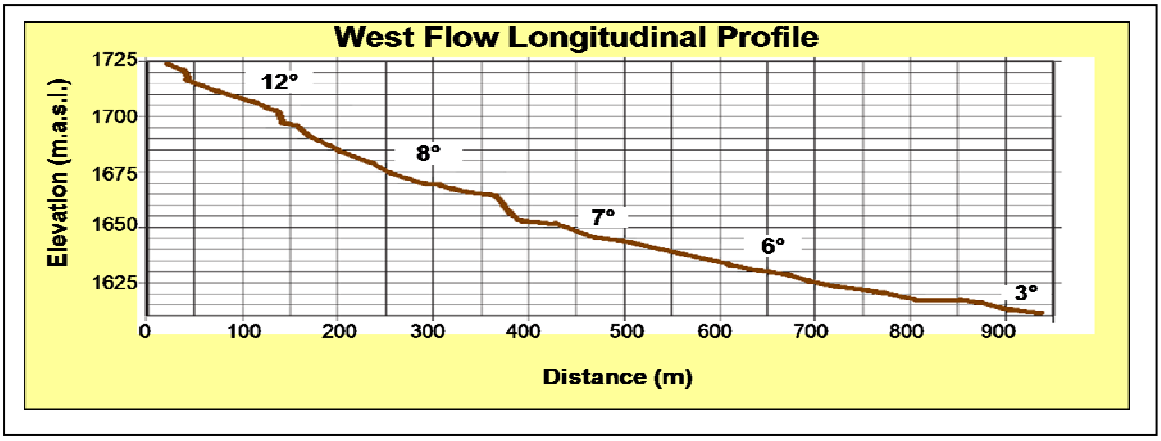

Fig.5.5. Longitudinal profile of the channel followed by the West flow.

Many affected families have been relocated in temporary shelters located within 100-300 m of the debris flow deposits of October 2005. This temporary housing is located on a gently sloping alluvial fan, a very broad geological deposit formed by the repeated inundation of the area by debris flows over a period of thousands of years or more. Because the temporary housing for people displaced by the debris flows is located in an area that is geologically and morphologically similar to the area inundated by flows in October 2005, this area may be inundated by debris flows as well. In addition to the thousands of people living in temporary shelters, many hundreds of people are currently reoccupying land adjacent to or on the October 2005 debris flows. It seems that a large fraction of the surviving Panabaj community still remains at risk from future debris flows.

6. Simulation of the Panabaj lahar with the program RAMMS

6.1 Description of the RAMMS program

The RAMMS (**Ra**pid **M**ass **M**ovement**s**) program was developed at WSL/ SLF (Swiss Federal Institute for Snow Avalanche Research) as a unified software package that can combine two and three-dimensional process modules for:

- Snow avalanches using a 2D model developed by WSL/SLF, for the description of dense avalanche dynamics with modules for avalanche-structures interactions and avalanche-forest interaction including the introduction of entrainment and deposition.
- Debris flows that uses a two-phase, 2-dimensional finite volume model, where the solid and fluid phases are described separately and coupled. The motion of the solid phase is based on a solution of the Savage-Hutter equations for granular flows. The fluid phase is similarly described as a Chezy-type fluid. The phases are coupled using a momentum exchange concept, and the equations are solved with a finite volume technique. Friction parameters consist of an internal Coulomb friction angle and a Chezy-type fluid friction parameter.
- Rock falls, still in development, that will allow the tracking of individual particles in 3D space over a DEM

The application of RAMMS involves predicting flow run-out distances, impact pressure and flow velocities. The development of RAMMS started two years ago and is still undergoing development (2007).

The model solves the governing mass and momentum equations using a first order TVD (total variation diminishing) scheme on triangular grids. The grid is generated from a digital terrain model. An automatic scheme determines the location and magnitude of the avalanche

release conditions. RAMMS includes an entrainment module based on the work of Sovilla (2004) and Sovilla et.al. (2007). It is possible to specify different layers of the bed which can be entrained according to an updated Grigorian and Ostroumov procedure. Three different entrainment mechanisms are described: frontal ploughing, step-entrainment, and basal erosion (Sovilla 2004). Entrainment rates are based on physical parameters such as the avalanche speed and the strength of the bed slope.

At the moment (2007), the program has the debris flow module included in the snow avalanche module. The debris flow module is based on a modified Voellmy-Salm friction relation incorporated into a hydraulic model based on the shallow-water equations which have been extended for granular flows.

6.2 Program characteristics

In the RAMMS program it is possible to handle all the input and output specifications and visualizations in the user interface. The data analysis ability of the program can handle large DTM (digital terrain model) data sets. The DTM data (together with other input specifications) is then used to describe the depth-averaged motion of dense flowing avalanches and debris flows in general terrain, employing a finite difference scheme that numerically solves the governing differential equations The numerical module is programmed in C which is linked to the interface. The binary output results are then read displayed and analyzed with interface.

The user interface uses GIS tools to define the boundaries of the computational grid and to simplify the definition of the source area for slopes instabilities. The system is linked with a GIS environment, making the RAMMS program a tool that can be used for hazard mitigation studies in mountainous regions that are affected by gravity driven processes. The graphical user interface is programmed using tools from IDL (Interactive Data Language). It is designed to facilitate the development of visualization tools by providing a set of

components that provide standard features: creation of visualization graphics, mouse manipulations of visualization graphics, management of visualization and application properties, data import and export, data filtering and manipulation and interface element event handling. The visualization objects are defined as polygons, where maps, orthophotos and input parameters can be mapped on top.

Results can be exported as ESRI shapefiles and compared in ArcGis with real data. ESRI shapefiles can also be imported into RAMMS. Additionally, GIF files, GIF animations and ASCII files can be exported.

6.3 The numerical model

The RAMMS program is a numerical simulation tool based on the generalization of the quasi-one-dimensional dense-snow avalanche model that contains a Voellmy-fluid flow law with longitudinal active and passive straining discussed in detail by Bartlelt (1999), and an entrainment model discussed by Sovilla (2004). The dense-snow avalanche flow with entrainment law is a hydraulic-based and depth-average continuum model that divides avalanche flow resistance into a dry Coulomb-type friction and a viscous resistance which varies with the square of the flow velocity. The models numerically solve the mass (volume) and momentum balance equations:

$$\frac{\partial A}{\partial t} + \frac{\partial Q}{\partial x} = Se - Sd \qquad (6.1)$$

$$\frac{\partial Q}{\partial t} + \frac{\partial}{\partial x}\left[\alpha \frac{Q^2}{A}\right] + \lambda g A\left[\frac{\partial h}{\partial x}\right]\cos\varphi = gA(So - Sf) \qquad (6.2)$$

where g is the acceleration due to gravity, $h(x,t)$ is the avalanche flow height, So and Sf are the acceleration and frictional slope, respectively, λ is the active/passive pressure coefficient and the α is the velocity profile factor. The equations are based on several assumptions: flowing

snow is a fluid continuum of mean constant density; the flow width, *w(x)* is known; a clearly defined top flow surface exists; the flow height, *h(x,t)* is the average flow height across the section; the vertical pressure distribution is hydrostatic and centripetal pressures which modify the hydrostatic pressure distribution are not accounted for; and flow velocity and depth are unsteady and non uniform (Christen, 2002).

The right-hand side of the mass equation contains the terms *Se* and *Sd* which are the volumetric snow entrainment and deposition rates. This is the entrainment model (Sovilla 2005) that has been implemented in the dense snow avalanche model and is discussed later in this chapter.

The parameter α *(x,t)* is the velocity profile factor. For a rectangular velocity profile, α *(x,t)*= 1. The *So*, acceleration slope, is given by:

$$So = \sin\varphi \qquad (6.3)$$

where φ*(x)* is the inclination of the bed slope from the horizontal. The friction slope, *Sf*, is found by depth-averaging the shear stress gradient:

$$\rho g Sf = \frac{1}{h}\int_0^h \frac{\partial \tau_{zx}}{\partial z} dz = \frac{1}{h}\left[\tau_{zx}(h) - \tau_{zx}(0)\right] = -\frac{1}{h}\tau_{zx}(0) \qquad (6.4)$$

It is assumed that no shearing deformation γ occurs in the avalanche body and at the top surface.

$$\gamma = \tau_{zx}(z) = 0 \quad \text{for} \quad 0 < z \le h \qquad (6.5)$$

The avalanche moves as a plug with a velocity that is constant over the depth of the flow, h. No fluidized shear layer exists since shear deformations are concentrated at the base of the avalanche; the shear layer is considered small compared to the avalanche flow height.

The basal shear resistance consists of a dry Coulomb-like friction and a Chezy-like resistance:

$$\tau_{zx}(0) = \mu\sigma_z + \frac{\rho g}{\xi}U^2 \qquad (6.6)$$

The stress σ_z is the overburden pressure at $z = 0$ and is dependent on the flow height:

$$\sigma_z = \rho g h(\cos\varphi) \qquad (6.7)$$

A hydrostatic pressure distribution is assumed. U is the plug flow velocity. The parameters μ and ξ are constants whose magnitudes depend, respectively, on snow properties and the roughness of the flow surface.

The friction slope for a Voellmy fluid is:

$$Sf = \mu\cos\varphi + \frac{U^2}{\xi h} \qquad (6.8)$$

The stress in the longitudinal direction is proportional to the hydrostatic pressure and is:

$$\sigma_z = \lambda\sigma_z \qquad (6.9)$$

where λ is the so-called active/passive pressure coefficient. The difference between active (extension) and passive (compression) cases are based on the sign of the velocity gradient (strain rate) in the longitudinal direction, $\partial U / \partial x$,

$$\lambda = \lambda_a \text{ for } \partial U / \partial x > 0 \qquad (6.10)$$

$$\lambda = \lambda_p \text{ for } \partial U / \partial x \leq 0 \qquad (6.11)$$

This allows different amounts of internal flow friction to be introduced depending on whether the plug is longitudinally pulled apart or compressed. Rankine's theory is applied to define the active/passive pressure coefficients:

$$\left.\begin{matrix}\lambda a\\ \lambda p\end{matrix}\right\} = \tan^2\left(45° \pm \frac{\phi}{2}\right) \qquad (6.12)$$

where ϕ is the internal friction angle, closely related to the angle of repose.

6.4 Entrainment model

An erodible cover of density $\rho_e\ (x)$ with depth $d_e\ (x)$ and a potential erosion area $A_e\ (x)$ are defined by the avalanche flow width $w\ (x)$, where x is the track length. Entrainment is localized at the head of the avalanche. The mass in flux rate is governed by mass and momentum conservation at the avalanche front but limited by mass availability. In this model the volumetric entrainment rate is:

$$S_e = \frac{\rho_e}{\rho} U_e w \qquad (6.13)$$

where U_e is the entrainment velocity, specifying the speed at which the snow cover height is decreasing. This velocity is

$$Ue = Cf\sqrt{\left(p - p^*\right)} / \rho_e \qquad (6.14)$$

where p is the applied pressure and p^* is the resisting strength of the snow cover. It is derived from mass and momentum conservation statements applied at the bottom boundary of the avalanche. C_f is:

$$Cf = \sqrt{1/\left(1 - \rho_e / \rho\right)} \qquad (6.15)$$

When the avalanche velocity *U(x,t)* is equal to the entrainment velocity *U(x,t)* the erosion front is inclined by an angle of 45°. It is difficult to define the avalanche pressure, p. This can be determined by redefining the applied pressure or limiting the entrainment velocity U_e by a coefficient. In this model it is assumed that the full impact pressure of the avalanche is exerted on the snow cover and therefore overestimates the entrainment rates and concentrates erosion at the front. This avoids the use of an additional empirical coefficient.

Once the entrainment model is implemented in the dense snow avalanche model (discussed above), the entrainment model defines the non zero $Se \neq 0$ volumetric snow entrainment rate on the right side of the mass continuity equation and defines *Sd* = 0. In the numerical solution of the governing equations the change in volume per calculation time Δt is: $\Delta Se = Se\Delta t$. The quantity Δ*Se* can never be greater than the available mass:

$$\Delta Se < \frac{\rho_e}{\rho} d(x,t) w(x) \qquad (6.16)$$

The avalanche density is assumed to be constant and as a result the avalanche mass balance corresponds to a volume balance. In the momentum equation mass is defined by the flow depth *h(x,t)* where an increase of mass will correspond to an increase in flow depth.

6.5 Use of the RAMMS program for the Panabaj lahar

A digital elevation model of the Atitlan study area with a 10 m grid was supplied by the USGS (U.S. Geological Survey). This map was turned into an ASCII file and was imported to the DEM folder file of the RAMMS program. A working directory inside the program was chosen on the preference window and a new project was ready to be started.

The RAMMS program has a set of windows with different steps that guide the user to start a new project. The first window displays the project information where the project name, project details and location of the project have to be specified. This information is used to name the input and output files. The second window displays the grid resolution and the GIS

information where the DEM and forest file can be loaded. The DEM of the Atitlan study area was loaded and no forest file was chosen for the simulation. The grid resolution of 25 m was chosen by default by the program and cannot be changed. The third window displays the project boundary coordinates. The coordinates from the ASCII file of the DEM for the Toliman volcano and Panabaj community were chosen. The coordinates of this area X min West = 688600, X max East = 696000, Y min South = 1614000, Y max North = 1620350. The fourth window gives a project summary with all chosen inputs so far. After confirming all the information, the DEM in three dimensions appears in the main window of the user interface.

The program is able to define automatic release areas or they can be defined by the user. The automatic release areas that the program chooses are depending on the lower and upper slope boundaries (°), minimum release length and area, altitude height and minimum continuous area. This option was run for the Toliman volcano and Panabaj study area with lower and upper slope boundaries of 30° and 55°, a minimum release length of 30 m, a minimum release area 10,000 m² and a fracture height of 1 m (Fig.6.1). This tool can be useful for hazard maps (RAMMS manual).

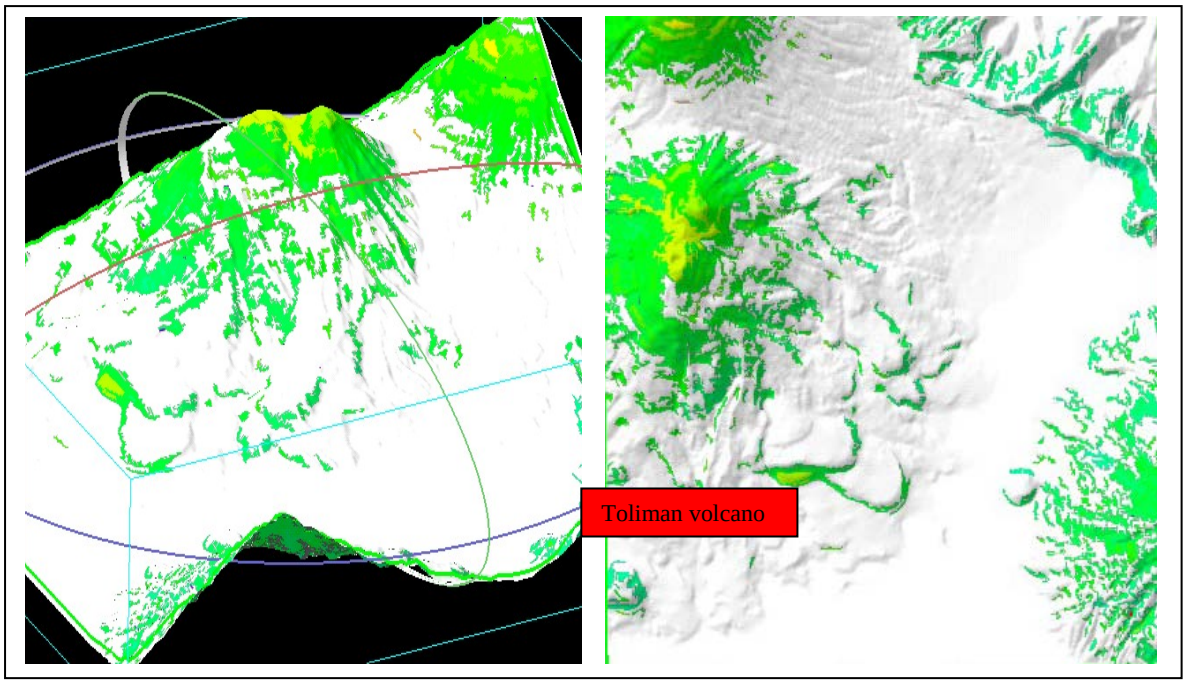

Fig.6.1. Automatic release areas made by RAMMS program for the Toliman volcano. Three dimensional view (right) and two dimensional view (left).

To simulate the Panabaj lahar in the RAMMS program, a release area was defined in the DEM with a polygon. To create this release area, the DEM has to be in the 2D switch, the option in the toolbar for creating a new release area was selected and the polygon defining the area was drawn. Measurements during the field work estimates that the release area has approximately 82,000 m² and a release volume of approximately 156,000 m³ (Fig.6.2).

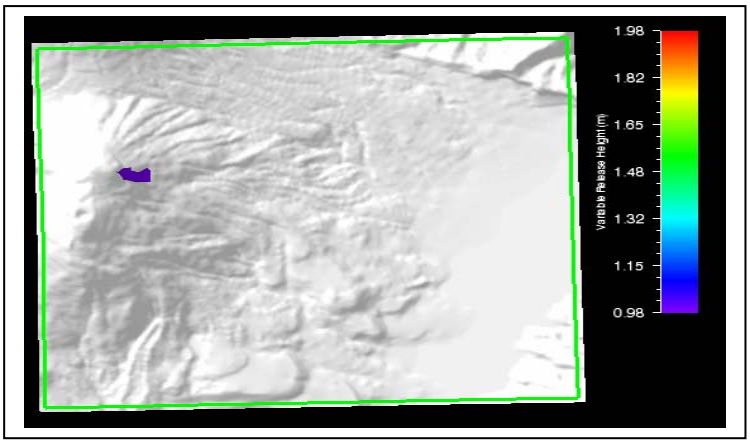

Fig. 6.2 Release area of the slope failure on the Toliman volcano in the RAMMS program.

The input of the parameters of the flow is done by the "edit avalanche input parameters" in the edit menu. A window with four options is displayed: General, Params, Mu/Xi and Release. The "general" option window displays automatically information of the project details and the output filename (the folder containing the simulation data will have this name). In the "Param" option window, the model used by the program is display, the grid resolution, the end time of the simulation, the dump steps of calculations, the density and lambda parameter. For the Panabaj case, the model used was the Voellmy-Salm model, the grid resolution was kept in 25 m, the end time chosen for the simulation was 370, and the dump steps for the calculation used were 5.

It should be noted that the following numerical values for the parameters used in the simulation of the Panabaj lahar have been adjusted such that the computed results match the observed characteristics of the lahar in the field. This is further discussed in Section 6.6 below. The density of the flow used was 1900 kg/m³ (density common in volcanic settings) and a

lambda of 1. In the Mu/Xi (in the Voellmy fluid model Mu = μ and Xi = ξ) option window, an option to choose a constant or variable Mu/Xi during the simulation and the parameters of Mu and Xi of the flow are displayed. For the Panabaj case, the Mu/Xi was kept constant during the flow because the flow followed the channels until reaching the alluvial fan. To make a variable Mu/Xi, a new file in the program has to be created specifying the changes in altitude (three changes of altitude are allowed by the program) and specifying the Mu and Xi values for an open slope, channel slope, gully slope, flat area slope and a forested area slope. The values of Mu/Xi in the Panabaj area were Mu = 0.04 and Xi = 450. In the "Release" option window, an option for selecting a constant or variable release area and to define the release height is displayed. To simulate the Panabaj lahar a constant release area was selected because the type of failure in the flank of the volcano was similar to the infinite slope condition. This type of failure is common in volcanic areas where the slope angles are steep and the soil is oversaturated with water. According to field measurements the mean height of the Panabaj release area was 1.9 m. The program calculates automatically the release volume of the release area.

To model the erosion process during the simulation, the snow cover (erosion) option in the input menu was selected. This displays a window where the user has to define the entrainment layers. Three different layers (top, intermediate and bottom layer) in the bed slope can be defined. The input parameters that are asked for are: height of the layer, density of the layer, a "Tao" which is a shear stress derived from the squared velocity and density of the flow, the height altitude and the change in altitude. For the Panabaj case, because of the angle of the channel slope and the geologic setting of the volcano, only one entrainment layer was selected with a mean height of 0.8 m. The entrainment layer was considered constant, the height altitude and change in altitude were not selected. The density of the channel slope material was set at 1750 kg/m^3. Based on the entrainment numerical model, this density has to be lower than the flow density to entrain. A Tao of 93100 pascals (93.1 kPa) was selected.

All of the inputs were introduced and selected in the user interface of the RAMMS program. There was no need to make an external text file or shape file. After choosing all the input parameters, the simulation was run. When the calculations were finished the output is displayed on the terrain model. Line profiles and points can be drawn and displayed in a plot.

6.6 Results and discussion of the simulation using RAMMS program

A series of criteria based on the information concerning both the dynamics (velocity, run-up heights) and features (deposit thickness) was created to compare the simulation results with the results observed in the field:

1. The run-out distances
2. Mean deposit thickness
3. Areal distribution
4. Diversion of the flow
5. Velocities

Before any simulations were done with the RAMMS program, the values of Xi, Mu, densities, velocity for entrainment, and height of the erodible layer were specified and boundary values for these parameters were established. These values were adjusted until the computed deposited volume, run-out length and velocities of the simulation matched the deposited volume, run-out length and velocities observed in the field. The results of the simulation with the adjusted values mentioned during the methodology that best fitted the event are presented below.

The mean velocities of the lahar estimated in the field were 11 m/s and 13 m/s. During the simulation with the RAMMS program the velocities from the lahar during the course of the flow varied from 19 m/s to 10 m/s with a mean velocity of the flow of 15 m/s. A plot of the velocities can be displayed with a feature built inside RAMMS where a line profile is drawn through the flow (Fig.6.3).

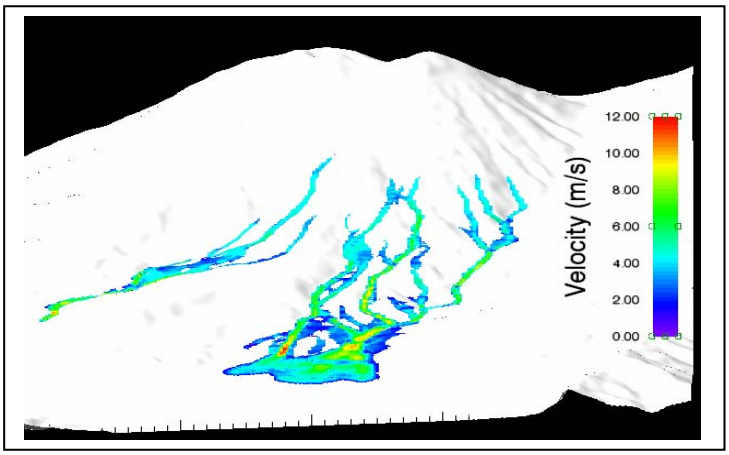

Fig.6.3 Velocity of the flow when it reached the alluvial fan (right).

In the field, the calculated mean value thickness of the deposit was 1.6 m. In the RAMMS program the thickness areas range from 1.0 m up to 5.50 m. With a mean deposit thickness of 1.9 m (Fig. 6.4).

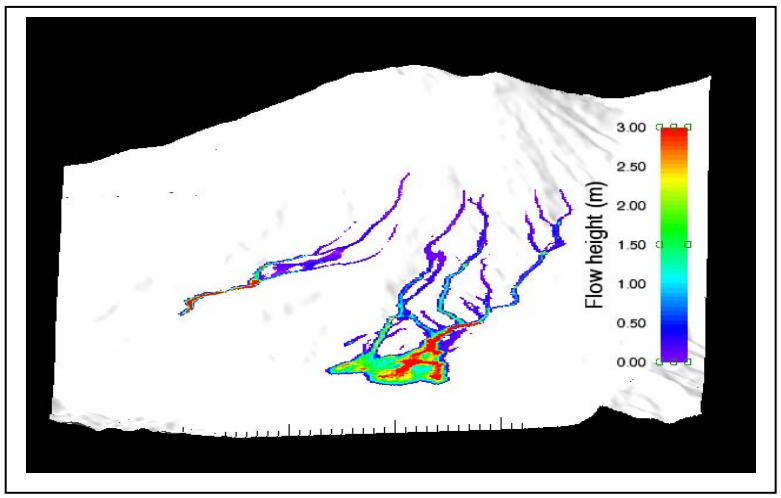

Fig. 6.4 Thickness of the deposit in the alluvial fan.

One of the most important features in the RAMMS program is the ability to model the erosion process during a flow. The erosive process during a lahar on a volcano is very high because of the geologic features of the soil. During the field investigation, a release volume of 156,000 m^3 was calculated and the volume deposited was approximately 400,000 m^3 (not taking into account the volume of hyperconcentrated material that was deposited into the lake). In the simulation with the RAMMS program the same release volume was selected as

the observed one and the deposited volume was 625,000 mts³. This volume did not reach the lake during the simulation (Fig.6.5).

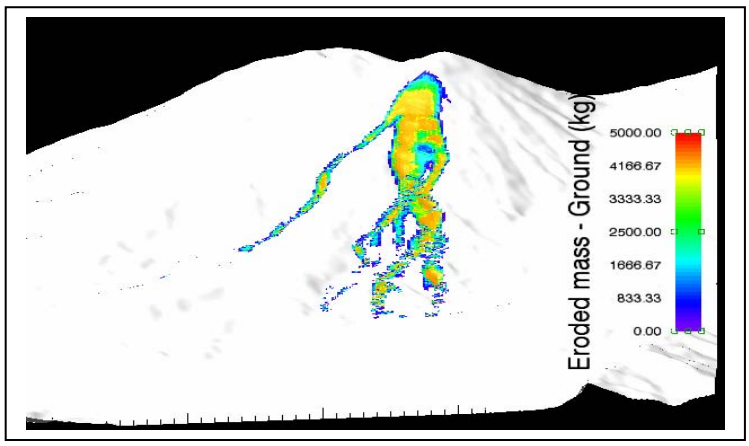

Fig. 6.5 Calculated eroded mass by the flow.

The RAMMS program can also simulate the maximum pressure force caused by the flow. This can be tool can be used to model the process and interaction of the flow with structures and mitigation measures (Fig.6.6).

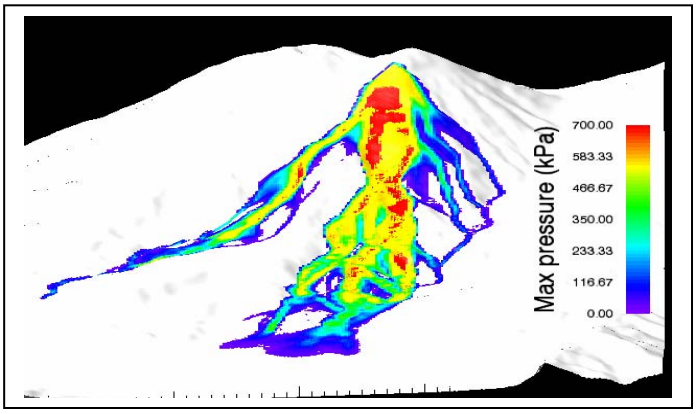

Fig.6.6 Max pressure of the flow.

The Panabaj lahar split in two during the evolution of the flow. Once the channel of the main flow was overtopped, the flow went into another channel. The new channel that the flow followed was steeper, making the flow gain velocity and mass by its erosive power. The population of the Panabaj community was affected by two flows that came from the same release area. This phenomenon was well simulated by the RAMMS program (Fig 6.7).

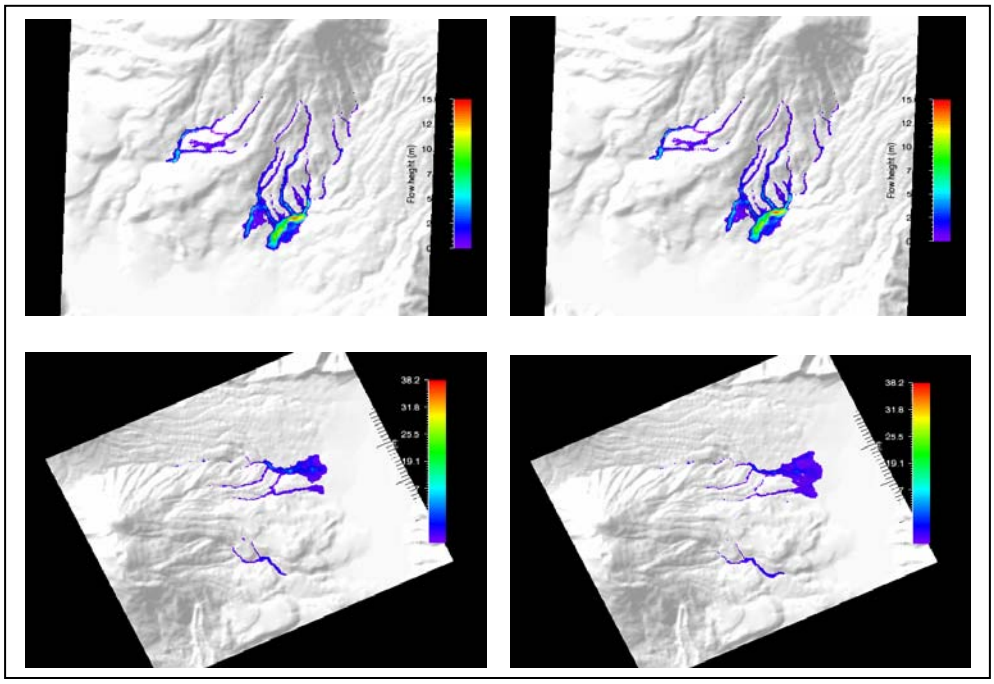

Fig 6.7. Simulation of the splitting phenomena suffered by the flow and its union in the alluvial fan

The shape of the RAMMS simulation was exported to ARCGIS and turned into raster to enhance the heights of the deposition. This raster was imposed on the DEM of the study area to observe the run-out of the simulated flow. The run-out in the deposition area simulated by RAMMS is similar to which happened in reality. However the simulated flow never reached the lake and left all the deposit in the alluvial fan (Fig. 6.8).

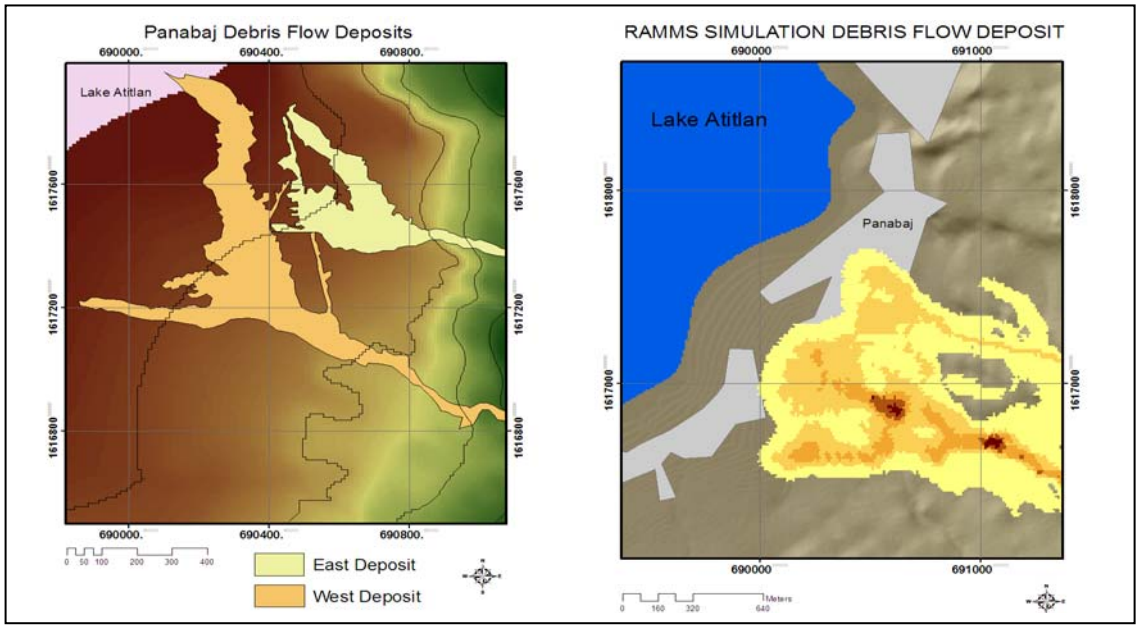

Fig.6.8 A map showing the flow deposits measured in the field (right). A map made with the RAMMS shape of the deposit left by the simulation. (left)

As shown in Fig. 6.3 and 6.4, plots of the velocities and flow depths can be displayed with a feature built inside RAMMS where a line profile can be drawn through the flow. This plot can also be animated according to the time steps of the animation (Fig. 6.9).

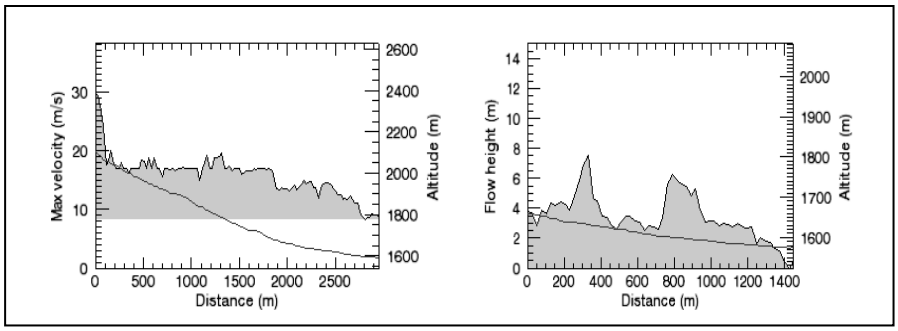

Fig.6.9 Plot of the velocity before reaching the alluvial fan (left). Plot of the Flow height when the flow before reaching the alluvial fan (right)

Having found the parameters that could best replicate the Panabaj lahar with the RAMMS program, the model results were compared against the data observed in the field. The ability of the model to model real behavior was evaluated using an informal measure of suitability determined by the following relationship:

Suitability = (Simulation result – Field measurement)/ (Field measurement) * 100

The lower the suitability number in %, the better the agreement.

Table.6.1 Results of suitability evaluation

Criteria	Simulation results	Field Measurements	Suitability
Mean velocity of the flow	15 m/s	12 m/s	25 %
Mean thickness of the deposit	1.9 m	1.6 m	19 %
Volume of the Flow deposit	624,583 m^3	400,000 m^3 aprox.	56 %

Table 6.1. Comparison of the RAMMS model with the field measurements.

6.7 Parametric study

To measure the sensitivity of the program to variations in the input parameters, several simulations were made. The μ (Mu) and the ξ (Xi) parameters were changed. The run-out length result of each simulation was compared with the simulation described in Section 6.6 that had a run out length of the flow of 4,900 m (Fig. 6.10).

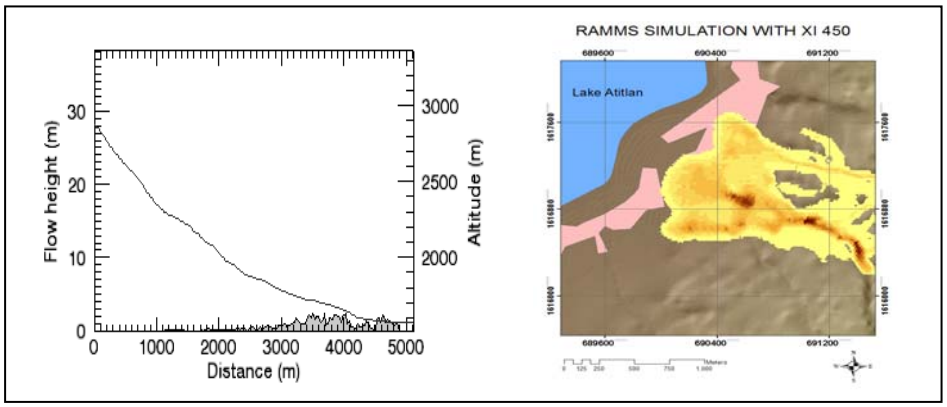

Fig.6.10. A plot of the run-out length of the simulation described in section 6.6 using a value of μ (Mu) of 0.04 and ξ (Xi) of 450 (left). Map of the deposition area (right).

6.7.1. Sensitivity to the ξ (Xi) parameter

Two different simulations were run using all the same parameters as in Section 6.6 except for the ξ (Xi) value. In the first simulation the value was changed from 450 to 200 and in the second simulation the value was changed from 450 to 900. The first simulation with the ξ (Xi) parameter of 200 had a run-out of 4,350 m, a decrease of 550 m compared to the results in Section 6.6. Only one part of the flow reaches an outer limit of the community while the rest is deposited inside the channel and a small area of the alluvial fan (Fig 6.11).

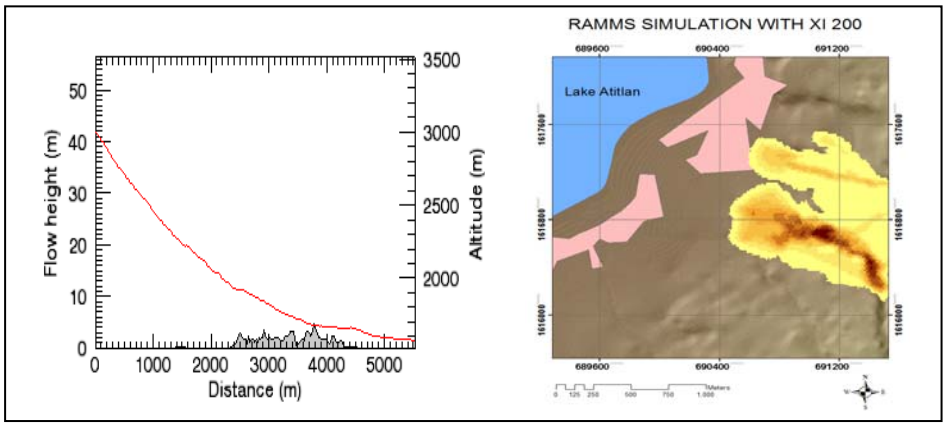

Fig.6.11. A plot of the run-out length of the simulation using a value ξ (Xi) of 200 (left). Map of the deposition area (right).

The second simulation with the ξ (Xi) parameter of 900 had a run-out of 4,750 m, a decrease of 150 m, but the flow spreads 200 m wider while depositing in the alluvial fan (Fig. 6.12).

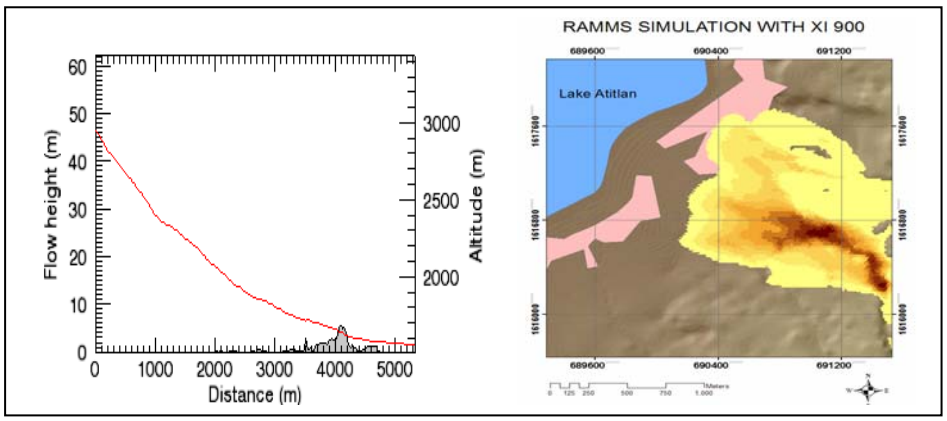

Fig.6.12. A plot of the run-out length of the simulation using a value ξ (Xi) of 900 (left). Map of the deposition area (right).

In all the simulations, the flow followed the same course and displayed the same splitting phenomena described in Section 6.6 and figure 6.7. As the ξ (Xi) parameter was increased, the ability of the material to spread out in the release and deposition area also increased.

6.7.2. Sensitivity to the μ (Mu) parameter

Another two different simulations were made using the same parameters as in Section 6.6, only this time the μ (Mu) value was changed from 0.04 to 0.1 and to 0.5. The run-out length from the simulation with the μ (Mu) value of 0.1 was 4,200 m, a decrease of 700 m. The flow stays inside the channel and never reached the alluvial fan (Fig. 6.13).

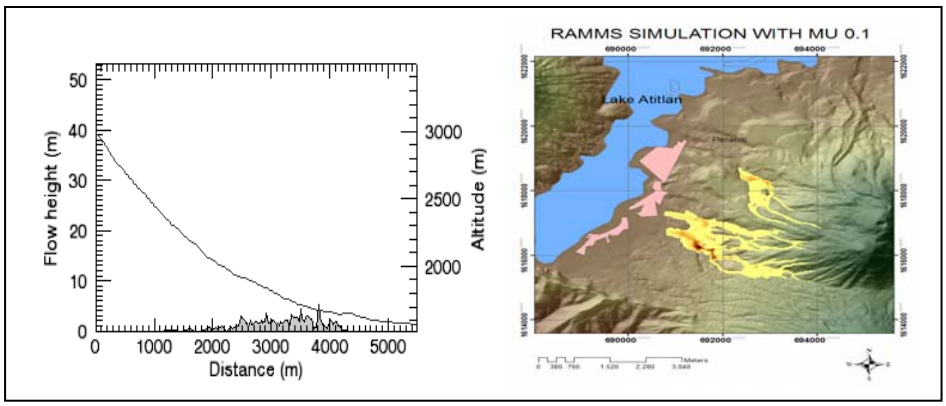

Fig.6.13. A plot of the run-out length of the simulation using a value μ (Mu) of 0.1 (left). Map of the deposition of the flow (right).

The run out length of the flow with a μ (Mu) value of 0.5 is 2,300 m, a decrease of 2600 m. The flow has very low mobility mainly staying at the flanks of the volcano (Fig. 6.14).

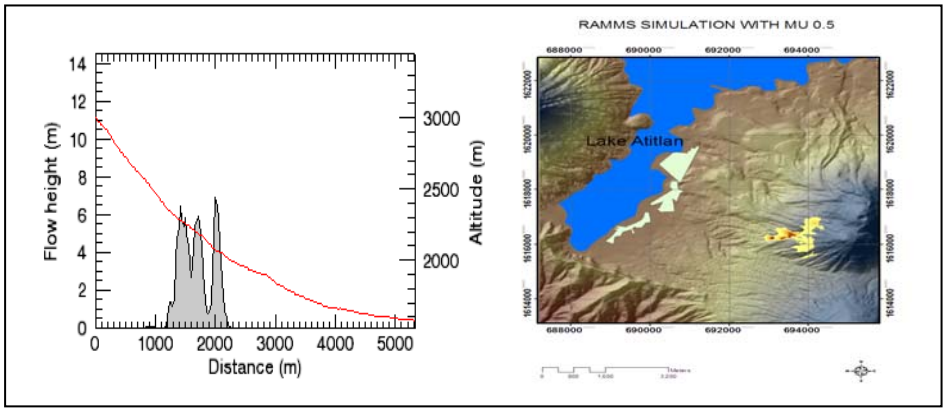

Fig.6.14. A plot of the run-out length of the simulation using a value μ (Mu) of 0.5 (left). Map of the deposition of the flow (right).

The parameter that affected the run-out distance the most was μ (Mu) since it is related to the friction of the flow as described in Section 6.3.

6.7.3 Sensitivity to entrainment

A simulation with the same calibrated parameters but with the erosion module turned off was also run. Since there was no entrainment, the volume from the release area was constant, 156,000 m³. The run-out of the flow was shorter, 4000 m, this is a decrease of 900 m, not reaching the alluvial fan and the Panabaj community (Fig. 5.10b).

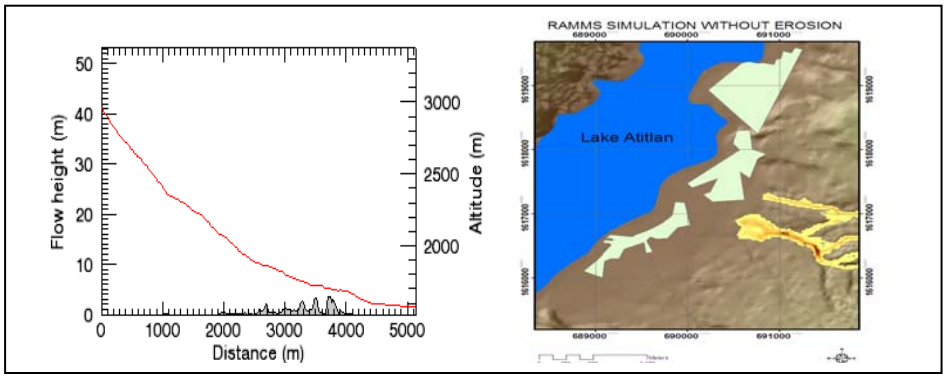

Fig.6.11. A plot of the run-out length of the simulation with the entrainment module turned off (left). Map of the deposition of the flow (right).

6.8 Summary

After adjusting the input parameters, the results of the RAMMS program are fairly similar to the event that happened in October 2005 in Panabaj in terms of velocity, run-out length, thicknesses of deposits and flow behavior. The RAMMS program simulation correctly showed the split of the flow. Although the program is originally designed for snow avalanches, it worked well the lahar in a volcanic setting.

An important feature of this program is the well designed and user-friendly user interface. There is no need to create files in another program or to make tedious calculations. All the inputs can be loaded without closing the user interface window. Once the user is familiar with the program, simulations can be created quickly, and the time for every simulation, depending on the end time selected, can be rather fast (20-30 minutes).

The outputs of the calculation in the program are displayed visually and cannot be manipulated. The simulation can be stopped, returned and continued with a time step slider in the user interface. GIF images can be created of every time step or the whole simulation can be created as a GIF. The results of the simulation can be seen in a two-dimensional or three-dimensional view. The program has good compatibility with ESRI FILES.

Another important feature of the program is the possibility to simulate the erosion process during the flow. The inclusion of entrainment in the simulation makes a more realistic prediction of run-out distances and a more accurate determination of the flow and deposition depths.

Over all, the RAMMS program with the right parameters can be a very useful tool for hazard mapping. However, the RAMMS program has some limitations:

- It does not take into account pore water pressure or collision of particles
- Cannot simulate the changes in rheology of the flow.
- It is sensitive with the quality of the DEM
- It has problems allocating memory when choose long time steps.
- The erosion is only simulated in the bed slope and not on the walls of the channel.

7. The San Juan La Laguna lahar

The San Juan La Laguna community is located in the south basin of the Lake Atitlan (Figure 7.1). Its coordinates are 14.669° North latitude and -91.286° West longitude and is 1590 meters above sea level. San Juan La Laguna is located inside a micro basin of the Atitlan Lake, belonging to the "Panatz´am" river with an area of 12 km² that drains to the lake in the north part of the town. San Juan La Laguna has a population of 10,000 habitants (Flores, 2005).

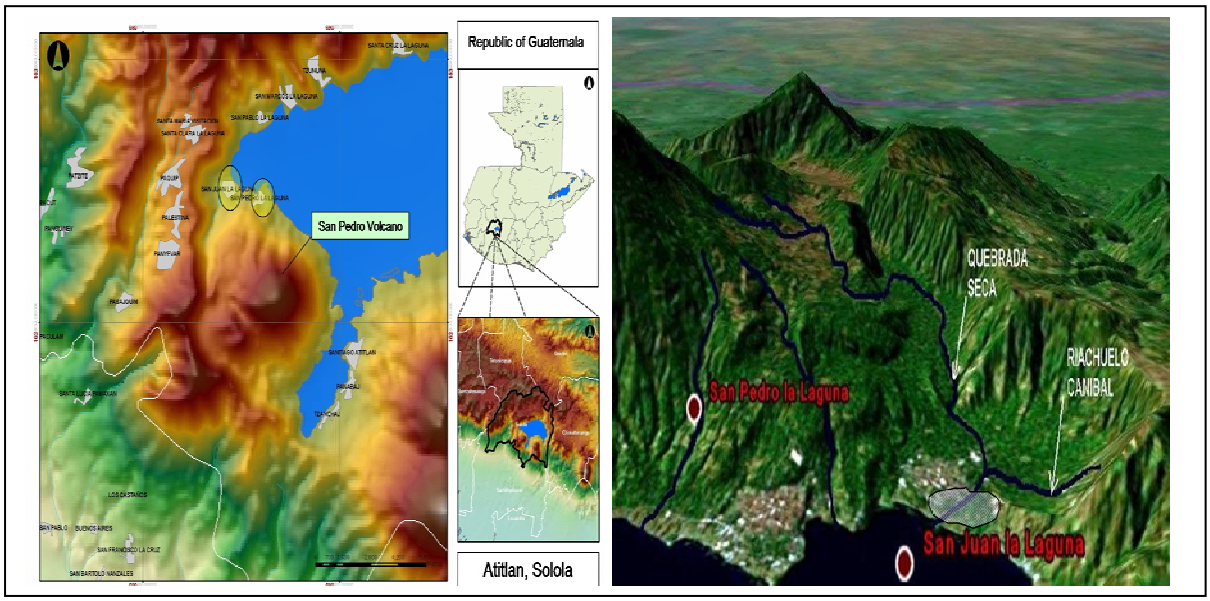

Fig 7.1. Map of San Juan La Laguna community (right) and location of the dry river "Panatz´am" (left).

In the surrounding areas of the San Juan La Laguna community, the intense precipitation caused by Hurricane Stan, created a series of landslides in areas with steep slopes and the rivers were overflowed causing great damage. The homes of 150 families, public buildings (school and churches) and all the crops in the area were completely destroyed. During this event, no casualties were registered. Even though it happened in the early hours of the morning, many inhabitants of the place evacuated their homes and went into a safe place.

The saturated soil started to erode and the dry river called “Panatz´am” or “Quebrada Seca” flooded all the human development and coffee plantations in the area near its banks. A settlement called “Barrio 5 de enero” located near the river bank, was destroyed almost completely by the debris and the rocks that were carried by the flood (Fig.7.2). The width of the stream bed in this area was 15 m and reached a height of almost 3 m. The drop of the “Panatz´am” river from its highest level is about 500 m in a length of 3 km. The width of the channel is influenced by the topographic features of the area and can vary from sections with 3 m to sections with 150 m. Before opening into the alluvial fan, there is one part of the channel that is very close to the San Juan La Laguna community (139 m). The deposits left by the debris flow all through the channel were varied. In the highest part of the channel, rocks with 3 m of diameter were found, while in the alluvial fan, fine sands and clay material were predominant.

Fig.7.2. Picture of the deposition area (top right). Pictures of the streamflow and the damage it caused in the San Juan La Laguna community.

The San Pedro volcano is located in the southeast side of the basin. The volcano still has a considerable vegetation cover but in the surroundings of the crater border, deforestation has occurred and this is the cause of many of the landslides.

Morphologically, the San Juan La Laguna town is located in a small plain that is a result of the deposition from the volcano that is less than 1km away. A depression made by a fault with orientation from north to south separates the volcano from the town. This creates a natural barrier against mudflows and debris flows that can originate from the northwest part of the volcano. Due to the high slopes on the border of the crater and the different mass movements that happened in the area, the threat of landslides in the zone is high, mostly in the highest part of the basin. Slopes of 60º to almost vertical ones with 80º on the crater border, covered with a thin coat of clay and organic soil that reaches a depth of approximately 1 m, makes this a very vulnerable zone.

During the field observations the longitudinal profile of the channel bed slope was determined (Fig.7.3). Following the same procedure of superelevation as in the Panabaj lahar in Chapter 5, the mean velocity of the lahar flow was calculated. Based on the field observations, the mean flow velocity calculated for the San Juan La Laguna debris flow was 5 to 7 m/s.

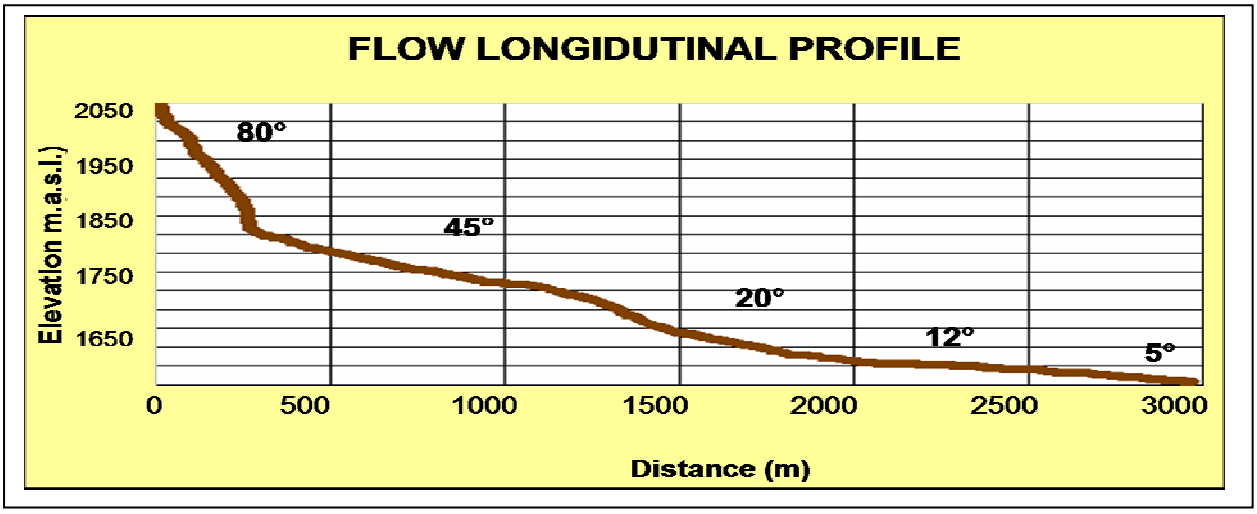

Fig.7.3. Longitudinal profile of the channel followed by the lahar in San Juan La Laguna.

More than 70 landslides in the area and the renewal of 12 springs of water in the zone contributed to the San Juan La Laguna lahar development and transition to a streamflow phase. The calculated areas that contributed to the flow were estimated to 731,500 m² (Fig.7.4 and 7.5). The deposition area is estimated to be 188,900 m² and the average measured deposition depth is 1.30 m. The total volume of deposited material in the alluvial fan is 246,700 m³. This value does not take into account the volume of debris flow that went inside the lake.

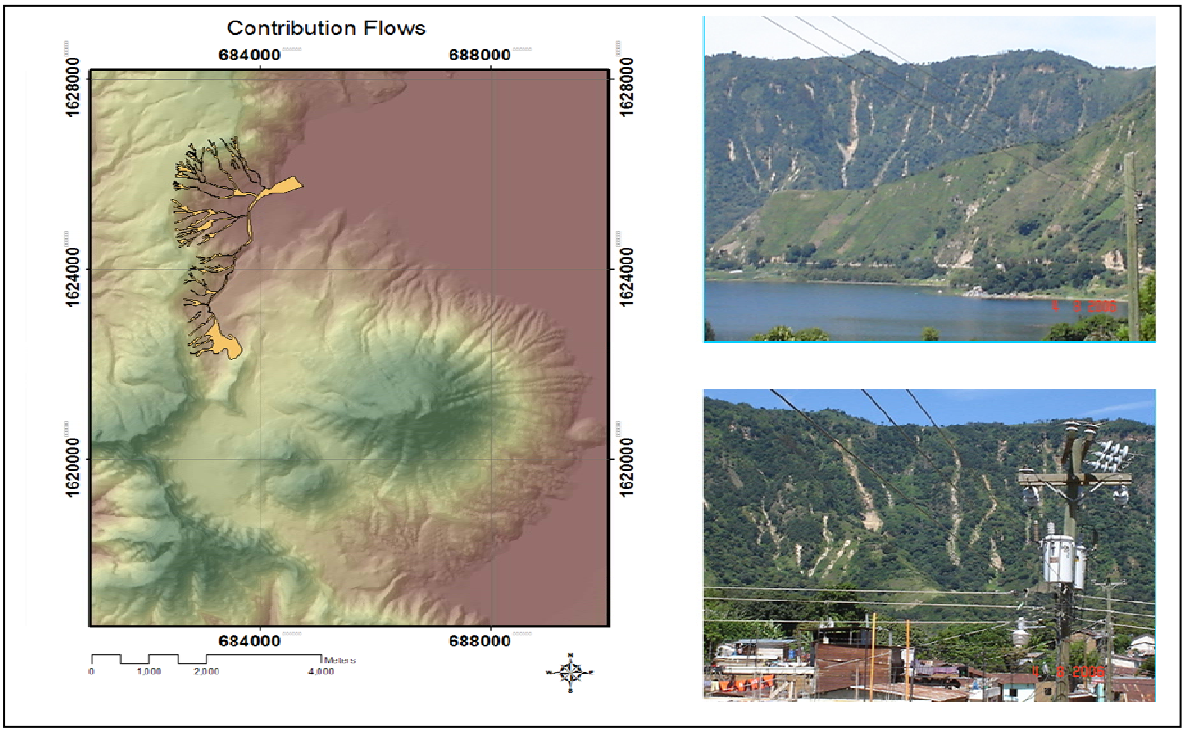

Fig.7.4 Map of the flows and landslides that contributed to the main flow (right). Pictures of contributive landslides (top and bottom left)

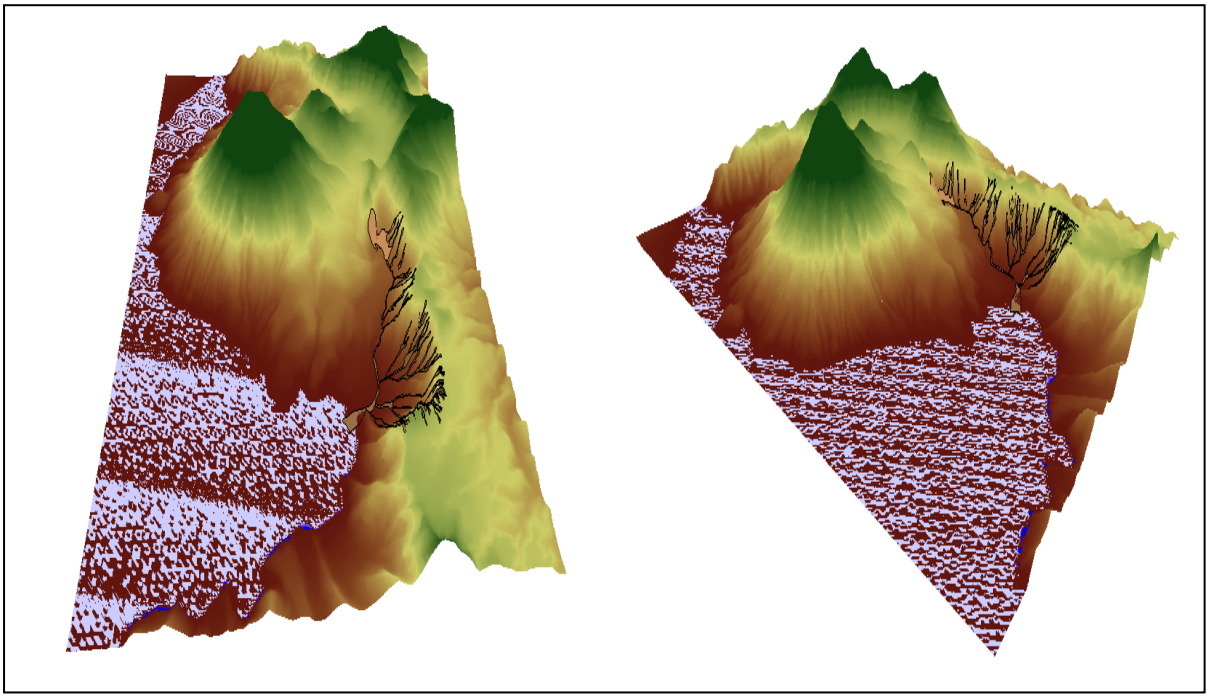

Fig.7.5 View of the position of the contributive landslides in the basin of the San Juan La Laguna.

8. Simulation of the San Juan La Laguna lahar with the program FLO 2D

8.1 Description of the FLO 2D program

FLO 2D is a dynamic flood routing model that simulates channel flow, unconfined overland flow and street flow. The program uses a volume conservation model that distributes a flood hydrograph over a system of square grid elements. It simulates a flood over complex topography and roughness while maintaining volume conservation. The model uses the full dynamic wave momentum equation and a central finite difference routing scheme (an explicit numerical technique) with eight potential flow directions to predict the progression of a flood hydrograph over a system of square grid elements. Floodwave progression over the flow domain is controlled by topography and resistance to flow. The FLO 2D model was originally created in 1988 to conduct a Federal Emergency Management Agency (FEMA) flood insurance study of an urbanized alluvial fan in Colorado (FLO 2D Users Manual, 2005). The FLO 2D model evolved from the diffusive hydrodynamic model (DHM), which is a simple numerical approach with a finite difference scheme that permits modification of the grid element attributes.

The two dimensional finite difference model FLO 2D was conceived for routing non-Newtonian flood flows on alluvial fans. The objective of this model was to estimate the probable range of flow properties (velocity and depth), predict a reasonable area of inundation, and simulate flow cessation. FLO 2D allows delineating flood hazards and designing flood mitigation. The model has a number of components which will add detail to a flood simulation including channel-floodplain discharge exchange, loss of storage due to buildings or topography, flow obstruction, rill and gully flow, street flow, bridge and culvert flow, levee and levee failure, mud and debris flow, sediment transport, rainfall and infiltration (Fig.8.1). Details can be added to the simulation by turning on or off switches for various components. Channel flow is one dimensional, with the channel geometry represented either by natural, rectangular or trapezoidal cross sections, while the overland flow is modeled

two-dimensionally and channel overbank flow is computed when the channel capacity is exceeded. When the flow overtops the channel, it will disperse to other overland grid elements based on topography, roughness and obstructions (FLO 2D Users Manual, 2005). FLO 2D can be applied to simulate a diverse realm of complex flood problems including (O'Brien, 2005):

- River over bank flooding
- Unconfined alluvial fan and floodplain flows
- Urban flooding with street flow, flow obstruction and storage loss
- Run-out of tsunami and hurricane storm surges
- Mud and debris flows
- Watershed rainfall and runoff
- Flood mitigation design

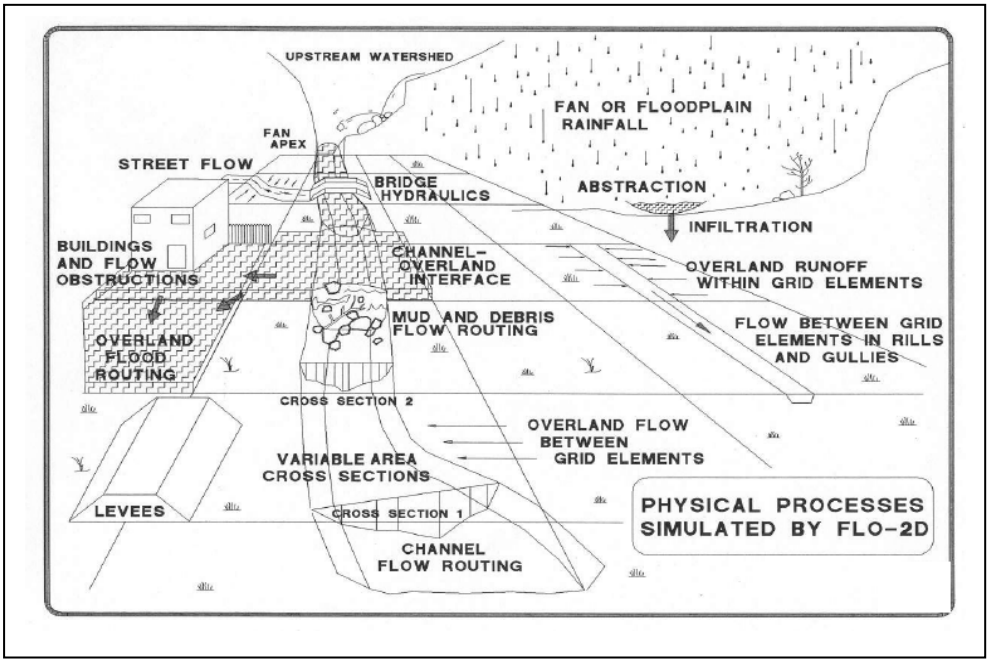

Fig. 8.1 Physical processes simulated by FLO 2D (O'Brien ,2005).

8.2 Numerical model

FLO 2D moves the flood volume around on a series of tiles for overland flow or through stream segments for channel routing. Floodwave progression over the flow domain is controlled by topography and resistance to flow. Flood routing in two dimensions is accomplished through a numerical integration of the equations of motion and the conservation of fluid volume for either a water flood or a hyperconcentrated sediment flow.

The general constitutive fluid equations include the continuity equation, and the two-dimensional equations of motion (dynamic wave momentum equation):

$$\frac{\partial h}{\partial t} + \frac{\partial hV_x}{\partial x} + \frac{\partial hV_y}{\partial y} = i \qquad (8.1)$$

$$S_{fx} = S_{ox} - \frac{\partial h}{\partial x} - \frac{V_x}{g}\frac{\partial V_x}{\partial x} - \frac{V_y}{g}\frac{\partial V_x}{\partial y} - \frac{1}{g}\frac{\partial V_x}{\partial t} \qquad (8.2)$$

$$S_{fy} = S_{oy} - \frac{\partial h}{\partial y} - \frac{V_y}{g}\frac{\partial V_y}{\partial y} - \frac{V_x}{g}\frac{\partial V_y}{\partial x} - \frac{1}{g}\frac{\partial V_y}{\partial t} \qquad (8.3)$$

where h is the flow depth, and V_x and V_y are the depth-averaged velocity components along the x and y coordinates. The excess rainfall intensity (i) may be nonzero on the flow surface (alluvial fan or floodplain). The friction slope components S_{fx} and S_{fy} are based on Manning's equation and are written as function of bed slope S_{ox} and S_{ox}, pressure gradient, and convective and local acceleration terms. A diffusive wave approximation to the equations of motion is defined by neglecting the last three acceleration terms of (2) and (3). Further, by neglecting the pressure term, a kinematic wave representation is derived. On most steep slope applications, the application of the kinematic wave (S_o=S_f) is sufficient to model floodwave progression. The addition of the pressure gradient term to create the diffusive wave equation

will enhance overland flow simulation with complex topography. The diffusive wave equation with the pressure gradient is required if the grid system has topographic depressions. The local and convective acceleration terms are important to the solution for channel flow especially for flat or adverse slopes or very steep slopes. Only the full dynamic wave equation is applied in FLO 2D model version 2006.

The equations of motion in FLO 2D are better defined as a quasi two-dimensional. The momentum equation is solved by computing the average flow velocity across a grid element boundary one direction at time. There are eight potential flow directions, the four compass directions (north, east, south and west) and the four diagonal directions (northeast, southeast, southwest and northwest). Each velocity computation is essentially one-dimensional in nature and is solved independently of the other seven directions. The stability of this explicit numerical scheme is based on specific criteria to control the size of the variable computational time step.

The rheological behavior of hyperconcentrated sediment flows involves the interaction of several complex physical processes. The non Newtonian behavior of the fluid matrix is controlled in part by the cohesion between fine sediments particles. This cohesion contributes to the yield stress, which must be exceeded by an applied stress in order to initiate fluid motion. By combining the yield stress and viscous stress components, the FLO 2D program models the shear stress in hyperconcentrated sediment flows, including those described as debris flows, mudflows and mud floods, as a summation of five shear stress components: the cohesive yield stress, the Mohr-Coulomb shear, the viscous shear stress, the turbulent shear stress and the dispersive shear stress. All these components can be written in terms of shear rates giving a quadratic rheological model function of sediment concentration that adds a turbulent and dispersive term to the Bingham equation (FLO 2D Users Manual, 2005).

The rheological behavior of hyperconcentrated sediment flows involves the interaction of several complex physical processes. The non-Newtonian behavior of the fluid matrix is controlled in part by the cohesion between fine sediments particles. This cohesion contributes to the yield stress τ_y, which must be exceeded by an applied stress in order to initiate fluid motion. By combining the yield stress and viscous stress components:

$$\tau = \tau_c + \tau_{mc} + \tau_v + \tau_t + \tau_d \qquad (8.4)$$

in which the total shear stress depends on the cohesive yield stress τ_c, the Mohr-Coulomb shear τ_{mc}, the viscous shear stress τ_v ($\eta \frac{\partial v}{\partial y}$), the turbulent shear stress τ_t, and the dispersive shear stress τ_d. When written in terms of shear rates ($\frac{\partial v}{\partial y}$), the following quadratic rheological model can be developed (O'Brien and Julien 1985):

$$\tau = \tau_y + \eta\left(\frac{\partial v}{\partial y}\right) + C\left(\frac{\partial v}{\partial y}\right)^2 \qquad (8.5)$$

where

$$\tau_y = \tau_c + \tau_{mc} \qquad (8.6)$$

and

$$C = \rho_m l^2 + f(\rho_m, C_v) d_s^2 \qquad (8.7)$$

in which η is the dynamic viscosity, τ_c is the cohesive yield strength; the Mohr-Coulomb stress $\tau_{mc} = p_s \tan\varphi$ depends on the intergranular pressure p_s and the angle of repose φ of the material; C denotes the inertial shear stress coefficient, which depends on the mass density of the mixture ρ_m, the Prandtl mixing length l, the sediment size d_s^2 and a function of the volumetric sediment concentration C_v. Bagnold (1954) defined the function relationship $f(\rho_m, C_v)$ as:

$$f(\rho_m, C_v) = a_i \rho_m \left[\left(\frac{C_*}{C_v}\right)^{1/3} - 1\right] \qquad (8.8)$$

where a_i (~ 0.01) is an empirical coefficient and C_* is the maximum static volume concentration for the sediment particles. It should be noted that Takahashi (1979) found that the coefficient a_i may vary over several orders of magnitude. Egashira et al. (1989) revised this relationship and suggested the following:

$$f(\rho_s, C_v) = \frac{\pi}{12}\left(\frac{6}{\pi}\right)^{1/3} \sin^2 \alpha_I \quad \rho_s(1 - e_n^2)\, C_v^{1/3} \qquad (8.9)$$

where the energy restitution coefficient e_n after impact ranges $0.70 < e_n < 0.85$ for sands, α_I is the average particle impact angle and ρ_s is the mass density of sediment particles (O'Brien, 2005).

The first two shear stress terms in the quadratic rheological model are referred to as the Bingham shear stresses, and represent the internal resistance stresses of a Bingham fluid (Fig.8.2). The sum of the yield stress and viscous stress defines the total shear stress of a cohesive, hyperconcentrated sediment fluid in a viscous flow regime. The last term is the sum of the dispersive and turbulent shear stresses and defines an inertial flow regime for a mud flood. This term is a function of the square of the velocity gradient.

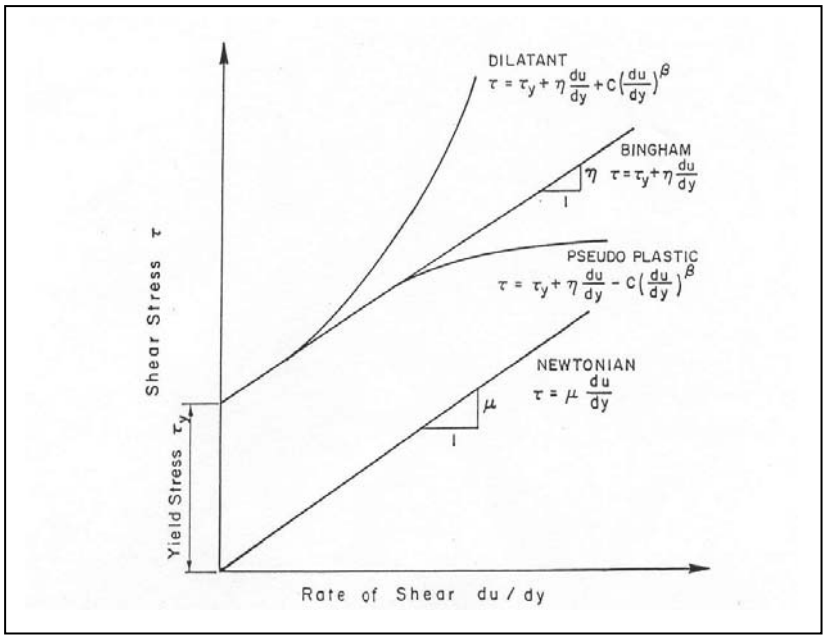

Figure8.2. Shear stress as a function of shear rate for fluid deformation models.

A mudflow model that incorporates only the Bingham stresses and ignores the inertial stresses assumes that the simulated mudflow is viscous. This assumption is not universally appropriate because all mud floods and some mudflows are turbulent with velocities as high as 8 m/s. Even mudflows with concentrations up to 40% by volume can be turbulent (O'Brien, 1993). Depending on the fluid matrix properties, the viscosity and yield stresses for high sediment concentrations can still be relatively small compared to the turbulent stresses. If the flow is controlled primarily by the viscous stress, it will result in lower velocities. Conversely, if the viscosity and yield stresses are small, the turbulent stress will dominate and the velocities will be higher.

To delineate the role turbulent and dispersive forces in water and non-cohesive sediment mixtures, Hashimoto (1997) developed simplified criteria involving only flow depth d and sediment size D_i. When $d/D_i < 30$, the intergranular forces are dominant. If $d/D_i > 100$, inertial forces dominate. In the range $30 < d/D_i < 100$ both forces play an important role in momentum exchange. It should be noted, however, that sediment concentration is a critical factor that is not accounted for in this criteria. To define all the shear stress terms for use in the Flo-2d model, the following approach was taken. By analogy with the work of Meyer-Peter and Müller (1948) and Einstein (1950), the shear stress relationship (4) is depth integrated and rewritten in the following form as a dimensionless slope:

$$S_f = S_y + S_v + S_{td} \qquad (8.10)$$

where the total friction slope S_f is the sum of the yield slope S_y, the viscous slope S_v, and the turbulent-dispersive slope S_{td}. The viscous and turbulent-dispersive slope terms are written in terms of depth-averaged velocity V. The viscous slope can be written as:

$$S_v = \frac{K\ \eta}{8\ \gamma_m}\ \frac{V}{h^2} \qquad (8.11)$$

where γ_m is the specific weight of the sediment mixture. The resistance parameter *K* for laminar flow equals 24 for smooth wide rectangular channels but increases significantly (~ 50,000) with roughness and irregular cross section geometry.

The flow resistance of the turbulent and dispersive shear stress components is combined into an equivalent Manning's *n* value for the flow:

$$S_{td} = \frac{n_{td}^2 V^2}{h^{4/3}} \tag{8.12}$$

At very high concentrations, the dispersive stress arising from sediment particle contact increases the flow resistance and by transferring more momentum flux to the boundary. To estimate this increase in flow resistance, the conventional turbulent flow resistance n-value is increased by an exponential function of the sediment concentration Cv.

$$n_{td} = n_t b e^{mCv} \tag{8.13}$$

where: nt is the turbulent n-value, b is a coefficient (0.0538) and m is an exponent (6.0896). This equation was based on unpublished paper by Julien and O'Brien (1998) that relates the dispersive and turbulent resistance in hyperconcentrated sediment flows as function of the ratio of the flow depth to the sediment grain size (O'Brien, 2005)

Accordingly, the friction slope components can be written as

$$S_f = \frac{\tau_y}{\gamma_m h} + \frac{K\eta V}{8\gamma_m h^2} + \frac{n^2 V^2}{h^{\frac{4}{3}}} \tag{8.14}$$

A quadratic equation solution to the above friction slope equation has been formulated in the FLO 2D model to estimate the velocity for use in the momentum equation. The estimated velocity represents the flow velocity computed across each grid or channel element

boundary using the average flow depth between the elements. Reasonable values of K and Manning's n-value can be assumed. The specific weight of the fluid matrix γ_m, yield stress τ_y and viscosity η vary principally with sediment concentration. Unless a rheological analysis of the mudflow site depositional material is available, the following empirical relationships can be used to compute viscosity and yield stress:

$$\eta = \alpha_1 \ e^{\beta_1 C_v} \tag{8.15}$$

and

$$\tau_y = \alpha_2 \ e^{\beta_2 C_v} \tag{8.16}$$

where α_i and β_i are empirical coefficients defined by laboratory experiments (O'Brien and Julien, 1993). The viscosity and yield stress are shown to be functions of the volumetric sediment concentration C_v of silts, clays and in some cases, fine sands and do not include larger clastic material rafted along with the flow. The viscosity of the fluid matrix is also a function of the percent and type of silts and clays and fluid temperature. Very viscous mudflows have high sediment concentrations and correspondingly high yield stresses and may result in laminar flow although laminar flows in nature are extremely rare. Less viscous flows (mud floods) are always turbulent. (O'Brien, 1993)

8.3 FLO 2D computational process

The surface topography is discretized into uniform square-grid elements. Each element is assigned a location on the grid system, an elevation, a roughness factor, and area and flow width reduction factors used to simulate flow blockage. Flow is routed through the grid system using estimates of the flow depth to estimate discharge. For a given element and time step, the discharge across each of the four boundaries is computed and summed. The resultant volume change is uniformly distributed over the available flow area in the element. Time steps vary according to the Courant-Friedrich-Lewy stability condition (Liggett and Cunge 1975), resulting in relatively short time steps (e.g. 1-30 s).

Mass conservation is maintained for both the water and mudflow sediment volumes as the flow hydrograph is routed over the grid system. When routing mudflows, the sediment

continuity is preserved by tallying the sediment volume for each grid element; thus tracking the sediment volume through the grid system. At each time step, the model computes the change in water and sediment volumes, and the corresponding change in sediment concentration. Flow cessation is simulated with the potential for remobilization. For mudflows, high sediment concentrations result in a very viscous flow, which may halt on mild slopes. When successive discharges of less sediment concentration enter a grid element with a halted flow, the diluted mixture may remobilize.

The differential form of the continuity and momentum equations in the FLO 2D model is solved with a central, finite difference numerical scheme. This explicit algorithm solves the momentum equation for the flow velocity across the grid element boundary one element at a time. The solution of the differential form of the momentum equation results from a discrete representation of the equation when applied at a single point. The solution domain in the FLO 2D model is discretized into uniform, square grid elements. The computational procedure for overland flow involves calculating the discharge across each of the boundaries in the eight potential flow directions and begins with a linear estimate of the flow depth at the grid element boundary. The estimated boundary flow depth is an average of the flow depths in the two grid elements that will be sharing discharge in one of the eight directions. Other hydraulic parameters are also averaged between the two grid elements to compute the flow velocity including flow resistance (Manning's n-value), flow area, slope, water surface elevation and wetted perimeter.

The flow velocity (dependent variable) across the boundary is computed from the solution of the momentum equation. Using the average flow area between two elements, the discharge for each time step is determined by multiplying the velocity times flow area. The net change in the volume of water in each floodplain grid element for each time step is the sum of the eight individual discharges across the boundary. The full dynamic wave equation is a second order, non-linear, partial differential equation. To solve the equation for the flow velocity at a grid element boundary, the flow velocity is calculated with the dynamic wave equation using the average water surface slope (bed slope plus pressure head gradient).

Manning's equation is applied to compute the friction slope. In the full dynamic wave momentum equation, the local acceleration term is the difference in the velocity for the given flow direction over the previous time step. The convective acceleration term is evaluated as the difference in the flow velocity across the grid element from the previous time step. For example, the local acceleration term $(1/g * \partial V/\partial t)$ for a grid element converts to:

$$\Delta(V_t - V_{t-1})/(g * \Delta t) \qquad (8.17)$$

where Vt is the velocity in the east direction for grid element at time t, Vt-1 is the velocity at the previous timestep (t-1), Δt is the timestep in seconds, and g is the acceleration due to gravity. A similar construct for the convective acceleration term $(Vx/g * \partial V/\partial x)$ can be made.

The discharge across the grid element boundary is computed by multiplying the velocity times the cross sectional flow area. After the discharge is computed for all eight directions, the net change in discharge (sum of the discharge in the eight flow directions) in or out of the grid element is multiplied by the time step to determine the net change in the grid element water volume (Figure 8.3). This net change in volume is then divided by the available surface area (storage area) on the grid element to obtain the increase or decrease in flow depth for the time step. The channel routing integration is performed essentially the same way except that the flow depth is a function of the channel cross section geometry and there are usually only one upstream and one downstream channel grid element for sharing discharge.

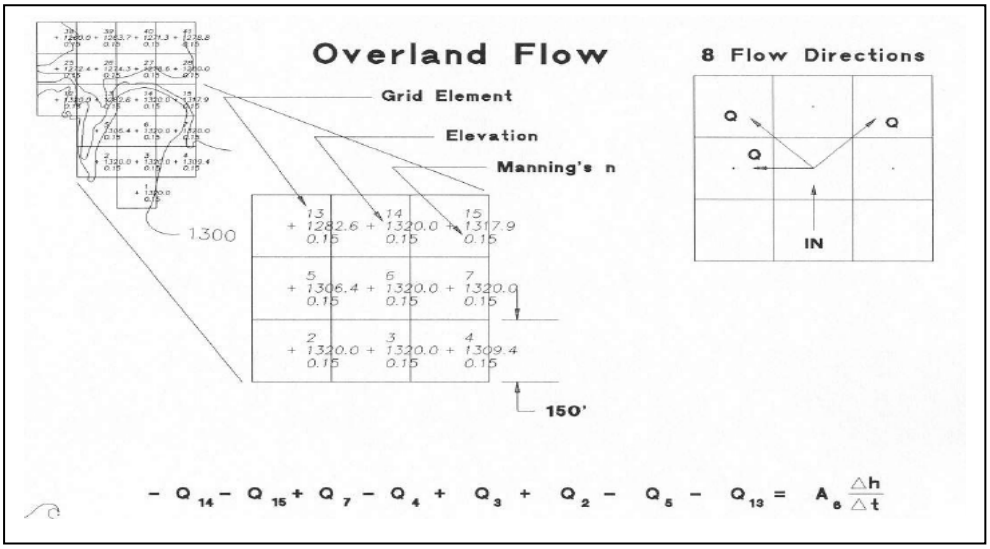

Fig. 8.3 Discharge flux of each grid (O'Brien, 2005),

The solution algorithm incorporates the following steps:

1. The average flow geometry, roughness and slope between two grid elements are computed.
2. The flow depth d for computing the velocity across a grid boundary for the next time step (i+1) is estimated from the previous time step using a linear estimate (the average depth between two elements).
3. The first estimate of the velocity is computed using the diffusive wave equation. The only unknown variable in the diffusive wave equation is the velocity.
4. The predicted diffusive wave velocity for the current time step is used as a seed in the Newton-Raphson solution to solve the full dynamic wave equation for the solution velocity. It should be noted that for hyperconcentrated sediment flows such as mud and debris flows, the velocity calculations include the additional viscous and yield stress terms.
5. The discharge Q across the boundary is computed by multiplying the velocity by the cross sectional flow area. For overland flow, the flow width is adjusted by the width reduction factors (WRFs).
6. The incremental discharge for the timestep across the eight boundaries (or upstream and downstream channel elements) is summed, and the change in volume (net discharge x timestep) is distributed over the available storage area within the grid or channel element to determine an incremental increase in the flow depth.

7. The numerical stability criteria are then checked for the new grid element flow depth. If any of the stability criteria are exceeded, the simulation time is reset to the previous time, the timestep increment is reduced, all the previous timestep computations are discarded and the velocity computations begin again.
8. The simulation progresses with increasing time steps until the stability criteria are exceeded.

When the stability criteria are exceeded, the time step is reduced by various functions depending on the previous history of stability success, and the computation sequence is restarted. If all the numerical stability criteria are successfully met, the time step is increased for the next grid system computational sweep. During a time step, discharge flux is added to the inflow elements. Flow velocity and discharge between grid elements are computed and the change in storage volume in each grid element for both water and sediment are determined.

All the inflow volume, outflow volume, change in storage or loss from the grid system area are summed at the end of each time step and the volume conservation is computed. The flood routing proceeds on the basis that the time step is sufficiently small to insure numerical stability (there is no numerical surging). The key to efficient finite difference flood routing is that numerical stability criteria limits the time step to avoid surging and yet allows large enough time steps to complete the simulation in a reasonable time. Most explicit schemes are subject to the Courant-Friedrich- Lewy (CFL) condition for numerical stability. The CFL condition relates the floodwave celerity to the model time and spatial increments. The physical interpretation of the CFL condition is that a particle of fluid should not travel more than one spatial increment Δx in one timestep Δt. FLO 2D uses the CFL condition for the floodplain, channel and street routing. The time step Δt is limited by:

$$\Delta t = C \Delta x / (v + c) \qquad (8.18)$$

where:
C is the Courant number (C _ 1.0)
Δx is the square grid element width
v is the computed average cross section velocity
c is the computed wave celerity

While the coefficient C can vary from 0.3 to 1.0 depending on the type of explicit routing algorithm, a value of 1.0 is employed in the FLO 2D model to allow the model to have the largest time step. The CFL stability criteria is hardwired in the model, the user does not input any data for its application .

For full dynamic wave routing, another set of the numerical stability criteria is applied that is a function of bed slope, specific discharge and grid element size. It is expressed as:

$$\Delta t < \zeta \, So \, \Delta x^2 / Qo \qquad (8.19)$$

where Qo is the unit discharge, So is the bed slope and ζ is an empirical coefficient. The coefficient ζ was created as a variable unique to the grid element and is adjusted by the model during runtime within a minimum and maximum range set by the user. Similar to the CFS criteria, when this numerical stability is exceeded, the hydraulic computations for that time step are dumped and the time step is decreased. Before the CFL and the full dynamic wave equation numerical stability criteria are evaluated during a FLO 2D simulation, the percent change in depth from the previous time step for a given grid element is checked. This percent change in depth is used to preclude the need for any additional numerical stability analysis. If the percent change in depth is greater than that specified by the user, the time step is decreased and all the hydraulic computations for that timestep are voided.

Time steps generally range from 0.1 second to 30 seconds. The model starts with the a minimum time step equal to 1 second and increases it until one of the three numerical stability condition is exceeded, then the time step is decreased. If the stability criteria continue to be exceeded, the timestep is decreased until the minimum time step is reached. If the minimum time step is not small enough to conserve volume or maintain numerical stability, then the minimum time step can be reduced, the numerical stability coefficients can be adjusted or the input data can be modified. The time steps are a function of the discharge flux for a given grid element and its size. Small grid elements with a steep rising hydrograph and large peak discharge require small time steps. Accuracy is not compromised if small time steps are used, but the computational time can be very long if the grid system is large.

8.4 Use of the FLO 2D program for the San Juan La Laguna lahar

The simulation for the San Juan La Laguna lahar with the FLO 2D model was divided in two parts. The first part was a simulation of the rainfall caused by the Hurricane Stan in the area to calculate a discharge hydrograph. The second part was a simulation of the lahar (streamflow) that affected the community using the hydrograph from the rainfall as an input. The DEM available for the Atitlan area was a 10 m grid model. This DEM had to be cut and resampled to a 25 m grid in ARCGIS because the FLO 2D calculations can become very slow (days) and the memory is unable to create small grids. Once the DEM was resampled it was converted into an ASCII grid. The rainfall information was obtained at the INSIVUMEH where pluviograph measurements of the days of the hurricane event were available. With these graphs it was possible to make a very detailed reading of the precipitation. For this simulation, the precipitation reading of every half hour during the period of 2nd and 9th of October was made.

FLO 2D has a preprocessor called Grid Developer System (*GDS*) that overlays the grid system on a digital terrain map or a DTM set of points and will interpolate and assign elevations to the grid elements. It establishes boundaries, imports background images and photos, and it will automatically generate most of the data files required to run the model. This preprocessor can work with DEMs in ASCII format or in DTM elevation points (DTM points are a series of random digital elevation points that may have been collected with aerial photogrammetry or Light Detection and Ranging (LIDAR) equipment). Once the ASCII file for the San Juan La Laguna study area is loaded into the GDS, the region limits are displayed (the program reads automatically the coordinates of the DEM map of the study area).

The GDS identifies then the number of points within the working region, for the San Juan La Laguna 102,979 elevation points were inside the study region and the DEM are displayed. It is possible to import aerial images such as *.jpg or *.tiff files or shape files. Having an image in the background helps to identify the FLO-2D computational domain and edit the grid element attributes**.** A 25 grid element size was selected to be overlaid as a grid system on the DEM points. A smaller grid element would improve the resolution but also

increases the computer runtime and memory requirements. For this reason, the DEM was resample from 10 m grid to 25 m grid (although the FLO 2D has an interpolation function also) (Fig. 8.4).

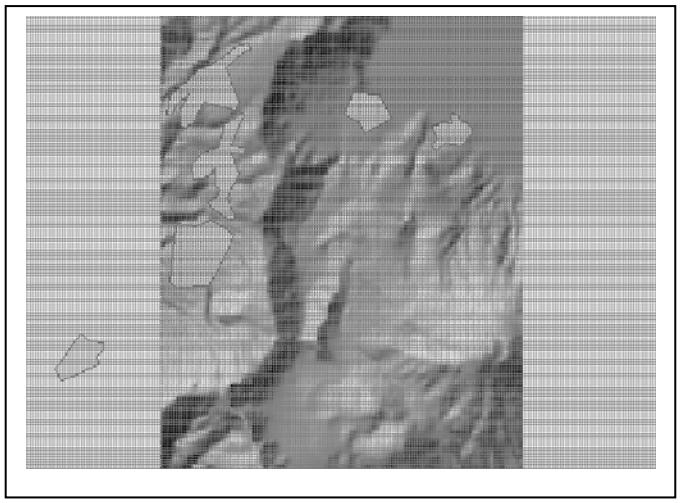

Fig. 8.4 Overlaying of the 25 m. grid system on the DEM

Once the grid is displayed on top of the DEM a computational domain has to be defined by marking the boundary grid elements of the specific area to be analyzed. The grid system outlines the project area. For the first part of the simulation, the rainfall simulation, a computational domain on the upper part of the basin and the San Pedro volcano was selected. For the second part of the simulation (simulation of the lahar), the area surrounding the whole basin was selected. When the computational domain is selected, the interpolation of the grid with the elevations of the DEM was made because the FLO-2D model requires that each grid element (center of the grid element) be assigned a representative elevation. For both parts of the simulation, a no filtering interpolation was selected since the grid size and the DEM size was of 25 m. When the FLO 2D grid has been interpolated, elevation points inside the computational domain are assigned to each grid.

8.4.1 Rainfall Simulation

Once the computational domain was selected in the upper part of the basin, a overland roughness value called Manning's roughness coefficients (n-value) of 0.05 was assigned to the whole computational domain because the flow follow a channel of a dry river. This value was taken from a table in the FLO 2D manual according to the characteristics of the soil and land use.

To simulate rainfall in the FLO 2D program, the accumulated rainfall during the period of the event was used as an input. (Fig. 8.5)

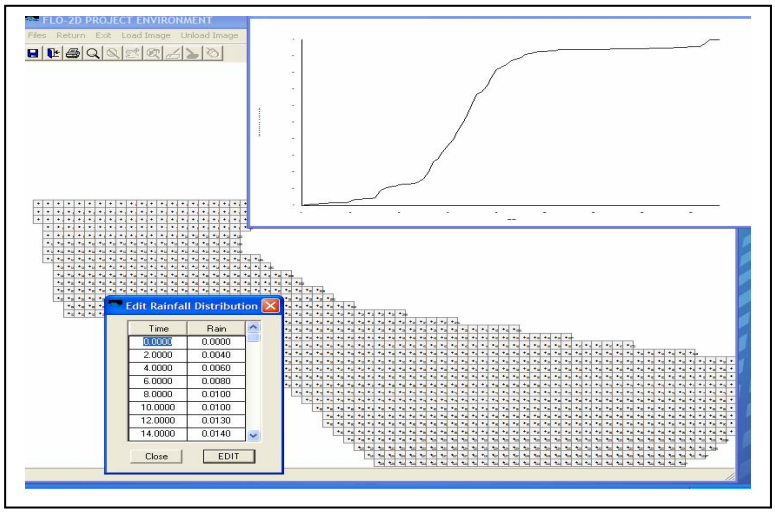

Fig.8.6 Accumulated rainfall used as an input in FLO 2D

The accumulated rainfall will be distributed all over the grid inside the computational domain selected in real time. Outflow grids have to be selected where the accumulated rain of the whole domain will be discharged. The outflow node is an artificial grid element whose sole purpose is to discharge flow off the grid system. For the San Juan La Laguna area, two different areas were selected with outflow grids. One area is located at the bottom of the San Pedro volcano, where the slope failure that occurred in the flanks started to follow the dry river channel. The other area selected with outflow grids was the area where the contribution flows that added material to the lahar were also canalized.

The discharge of every outflow grid selected is calculated by the program and displayed as an output. The discharges of each outflow grid of the two selected areas were added to have the total discharge value in each area. The result is two discharge hydrographs that were used as an input to simulate the streamflow that affected the San Juan La Laguna community (Fig.8.6).

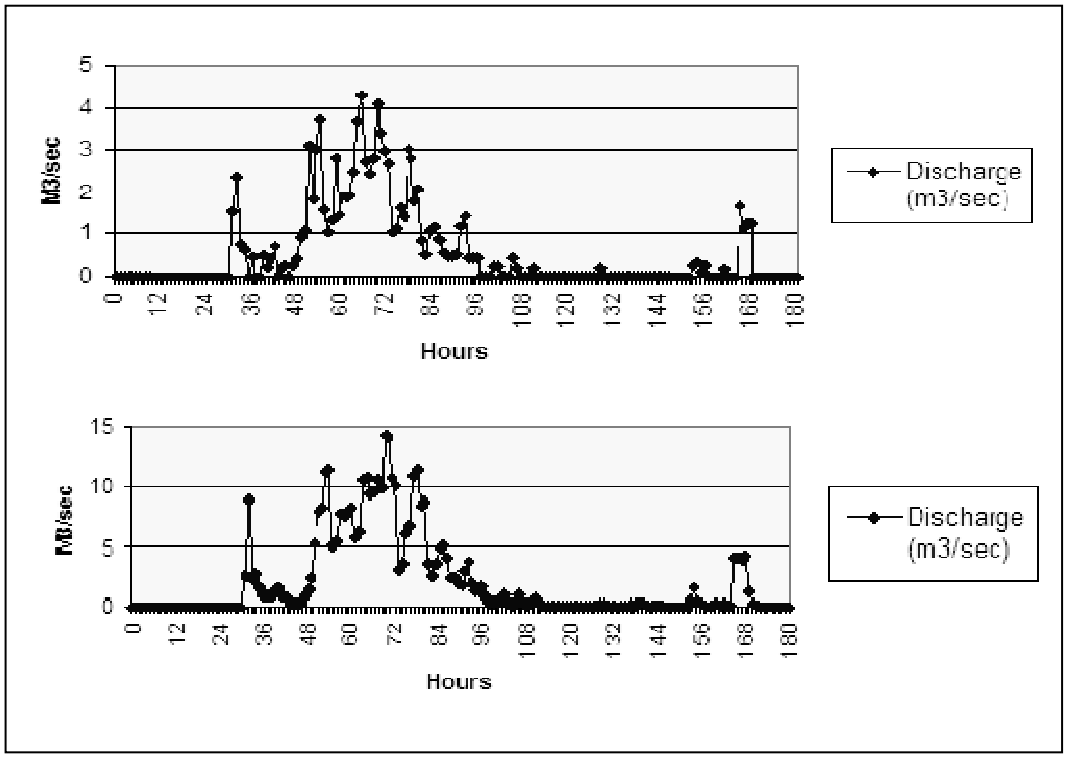

Fig.8.6 Hydrographs of the contributive flows (top) and from the lahar in the San Pedro volcano (bottom)

8.4.2 Lahar Simulation

To simulate the lahar, a second simulation had to be done. A new computational domain was selected (the whole basin). The value for the Manning roughness coefficient selected was the same as for the rainfall simulation, 0.05. For this simulation inflow grids has to be selected, these grids will discharge the hydrograph through the DEM. It is important to select the inflow grids correctly. For this simulation, the inflow grids were located inside the channel of the dry river and at the same location where the outflow grids in the "rainfall simulation" were selected. The input for this inflow grid was the hydrograph and the sediment in the flow.

A sediment volume must be assigned to the water discharge for a time step in the inflow hydrograph. The inflow sediment volume may represent channel and bank erosion and slope failure. The incremental sediment volume is tracked through the simulation. When routing the mud flood or mudflow over an alluvial fan or floodplain, the FLO-2D model preserves continuity for both the water and sediment. The percentage concentration selected for this flow was 24%. This percentage of concentration was taken from a table of the FLO 2D manual (2005) for stream flows. The viscosity and yield stress variables for the sediment must be specified also. Values of α and β for the viscosity and yield stress have to be assigned (Equations 8.15 and 8.16). The values selected for the simulation were: Viscosity $\alpha_1 = 0.152$ and $\beta_1 = 18.7$; Yield stress $\alpha_2 = 0.00136$ and $\beta_2 = 28.4$. These values were taken from a table of the FLO 2D manual (2005). The extent of mudflow inundation and the maximum flow depths and velocities are a function of the sediment volume and concentration.

The outflow nodes selected for this simulation were placed at the shores of the Lake Atitlan. No infiltration value was selected because the event happened during the latter days of the rainy season when the soil was already saturated with water

8.5 Results and discussion of the simulation using FLO 2D

For the simulation with the FLO 2D program, no adjustment of parameters was done as was the case for the situation described in Chapter 6. The results of the simulation of the lahar in the San Pedro volcano that affected the San Juan La Laguna community are:

The maximum velocity reached by the flow was of 7.2 m/s and the velocity of the flow when it reached the alluvial fan was 2.4 m/s. A mean velocity of the flow was 4.5 m/s. According to the field measurements, the mean velocity of the flow was 6 m/s (Fig. 8.7).

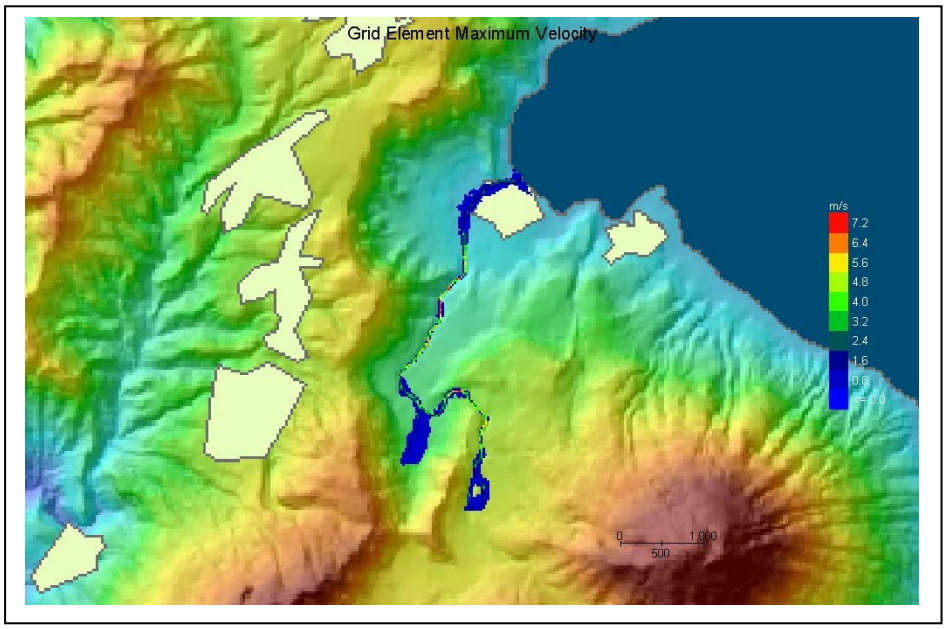

Fig.8.7 Velocity of the flow.

The computed maximum depth reached by the flow was 2.9 meters. When the flow reached the alluvial fan the computed depth of the flow was 1.6 meters. The field measurement of the mean depth in the alluvial fan was 1.3 meters. The program FLO 2D has a function to plot a graph of the depth of the flow with respect to the bed slope by drawing a profile line following the course of the flow (Fig.8.8).

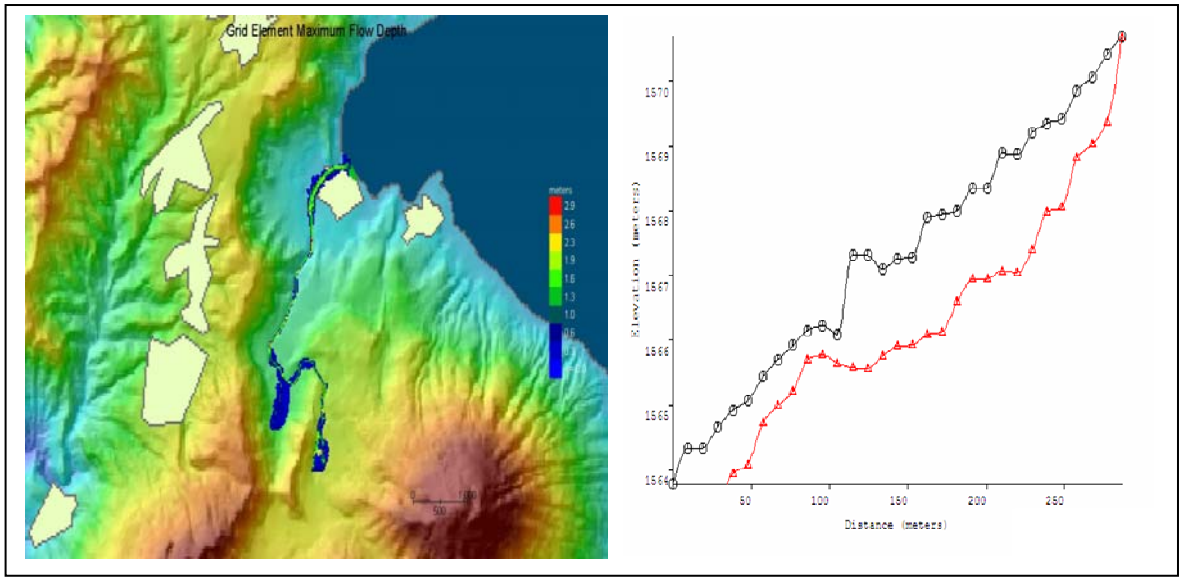

Fig. 8.8 Maximum depth of the flow (left), and plot of depth flow through the course of the channel showing the elevation of the flow.(right)

The amount of discharge calculated by FLO 2D of the flow during the San Juan La Laguna lahar with the contributive flows was 7,556,000 m³ . The deposited volume in the deposition area was 78,300 m³. The computed volume that was deposited in the lake was 7,478,000 m³. The area that contributed to the flow is 689,400 m². According to field measurements the deposited volume in the deposition area was 246,662 mts³ and the area of the contributive flows were 731,500 m².

The FLO 2D program is able to produce hazard maps. The hazard map of San Juan La Laguna was made selecting values of High event intensity = 3 m, Medium event intensity = 1 m, Low event intensity = 0.5 m (Fig8.9a). Another feature of FLO 2D is to compute impact forces, static pressures and specific energy of the flow for each grid. This tool can be useful for designing mitigation measures. The flow when it reached the population had an impact pressure of 19 kPa (Fig 8.9b).

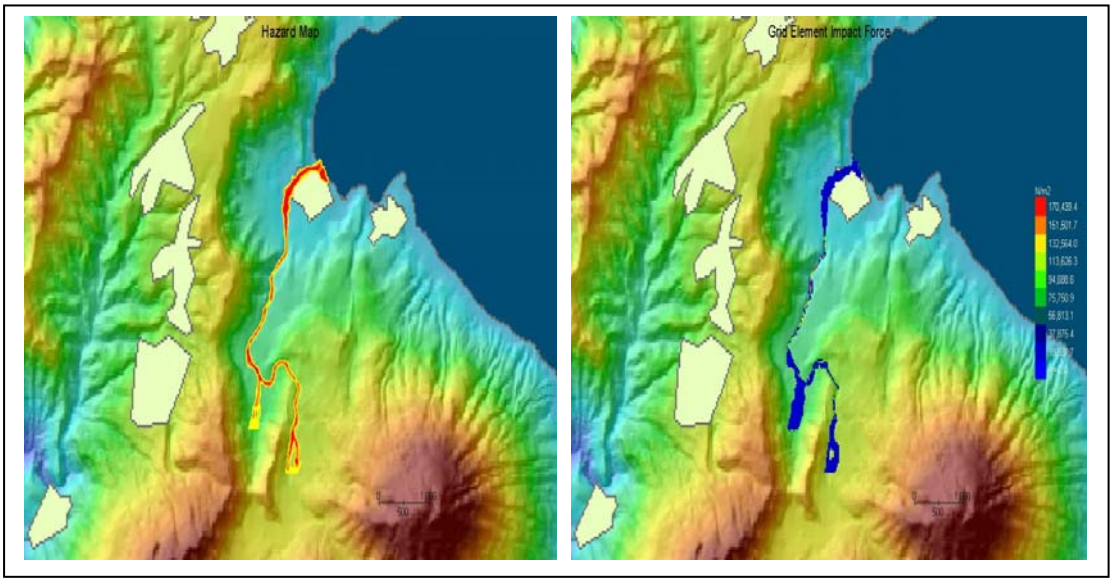

Fig 8.9. a) Results of a hazard map produced by FLO 2D (left), b) Display of the impact force of the flow calculated by FLO 2D (right).

The model results were compared with the data from the field measurements in San Juan La Laguna. The ability of the model to simulate field behaviors was evaluated with an informal measure of suitability determined by the following relationship:

Suitability = (Simulation result – Field measurement)/ (Field measurement) * 100

The lower the suitability number in %, the better the agreement.

Table.8.1 Results of the suitability evaluation

Criteria	Simulation results	Field Measurements	Suitability
Mean velocity of the flow	6 m/s	4.5 m/s	33 %
Mean thickness of the deposit	1.6 m	1.3 m	23 %
Volume of the Flow deposit	78,000 m^3	247,000 m^3 aprox.	- 68 %

Table 8.1. Results of the comparison of the FLO 2D program with the field measurements

After performing several simulations, it was found out that the parameter that most influence the output values of the program is the hydrograph, selection of the grid size and the quality of the DEM .

A simulation using the same hydrograph but using a 100 m grid was run and the results were compared with the previous 25 m grid simulation. The result was a reduction in the mean velocity from 6 m/s to 2.2 m/s and a decrease in the mean thickness of the deposit from 1.6 m to 0.6 m.

Another simulation was run using the same grid but reducing the input hydrograph by 45 %. The mean velocity decreased from 6 m/s to 4.5 m/s and the mean thickness from 1.6 m to 1.3 m (Fig. 8.10a and b)

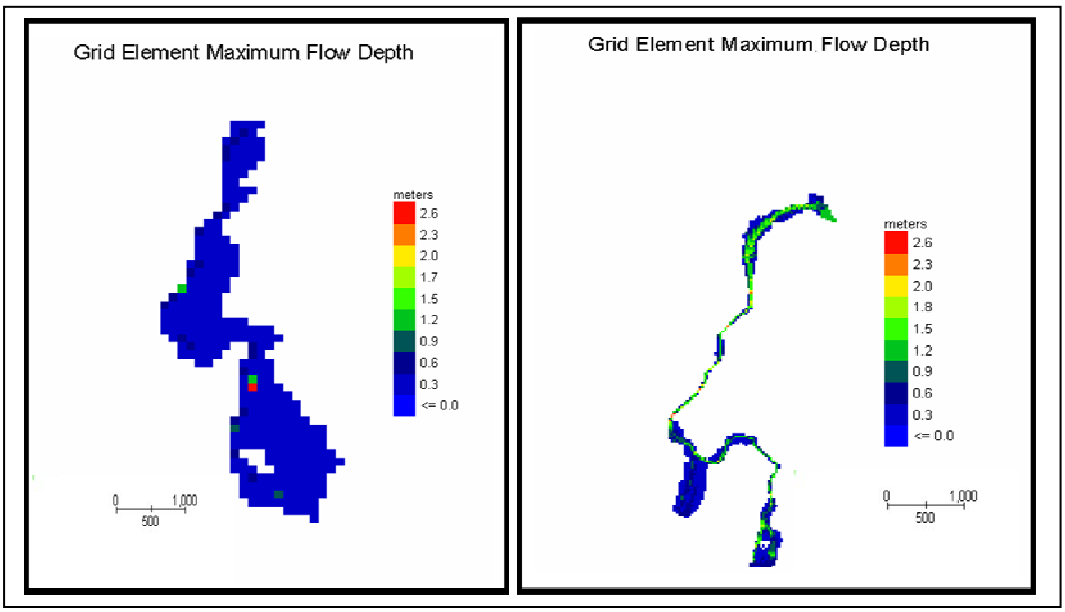

Fig. 8.10. a) Display of the results of the flow depth in a simulation run with a 100 m grid (left), b) Display of the results of the flow depth in a simulation run with a decrease in discharge of 45% (right).

8.6 Summary

The simulation with the FLO 2D program for the San Juan La Laguna event manage fairly well to simulate the observations in the field in terms of velocities and flow depth. accurate to the observations in the field in terms of velocities and flow depth. However, the program has some limitations as described below.

The results of the FLO 2D program are strongly influence by the topography. The detail and accuracy of a simulation is related to grid size because the program interpolates the topography into a system of square grid elements. The topography of each grid element is represented by a single elevation and roughness. Variations in topography such as mounds and depressions within the element are sometimes ignored. Alluvial fans and floodplain topographic features can be affected by this interpolation. Map resolution and accuracy should be considered when selecting the grid element size. Finer grid resolution requires more computer run time, more extensive data files, and more detailed boundary conditions.

The program assumes a steady flow for the duration of each time step. It can not distinguish between subcritical and supercritical flow and has no restrictions when computing the transition between the flow regimes. It also assumes a rigid bed model and does not simulate erosion or entrainment. Simulations with sediment transport and mudflow cannot be made simultaneously.

The centrifugal forces in the flow are not considered. Very detailed flow hydraulics such as hydraulic jumps, flow in bends or around circular structures can not be simulated with the model. The program has a hardwired rheology in the mudflow simulation and some parameters are chosen by default by the program and cannot be changed. The program does not take into account: particle-particle interaction, pore pressure within the flowing mass and accurate changes in the bed friction due to change in the surface material.

The calculation of input hydrograph is not always straightforward and problems occur when hydrograph has sharp peaks.

Overall, the FLO 2D program has many features (velocities, depths, impact force, static pressure and specific energy of the flow) that can make this program a useful tool for prediction of floods, calculation of flood hydraulics, identification of inundation areas, designing options for flood mitigation and hazard mapping.

In the Appendix B it is demonstrated how the program RAMMS and FLO 2D are used to analyze the run-out of a tsunami caused by a lahar into the Lake Atitlan.

9. Conclusions and recommendations

9.1 Conclusions

The October 2005 lahar events that occurred in the communities of Panabaj and San Juan La Laguna exemplify the typical mechanism of rapid flows on volcanic settings: significant entrainment of debris following the initial failure and high flow velocities. Triggered by the intense rainfall caused by Hurricane Stan, these landslides were very destructive, although the initial failure volumes were moderate. This resulted from the transformation of an initial failure mass into a large lahar with a high velocity.

The behavior and processes of the flow during their trajectories were well simulated by the RAMMS and FLO 2D programs, respectively. A calibration of the parameters by means of a back analysis that best fitted the observed event in Panabaj was performed to simulate the lahar with the RAMMS program. Although the RAMMS program was originally designed for snow avalanches, it worked fairly well for a volcanic setting. The inclusion of entrainment in the simulation made a better prediction of the run-out distance and a more accurate determination of the flow and deposition depths. RAMMS program is suited when a landslide occurs and the resulting flow entrains material on its way, as seen in the Panabaj event.

A selection of the best suited input parameters and a discharge hydrograph based on the accumulated rainfall was used to produce a FLO 2D simulation of the San Juan La Laguna slide. The FLO 2D program has many features (velocities, depths, impact force, static pressure and specific energy of the flow) that make this program a good tool for prediction of floods, calculation of flood hydraulics, identification of inundation areas, designing options for flood mitigation and hazard mapping. The FLO 2D program was precise as a routing tool for the flow in the San Juan La Laguna lahar. It was consistent when simulating the velocity and depth of the flow, although it underestimated the volume of deposition. The program is

applicable when the flow turns into a streamflow phase and the entrainment does not have a big influence on the mobility of the flow as observed in the San Juan La Laguna event.

The two lahars events that happened in October 2005 had different behavior, activity and rheology during its flow. One computer model cannot simulate all the alterations that occur during the course of a flow. For this reason, it is important to choose the right program for the right flow characteristics. A challenge for the future will be to develop a program that can simulate a broader range of flow and bed characteristics and the dynamic processes that take places in and with them.

In the Appendix B, a simulation of a tsunami that took place in the Lake Atitlan one hour after the Panabaj lahar happened, was done combining the RAMMS and the FLO 2D program. The tsunami was generated by a lahar from the San Pedro Volcano into the Lake Atitlan and affected the shores of Santiago and Panabaj communities.

It is important to note that to the use computer programs as simulation tools there is a necessity to make many assumptions and simplifications. All results will be subjected to the validity of the assumptions made. Nevertheless, the careful use of such tools can provide much valuable insight and assist in the hazard analysis process. Together with careful field observation, the application of a computer model can help produce a useful reconstruction of a complex multiphase movement and assist in landslide hazard assessment in volcanic settings.

Disasters associated with debris flows can be minimized through outreach to potentially affected communities. The local population and authorities must be provided with the information they need to take action in the event of future debris flows. The computer models RAMMS and FLO 2D, although they cannot predict the occurrence of the event, they can be a useful tool for hazard zonation of an area.

9.2 Recommendations for further work with RAMMS and FLO 2D programs

Based on the different features and the capabilities of the two programs, I recommend that further work should be performed. My suggestions for additional work with the RAMMS program are:

Modeling and calibration of a submarine slide.

An evaluation of the program with the adjusted parameters used for the Panabaj lahar in another volcanic setting with a well documented case, for example the Casita Volcano landslide in Nicaragua.

To model and adjust the parameter values in others well documented debris flows in different geological settings where erosion played a big role in the development of the flow. As the case of the Fjærland debris flow in Norway.

To model a debris flow where the bed slope characteristics change during the course of its trajectory, using the variable Mu/Xi feature in the program.

To model a debris flow where the flow followed a complex topography (close curves).

To model the interaction of a debris flow with planned or already built mitigation structures.

To model snow avalanches.

For the FLO 2D program:

To make a parametric study and measure the sensitivity of the program to changes in sediment concentration, n-value (roughness coefficient) and the values α and β of the viscosity and yield stress.

To model a dam breach or a levee failure that includes sediments and routing the discharge.

To model the interaction of the flow with mitigation and other type of structures (buildings and houses). Producing a detailed hazard map and making a damage assessment. Estimating the damage (cost) caused by a flood in an area is another feature of FLO 2D.

To make a flood delineation of an area based on return periods of precipitation.

9.3 Mitigation measures for the Atitlan area

It is important to asses the hazards owing to lahars and to adopt mitigation strategies for dealing with the hazards that derive from them. For this reason, I suggest the following mitigation measures for the Panabaj and San Juan La Laguna community:

Strict land use regulation and relocation of the communities: A careful inspection and recognition of the potential high risk areas at the skirts of the volcanoes should be done. After a lahar hazard map is prepared, governmental agencies should prohibit residential and commercial building in areas potentially at risk. In both communities, planned new infrastructure, temporary shelters and new housings are located close to the deposition area of the flow and located on the same alluvial fan that hosted the October lahars. This location was chosen shortly after the disaster and no safety guidelines were followed but undoubtedly these areas will be affected by lahars in the future. In any given year, any location on the alluvial

fan is at potential risk from lahar flows. In the very near future, small volume debris flows are more likely than normal, due to slope instabilities created by the October 2005 lahars.

Sediment diversion dams and dikes and sediment retention dams should be built. This structures work well for lahars of modest volume. It is inevitable that a significant number of people will choose to stay on the alluvial fan for economic reasons. These families will remain at risk, because eventually all areas of the alluvial fan will experience debris flows and mud flows as part of the normal sedimentation process.

Monitoring and evacuation plans are required. Lahars pose a big risk to people and property downstream because of their high velocities, their mobility and destructive power. The main hazards to these communities are represented by small volume lahars (debris flows and mudflows) that are triggered by rainfall. A meteorological station and a seismometer should be built near the crater of a volcano. A threshold value of rain and a critical hourly intensity for both long term (more than 1 day) and short term rainfall (1 or 2 hours) that relates duration-intensity of the rain, climate and topographical conditions using a statistical methods that relate rainfall intensities to a certain return period (Domaas et.al 2003) should be estimated. This will give warnings concerning lahar potential for a fast and safe evacuation.

References

- Bartelt, P; Salm, B.; Gruber, U.. 1999. **Calculating dense-snow avalanche runout using a Voellmy-fluid model with active/passive longitudinal straining.** *Journals of Glaciology 45*, 242-254

- Bertolo, P; Wieczorek, G.F.. 2005. **Calibration of numerical models for small debris flows in Yosemite Valley, California, U.S.A**. *Natural Hazards and Earth System Sciences # 5* p. 993-1001

- Buckman, Robert C.; Coe, Jeffrey A.; Mota, Manuel; Godt, Jonathan W.; Godt, Arthur C.; Tarr, Lee-Ann; Rafferty, Sharon; Hanckock, Dean; Dart, Richard and Johnson, Margoth. 2001.**Landslides triggered by Hurricane Mitch in Guatemala—Inventory and Discussion.** *US Geological Survey*. Denver Federal Center, Denver, Colorado U.S.A. 80225.

- Christen, M.; Bartelt, P.; Gruber, U.. 2002. **Aval -1: An avalanche dynamics program for the practice.** *International Congress INTERPRAEVENT 2002 in the Pacific Rim – MATSUMOTO / JAPAN Congress publication, vol. 2*, pp. 715-725

- Coe, J.A.; Godt J.W.; Baum, R.L.; Buckman, R.C. & Michael, J.A.. 2004. **Landslide susceptibility from topography in Guatemala**. *U.S. Geological Survey*, MS 966, Denver Federal Center, Denver, Colorado U.S.A. 80225.

- Domaas, U.; Heyerdal, H.; Harbitz, C.; Sandersen, F.; Tronstad, K; Nowacki, F.; Engen, A.; Kjestad, O; Devoli, G.; Buezo, G.; Diaz, M.R.; Hernandez, W.. 2003. **Rainfall induced lahars in volcanic debris in Nicaragua and El Salvador. Practical mitigation.** *Presented in proceeding from International Conference FSM2003-Naples,* May 2003.

- Evans, S.J.; Hungr, O. Clague, J.J.. 2001. **Dynamics of the 1984 rock avalanche and associated distal debris flow on Mount Cayley. British Columbia, Canada; implications for landslide hazards assessment on dissected volcanoes**. *Engineering Geology 61* p.29-51.

- Flores, Omar. 2005. **Technical report to assist and reconstruct the damage cause by Hurricane Stan in the municipality of San Juan La Laguna**. *Disaster Committee, University of San Carlos*, Guatemala.

- Giron, Jorge R. and Garavito, Fulgencio. 2006. **Evaluation of the lahar landslide in Panabaj and Tzanchag, municipality of Santiago Atitlan**. *INSIVUMEH report. (Institute of Meteorology, Vulcanology, Hydrology and Seismology, Guatemala).*

- Graf, C.; Rickenmann, D.; Hurlimann, M.. 2003. **Field and monitoring data of debris-flow events in the Swiss Alps.** *Can. Geotech. J. 40*: 161–175 (2003)

- Haapala, J.M.; Escobar Wolf , R.;Vallance J.. 2005.**Volcanic Hazards at Atitlán Volcano, Guatemala** *U.S. Geological Survey*, Reston, Virginia: 2005

- Hayashi, J.N. and Self, S.. 1992. **A comparison of pyroclastic flow and debris avalanche mobility**. *J. Geophys. Res. 97*, 9063-9071.

- Hungr. O.. 1995. **A model for the runout analysis of rapid flow slides, debris flows and avalanches.** *Canadian Geotechnical Journal 32* p. 610-623.

- Iverson, R.M.; Schilling S.P. and Vallance J.W.. 1998. **Objective delineation of lahar inundation zones.** *Geol. Soc. Am Bull. 110*, 972-984.

- Iverson, R.M; Denlinger, R.P.. 2001. **Mechanics of debris flows and debris-laden flash flood.** *Proceeding of the 7th. Federal Interagencies Sedimentation Conference.* March 25-29 of 2001. Reno, Nevada

- Legros, F.. 2002.**The mobility of long-runout landslides.** *Eng. Geol*. *63*:301-331.

- Malin, M.C. and Sheridan, M.F.. 1982.**Computer assisted mapping of pyroclastic surges.** *Science, 217*, 637-640.

- Newhall, C.. 1987, Geology of **the Lake Atitlán Region, Western Guatemala**: *Journal of Volcanology and Geothermal Research, V. 33*, p 23-55

- Newhall, C., Braddbury, P., Higuera, J., Poppe, A., Self, S., Sharpless, N., and Ziagos, J.. 1987, **Recent Geologic History of Lake Atitlán, A Caldera Lake in Western Guatemala.** *Journal of Volcanology and Geothermal Research, V. 33,* p. 81-107.

- NOAA. 1999. **Hurricane Basics.**

- O'Brien, Jimmy. 2005. **FLO 2D Users Manual**. *Tetra Tech ISG*, Nutrioso AZ.

- O'Brien, Jimmy and Zhao, Bing. 2004. **Real time rainfall-runoff modeling on alluvial fans, floodplains and watersheds.** *Tetra Tech, FLO-2D Software Inc.*, Nutrioso Arizona, USA.2004.

- O'Brien, Jimmy; Julien, P.Y. and Fullerton, W.T.. 1993. **Two dimensional water flood and mudflow simulation.** *Tetra Tech, FLO-2D Software Inc*., Nutrioso Arizona, USA.

- Pasch, R.J.; Roberts, D.P.. 2006. **Tropical Cyclone Report, Hurricane Stan**. *National Hurricane Center.*

- Pierson, T.C.; Costa, J.E.. 1987. **Rheologic classification of subaerial sediment-water flows.** *Reviews in Engineering Geology Vol. 7* 1987

- Pitman, E.B.; Nichita, C. C.; Patra, A.; Bauer, A.; Sheridan, M.F. and Bursik, M.I.. 2003. **Computing granular avalanches and landslides.** *Physics of Fluids, 15* p.3638-3646.

- Pudasaini, S; Hutter, K.. 2003. **Rapid Motion of free-surface avalanches over natural terrains and their simulation through curved and twisted channel**. *Isaac Newton Institute for Mathematical Science.*

- Sandersen, F; Bakkehoi, S; Hestnes, E; Lied. K.. 1996**. Influence of meteorological factors on the initiation of debris flows, rockfalls, rockslides and rock mass stability.** *Landslides Proceedings of the 7th symposium on landslides*, Trondheim pp. 97-114.

- Savage, S.B.; Hutter, K.. 1991. **The dynamics of avalanches of granular material from initiation to run/out. Part I analysis**, *Acta Mechanica 86* pag. 201-233

- Sheridan, M.; Connor, L.; Connor, C.. 2006. **Assessment of October 2005 Debris Flows at Panabaj, Guatemala.** *Document prepared for Oxfam.*

- SLF, Swiss Federal Institute for Snow and Avalanche Research.2007. **RAMMS draft users manual.**

- Sovilla, B.. 2004. **Field experiments and numerical modeling of mass entrainment and deposition processes in snow avalanches**. *PhD Thesis. No. 15462*, ETH Zurich, Switzerland.

- Sovilla, B.. 2002. **Observation and modeling of snow avalanche entrainment**. *Nat. Hazards Earth Syst. Sci. 2*, 169-179

- Sovilla, B, Margreth, S, Bartelt, P.. 2007. **On snow entrainment in avalanche dynamics calculations**. *Cold Regions Science and Technology 47* p. 69-79

- Tilling, R.I.. 1989. **Volcanic hazards and their mitigation: progress and problems.** *Reviews of Geophysics, 27*, 237-269.

Appendix A
Chronology of Hurricane Stan
in Guatemala

This description of the event is based on a report made by INSIVUMEH (2005).

Day 28 of September 2005: A strong low pressure system was located in the Caribbean Sea between Jamaica and Honduras. It was moving in a Northwest direction and had a potential to become a Tropical Depression. The Intertropical Convergence Zone was very near to the coasts of the Pacific Ocean in Guatemala (Fig.A.1.a)

Day 29 of September 2005: The low pressure system was becoming stronger in the Caribbean Sea with a slow movement towards the Northwest. Cloudy weather in the Pacific coasts of Guatemala associated the Intertropical Convergence Zone (Fig.A.1.b).

Day 30 of September 2005: The low pressure system in the Caribbean Sea moved slowly and located itself in front of Honduras. The Intertropical Convergence Zone in front of the Pacific coast was very active, creating rainfall and thunderstorms (Fig.A.1.c).

Day 1 of October 2005: At 12:00 hrs, Guatemala local time, the National Center for Hurricanes informed that the low pressure system in the Caribbean has formed into the Tropical Depression # 20, with a minimum pressure of 1007 milibars and maximum sustained winds of 45 km/hr, moving West-Northwest with a speed of 9 km/hr. The depression was located 500 km off to the Atlantic coast of Guatemala. The Intertropical Convergence Zone in front of the Pacific coast kept being active creating more rainfall on the Pacific coast of Guatemala (Fig.A.1.d).

Day 2 of October 2005: Around 2:00 a.m., the Tropical Depression became stronger, transforming into Tropical Storm “Stan”, with a minimum pressure of 1003 milibars and maximum sustained winds of 75 km/hr., moving West-Northwest with a speed of 10 km/hr. Heavy rainfalls at the Pacific coast because of the Intertropical Convergence Zone associated with a low pressure system located in that area. Stan crossed the Yucatan Peninsula with West-Northwest direction. The interaction of the storm and the land, made “Stan” weak, turning (at evening) in a Tropical Depression again. During this day, the first records of rain in Atitlan (Santiago station) were recorded. The station recorded 13.4 mm. accumulated rain for this day (Fig.A.1.e).

Day 3 of October 2005: At 3:00 a.m. the tropical depression became a Tropical storm. At this moment the storm is located in the Gulf of Mexico waters, 615 km of the coast of Tuxpan, Mexico. The minimum pressure was of 1002 milibars, maximum sustained winds of 65 km/hr, moving to the West with a speed of 17 km/hr. The secondary bands of the Tropical storm favored the increase in humidity from the Pacific Ocean, this included the low pressure system in the Pacific created high precipitation in the Pacific coast and the Guatemala Highlands. The Santiago station recorded 57.2 mm. accumulated rain for this day (Fig.A.1.f).

Day 4 of October 2005: At 3:00 a.m. the Tropical Storm "Stan" became a Category 1 Hurricane. The eye of the hurricane was located at 195 km to the East-Southeast of Veracruz, Mexico, with a minimum pressure of 982 milibars, maximum sustained winds of 120 km/hr and moving Southeast with a velocity of 19 km/hr. Stan kept moving until it reached land at 9:00 a.m. where it became a Tropical Storm again. By evening, the Tropical storm degraded to Tropical Depression. This caused cloudiness and strong precipitation in the central plateau and the West part of Guatemala. The Low Pressure system in the Pacific Ocean became a part of the Cyclone and the Intertropical Convergence Zone kept presence in the Pacific coast. At night, a new small tropical wave came also to the Pacific coast, this added more humidity and cloudiness to Guatemala. The Santiago station recorded 297.5 mm. accumulated rain for this day (Fig.A.1.g).

Day 5 of October 2005: At early hours of this day, the Tropical Depression kept becoming weaker, dissipating finally over the mountains of Oaxaca, Mexico. High amounts of rain still fell over Guatemala associated with the new tropical wave and the Intertropical Convergence Zone that kept very near to the Pacific Coast of Guatemala. The Santiago station recorded 144 mm. accumulated rain (Fig.A.1.h).

Day 6 of October 2005: Humidity remaining from the Tropical Depression was still in the Mexican territory, this, and a complex system of Low Pressures located in the Caribbean Sea allowed more humidity from the Pacific Ocean in Guatemala. Cloudiness and heavy rain fell over the pacific coast and the Guatemala Highlands. The Santiago station recorded 9.8 mm. accumulated rain for this day (Fig.A.1.i).

Day 7 of October 2005: High humidity still in the coasts of the Pacific Ocean associated with the Intertropical Convergence Zone. This condition was maintained during the next two days. The Santiago station recorded 2.4 mm. accumulated rain for this day (Fig.A.1.j).

Fig. A.1 Evolution of the tropical storm Stan

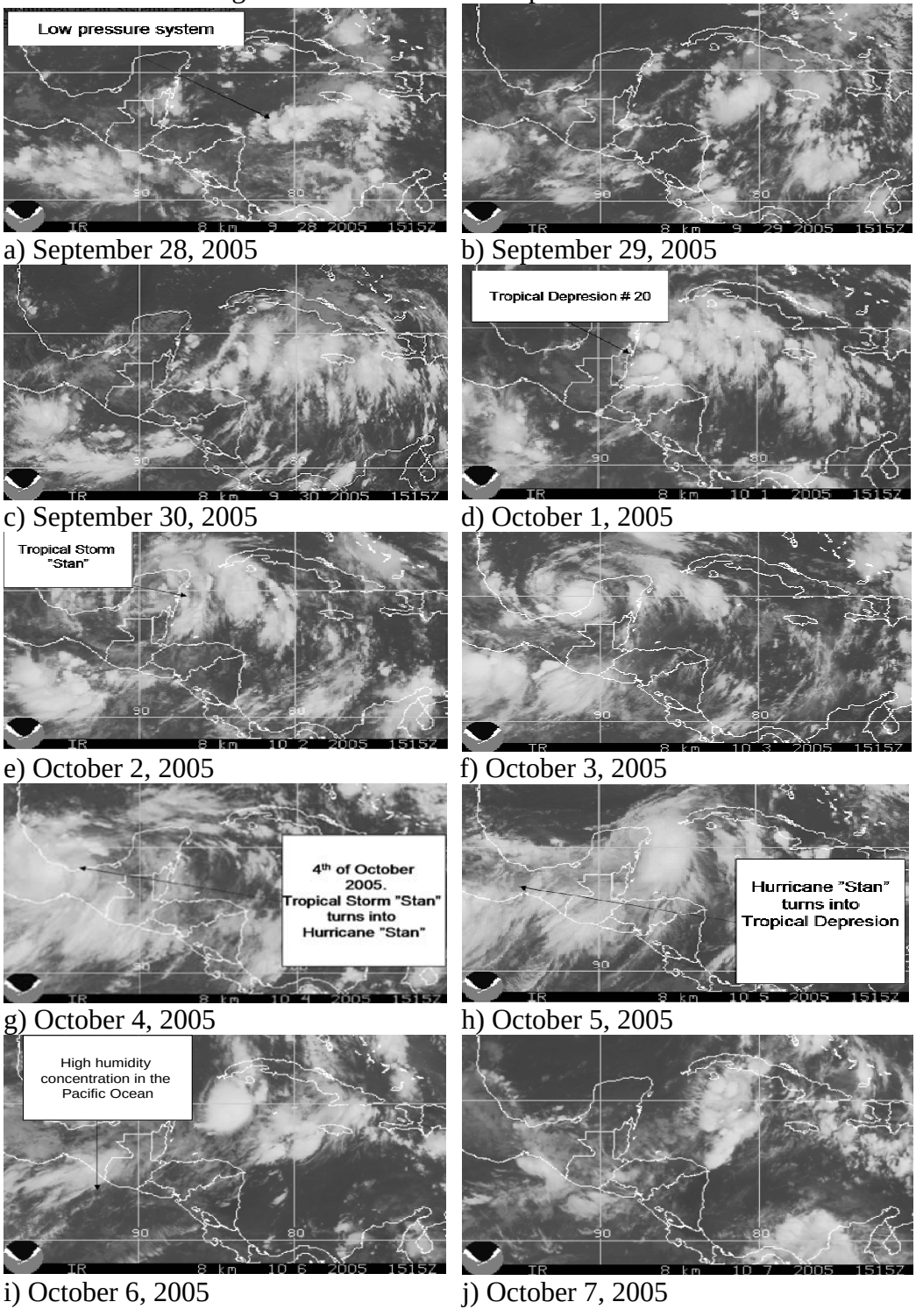

a) September 28, 2005 b) September 29, 2005

c) September 30, 2005 d) October 1, 2005

e) October 2, 2005 f) October 3, 2005

g) October 4, 2005 h) October 5, 2005

i) October 6, 2005 j) October 7, 2005

References to appendix A

INSIVUMEH. 2005. **Impact study associated with the Hurricane Stan in Guatemala**. *Report of the Institute of Seismology, Vulcanology, Meteorology and Hydrology for October 2005*.

Appendix B

Tsunami (seiche) caused by a lahar flow into the Santiago Bay, Lake Atitlan, simulated by RAMMS and FLO 2D

So might be heard,
when together came
the tempest sister[1]
and the long keels,
as when rock and surge
on each other break.

[1] Kolgu sister. Kolgat was one of the daughters of Aegir (Norse myth god of Sea) and Ran; they were waves.

(Verse 28 of "The Poetic Edda")

B.1 Introduction

One and a half hour after the slope failure in the southwestern part of the San Pedro volcano that affected the community of San Juan La Laguna, another slope failure in the eastern part of the volcano took place. This collapse failure created a lahar flow that was canalized for most of the trajectory inside a gully known by the name of "Chuitunamit", in the direction to the Santiago Bay where the communities of Panabaj and Santiago are located. This flow eroded big quantities of the channel material which deposited inside the Lake Atitlan. The impact of the lahar with the lake generated a series of water wave oscillations that traveled to the other side of the shore. These waves are known as "tsunamis" or if the wave oscillations happen in an enclosed basin are called "seiches" (Fig.B.1).

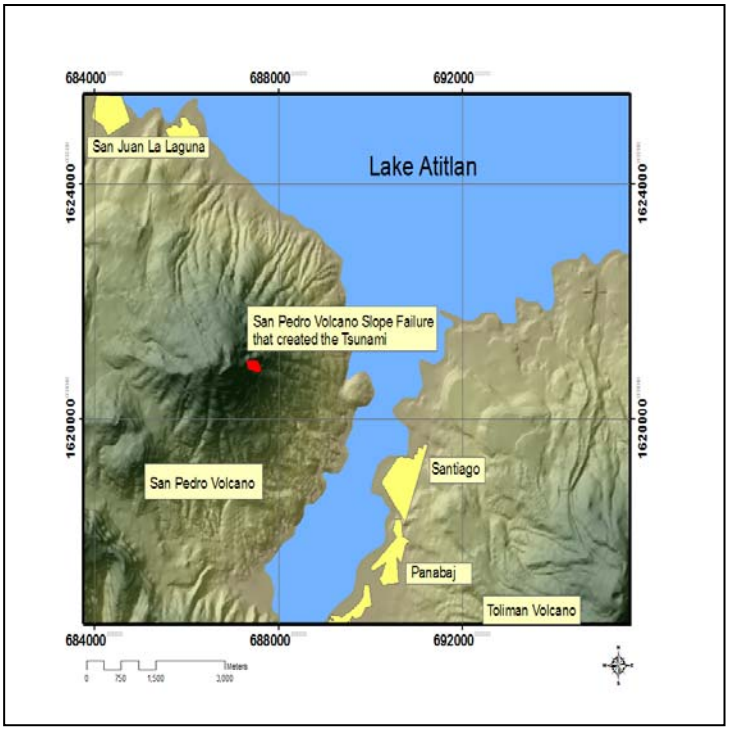

Fig.B.1. Location of the slope failure in the San Pedro volcano that produce a tsunami in the Santiago bay.

A seiche is the free oscillation of the water in a closed or semi-enclosed basin at its natural period. A seiche can be compared to the free oscillation of water in a dish (Fig.B.2). Seiches are frequently observed in harbors, lakes and bays. The initial displacement of water from a level surface can arise from a variety of causes, and the restoring force is gravity, which always tends to maintain a level surface. Once formed, the oscillations are characteristic only of the geometry of the basin and may persist for many cycles before decaying under the influence of friction (Miles, 1974). Seiches are not apparent in the main ocean basins, probably because there is no force sufficiently coordinated over the ocean to set a seiche in motion (Apel, 1987). A variety of seiche periods may appear in the same water level because the main body of water may oscillate longitudinally or laterally at different periods. Seiches generally lasts for only a few periods, but may be frequently regenerated.

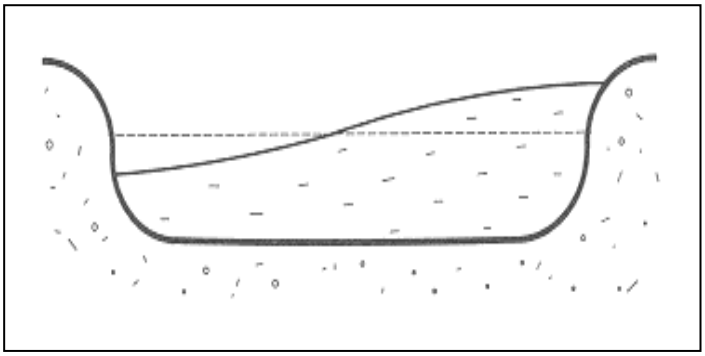

Fig.B.2. Diagram of the wave oscillation in a seiche.

Seiches can be generated when the water is subject to changes in wind or atmospheric pressure gradients. Other frequent causes of seiches include heavy precipitation over a portion of the lake, flood discharge from rivers, seismic disturbances, submarine or subaereal mudslides. The amplitude and persistence of the resulting seiche depend not only on the magnitude of the energy source but also on the energy losses within the water body. Such losses include dissipative effects resulting from friction on the sides or bottom of the basin.

If the seiche is generated by an impulsive event, the seiche amplitude is seen to decay by a nearly constant fraction with each succeeding period. In general, the rate of decay is greater for basins that are shallow or have narrow constrictions and complex topography.

B.2 Description of the event

The description of the event is based on personal interviews with local fishermen and by a report made by Giron and Matias (2006).

A collapse failure in the east part of the San Pedro Volcano produced a lahar at 5:50 a.m. on the 5th of October 2005 triggered by the intense rains caused by the Hurricane Stan in the area (Fig.B.3. a and b). The elapsed time from the collapse failure to the lahar reaching the lake was around 6 minutes. The lahar was composed of 25% of rocks, 30% of lapilli and the rest was clay, organic materials and debris.

Fig.B.3. a) San Pedro volcano view, and the channel where the lahar flowed (left) b.) Picture of one of the channels where one part of the lahar was deposited in the lake (INSIVUMEH, 2006).

The first wave that arrived to the other side of the shore was around 6 to 7 m high and was followed by two waves of 3 m high (Fig.B.4). The first wave reached the shore in 7 or 8 minutes after the collapse took place (this is based on the sound heard by the fishermen). The distance that the waves traveled is 2.15 km. This gives the waves a mean velocity of 130 km/h (36.11 m/s). The frequency of the following waves when they crashed the shore was 1 or 2 minutes. The entire event lasted around 1 minute. After the impact of the three waves in the Santiago Bay, the shores were inundated even two hours after the event. The lake changed its color from the emerald green to brown coffee for a 72 hours period.

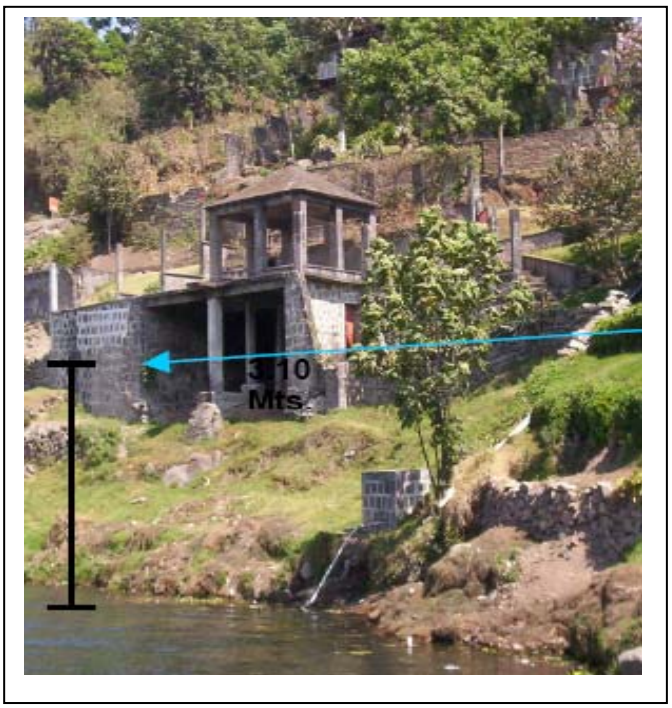

Fig.B.4. Shows the marks left by one of the waves when they reached the shore in Santiago. The arrows indicate a height of 3.10 m. (INSIVUMEH, 2006).

The seiche destroyed the grains and vegetable crops cultivated along the shores of the bay. The boats of the fishermen were overturned and knocked over. Two docks in the bay were affected. No casualties were reported during the seiche. No more information of this event was available, and the challenge was to simulate the event as accurately as possible with the use of the computer programs RAMMS and FLO 2D to understand the whole process of the event for future hazard assessments.

B.3 Methodology

A simulation of the whole event was made in three parts. The first part was simulating the slope failure and the behavior of the lahar that occurred on the volcano using the RAMMS program. The adjusted parametric values used for simulating the Panabaj lahar were used to

calculate the velocity, depth and volume of the lahar when it reached the lake (see Section 6.5). The second part was done by calculating the behavior of the waves. This was made by calculating the wave velocity and frequency with established formulas (see Section B.5). The third part was done by running a simulation of the run-out of the waves with the FLO 2D program when they reach the shores. The input parameters used in the FLO 2D program were taken from the calculations made in the Section B.5.

B.4 Simulation with the RAMMS program

A volume of 57,600 m³ was calculated for the release area from field measurements. The depth of the release area was 1.8m. The value chosen for $\mu = 0.04$ and $\xi = 450$. The density of the flow selected was 1900 kg/m³. The depth of the entrained bed used for the entrainment module was 0.7 m with a density of 1750 kg/m³ and a Tao of 93100 pascals (these are the same adjusted parameters as used in the Panabaj lahar simulation). The simulation was run with the following results:

The velocity of the flow when it reached the lake was 16 m/s (Fig.B.5 and B.6).

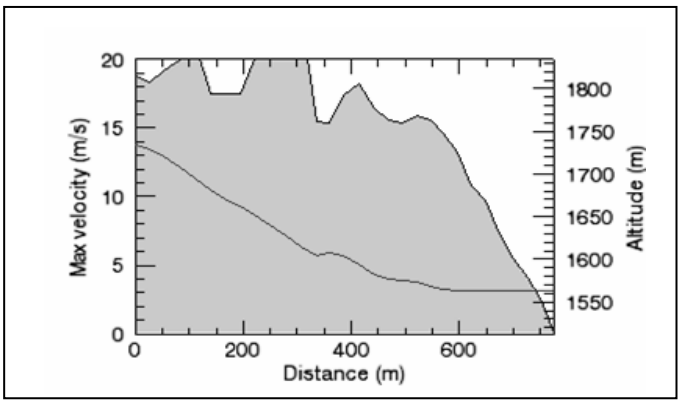

Fig.B.5. Plot of the velocity of the lahar when it reached the lake made with RAMMS program.

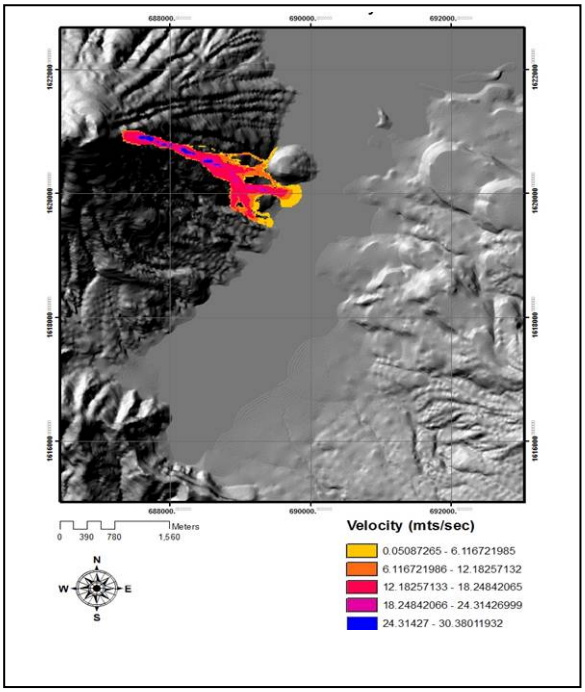

Fig.B.6. Map showing the maximum velocities reached by the flow through its trajectory.

The maximum depth of the flow was 15 m. The depth of the flow when it reached the lake was approximately 5 m (Fig.B.7 and B.8).

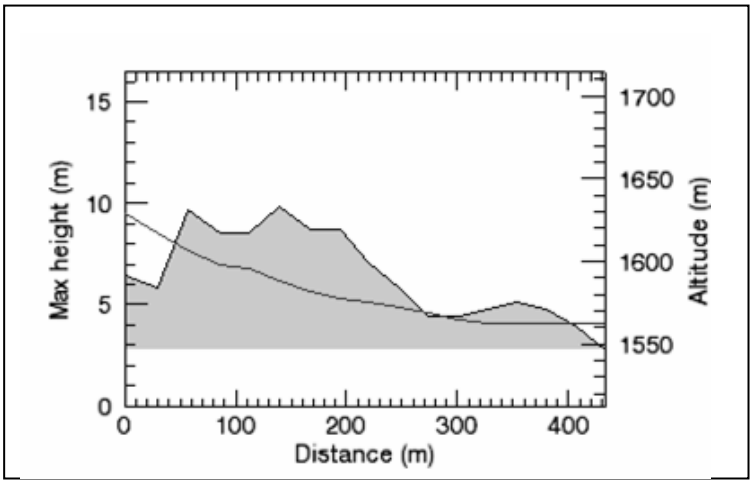

Fig.B.7. Plot of the maximum depths of the lahar when it reached the lake made with RAMMS program.

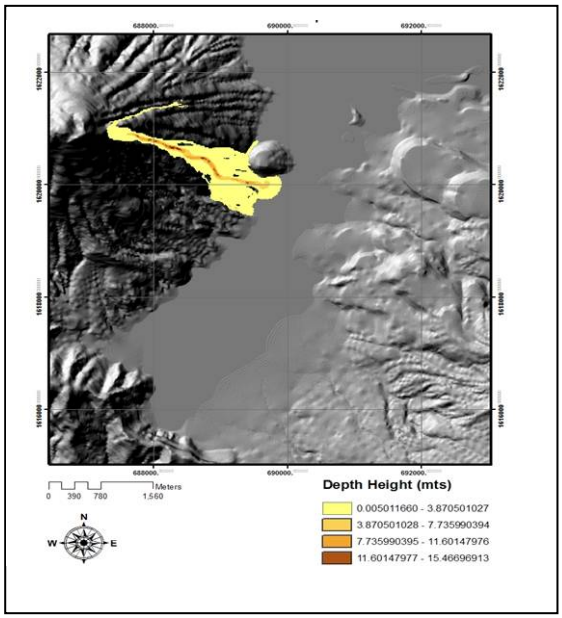

Fig.B.8. Map showing the maximum depths reached by the flow through its trajectory.

The volume of the eroded material was 195,400 m³ (Fig.B.9).

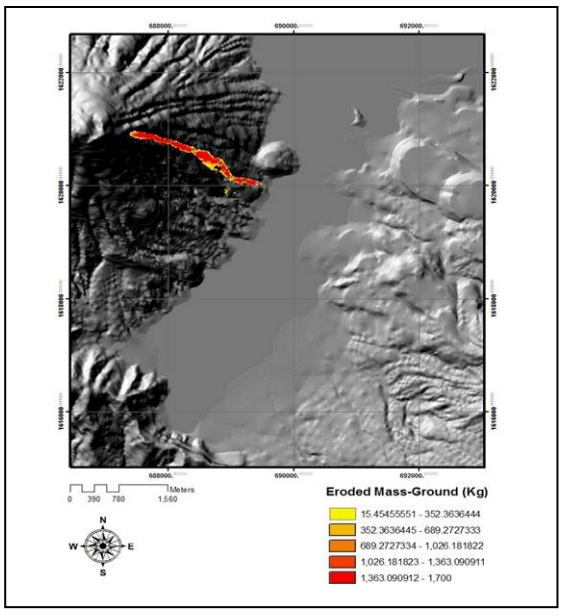

Fig.B.9. Map showing eroded mass of the flow in the channel.

The total flow when it reached the lake was 255,390 m³ (Fig.B.10).

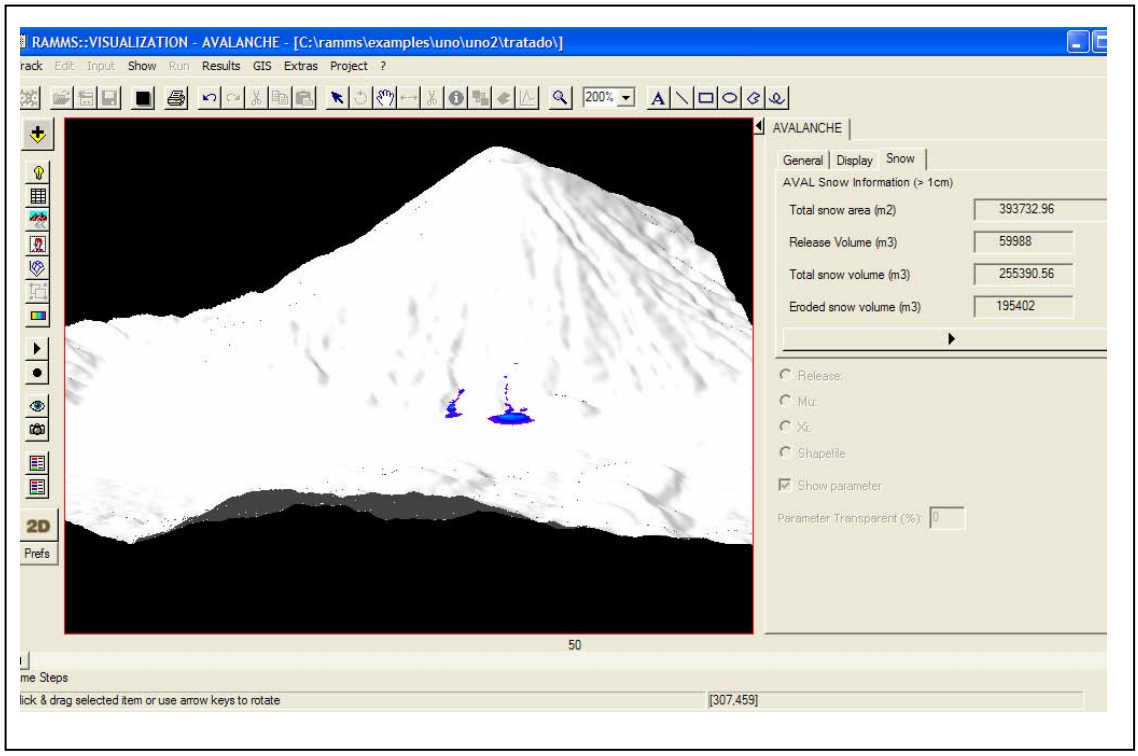

Fig.B.10. Picture of the RAMMS graphical user interface displaying the deposited lahar and the eroded mass in the panel. The panel displays “snow volume” because it was designed for snow avalanches, but in this cases this is equal to the lahar volume.

With the results given from the RAMMS simulation a calculation of the behavior of the waves in the lake was done with different formulas, as explained below, to match the results with the values observed in the field. To make these calculations it will be assumed that the basin is uniformly deep and rectangular in shape.

B.5 Calculations of the behavior of the waves

B.5.1 Wave Height

1) According to Noda (1970), the wave height can be modeled as:

$\eta = F \lambda$

where: η = wave height (m), F = Froude Number = $\frac{v}{\sqrt{g * d}}$, v = landslide velocity (16 m/s)

g = acceleration of gravity (9.81 m/s^2), d = water depth (132 m) the depth of the lake is the mean depth of the lake in the area taken from the bathymetry study in the lake by Newhall, 1987. λ= maximum thickness of landslide mass (15 m).

The wave height using the NODA model is = 6.67 m.

2) According to Huber and Hager (1997) model.

$$H = 0.88 \sin\alpha \left[\left(\sqrt{\frac{\rho s}{\rho}} \right) \left(\sqrt{\frac{Vs}{b}} \right) \left(\sqrt{\frac{d}{x}} \right) \right]$$

where α is the slope angle at the impact site (22.15°) (Fig.B.11).

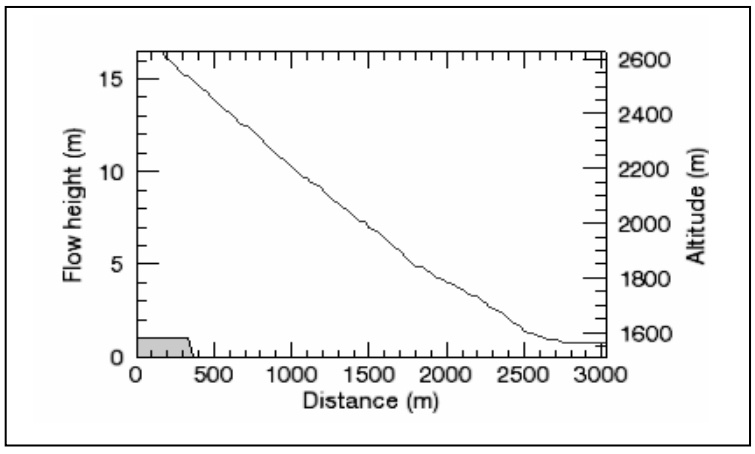

Fig.B.11. Plot of the profile of the San Pedro volcano where the lahar flowed.

ρs is the density of the flow (1.90 g/cm^3), ρ is the density of water (1 g/cm^3), *Vs* is the volume of the sliding mass (255,390 m^3 value given by RAMMS model), b is the finite shore distance equal to the width of the slide at impact with water (90 m), *d* is the water depth (132 m), *x* is the distance from the impact site to the location under consideration (2,150 m).

The wave height using the Huber and Hager (1997) model is = 6.09 m

These values of wave height agree with the wave height observed in the field.

B.5.2 Wave Velocity

According to the formulation of Huber and Hager (1997):

$$C = \sqrt{g * d}$$

where *g* = acceleration of gravity (9.81 m/s^2) and *d* is the lake depth (132 m).

This gives a wave celerity of 35.98 m/s (129.52 km/h)

This result also agrees with the field observations.

Landslide generated waves propagate in semi-circles; the wave height will vary with propagation direction and travel distance. The largest waves travel in the direction of maximum momentum, while lateral waves traveling along the shore are significantly smaller.

B.5.3 Frequency of the following waves

A standing wave can be represented by the sum of two waves traveling in the opposite direction, each being reflected at the ends of the basin. The natural period of oscillation is given by this formula:

$$T = \frac{2L}{n\sqrt{gh}}$$

where L is the length of the basin and n is the number of nodal lines present, one for the fundamental or uninodal seiche, two for the binodal seiche, and so on (Fig.B.12).

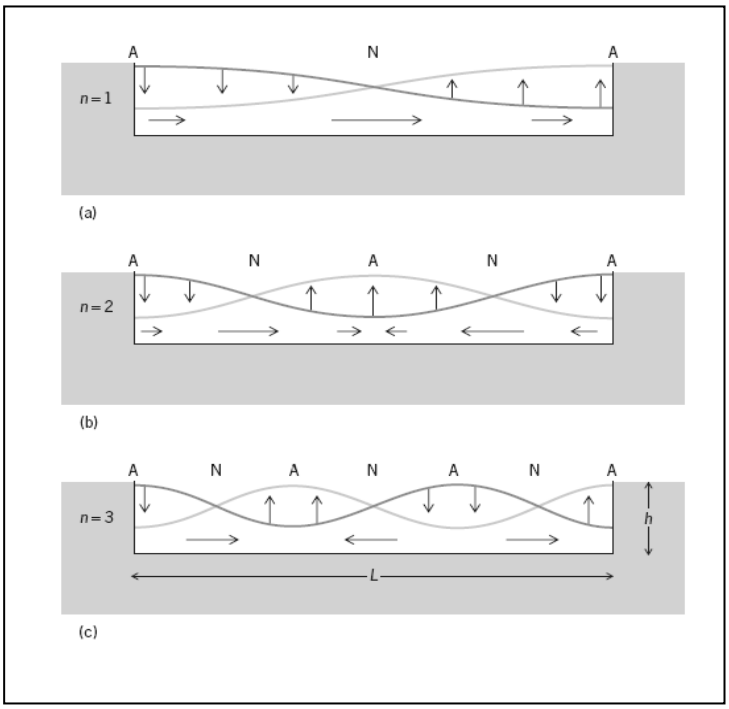

Fig.B.12. Diagram of a) uninodal b) bimodal and c) trinodal seiche in a rectangular basin. The arrows shows the direction of the flow corresponding to the change in water surface (McGraw-Hill, 2003).

This gives a frequency of 119.5 seconds or 2 minutes.

It is assumed that the event was a uninodal seiche because it was caused by a landslide and the periodicity of the waves was assumed constant.

B.6 Simulation with FLO 2D program

With the already known heights of the initial wave and the frequency of the following ones, a simulation with FLO 2D was run to estimate the run-out of the waves. FLO 2D can simulate tsunamis assigning a time-stage hydraulic control over unconfined floodplains where elevation (stage) rather than a discharge is the available data. By setting the water stage higher than the ground surface, inflow to areas can be simulated without knowing the discharge.

To simulate the seiche that occurred in the Santiago bay the time-stage data with the wave height and frequency was used as an input. Figure B.13 shows the time stage table created for this event. The duration of the wave was also selected according to the assumption of a uninodal type of seiche.

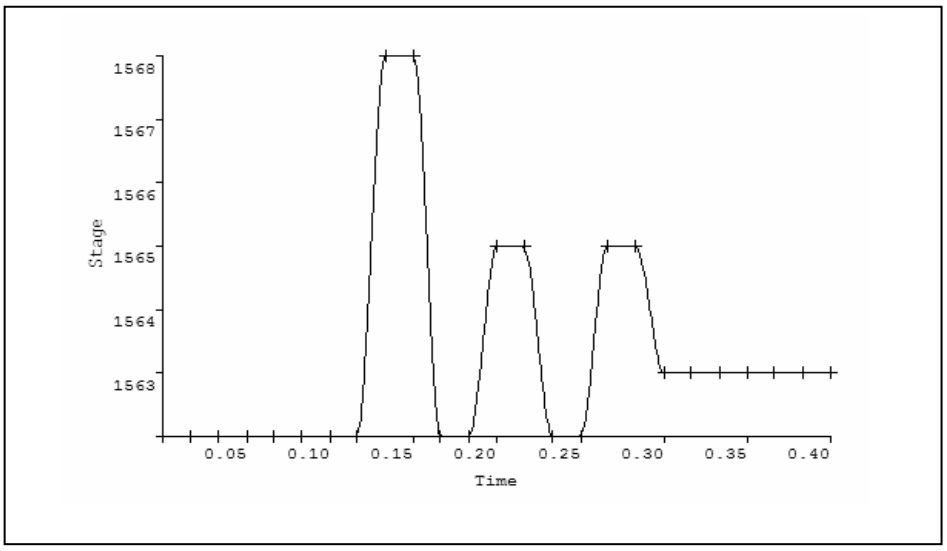

Fig.B.13. Time-stage data plot used to simulate the seiche with FLO 2D.

Using the grid developer system (GDS) included in the program and following the same steps as used in the simulation of San Juan La Laguna (see Chapter 8, Section 8.4) a 50 m square grid system was overlaid on the DEM. The data from the DEM was interpolated. Once the grid was assigned with elevations, the GDS was used to select the multiple grid elements representing the coastline where the seiche occurred. Once the shore grid elements are identified, the time-stage data was assigned to all of them simultaneously (Fig.B.14).

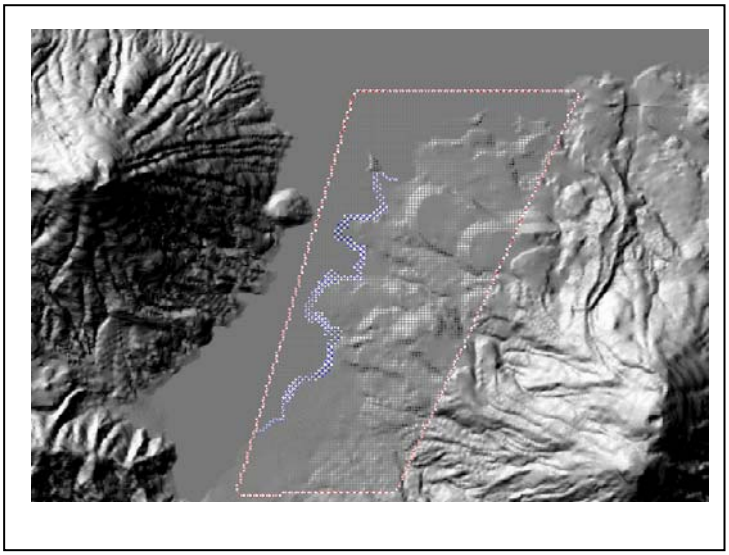

Fig.B.14. Picture of the selected grid, computational domain and outflow grids.

The simulated inundation did not reach any of the communities, most of the damages occurred at places near the shore (Fig.B.15). The total amount of water that reached the shores by the seiche was computed to be 17,475,000 m³. The amount of water that kept the area inundated after the event was 111,913 m³. The maximum inundated area was 1,097,500 m² (Fig.B.16 and B.17).

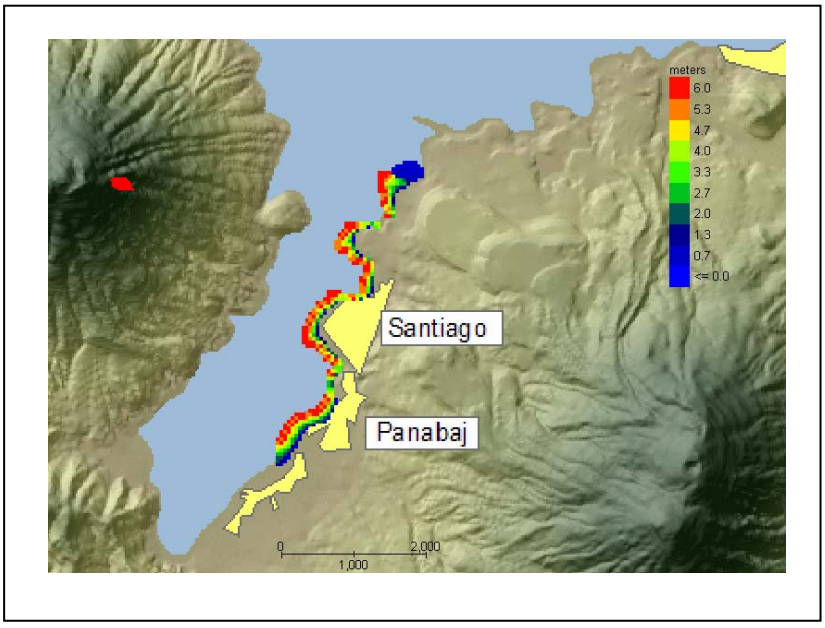

Fig.B.15. Map of the maximum flow depth of the inundation.

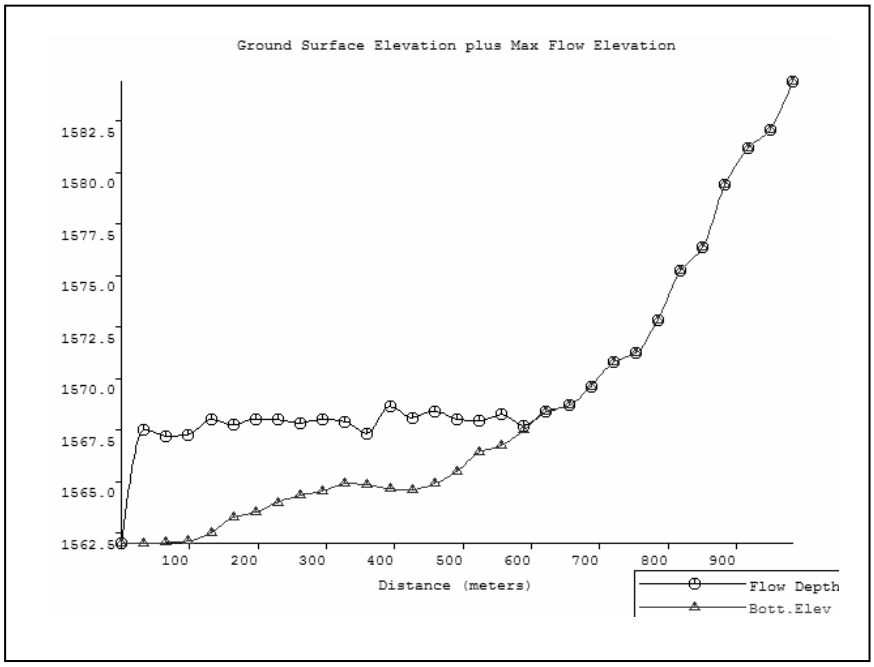

Fig. B.16. Plot of the inundation depth caused by the seiche in the Panabaj community.

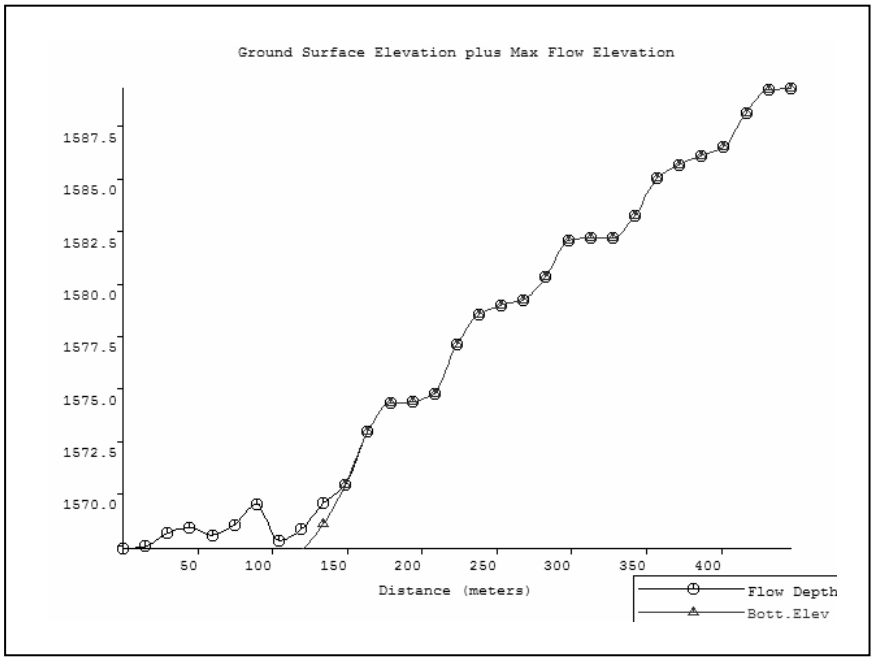

Fig.B.17. Plot of the inundation depth caused by the seiche in the Santiago community.

The velocity estimated by FLO 2D of the first wave (6 m high) when it reached the shore was 13 m/s (46.8 km/h) and a maximum impact force of the wave is 144 kilopascals in most of the shore area (Fig.B.18 a and b).

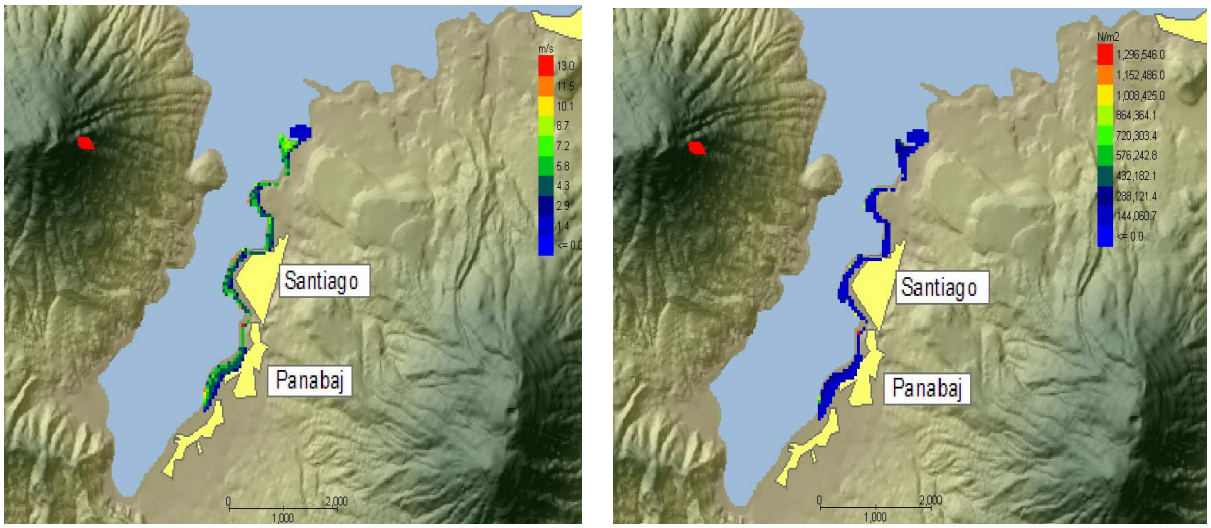

Fig.B.18. a) Map of maximum velocity reached by the waves when they reached the shore (left). b) Map of the maximum impact pressure of the waves (right).

B.7 Summary

It is possible to simulate a complex event as the seiche that occurred in the Santiago bay making use of different computer simulation programs. Using the best features of each program with a good calibration of parameters of input for a specific area using back analysis of past events, makes it possible to get an accurate representation of an event and can be very helpful to describe future possible scenarios (Fig.B.19 and B.20).

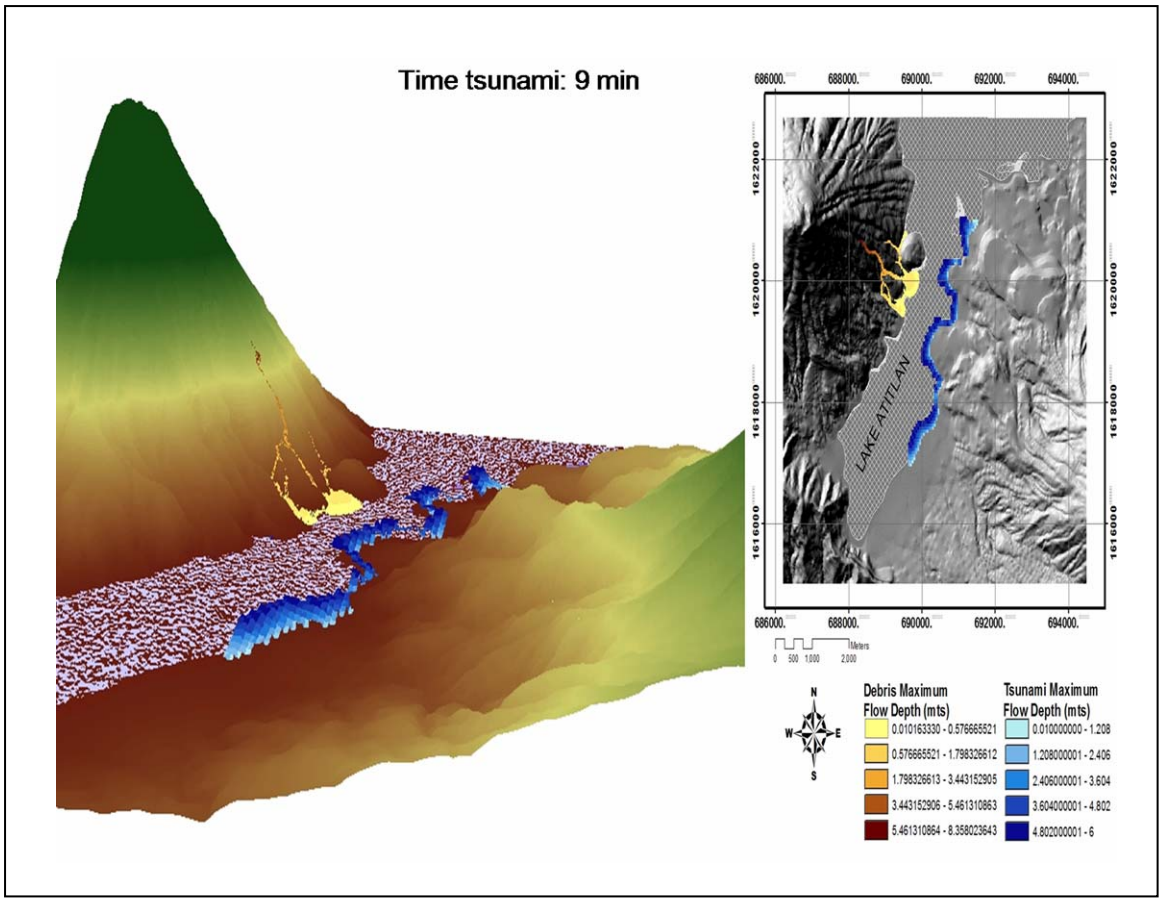

Fig.B.19. Result of the combined simulation between RAMMS program and FLO 2D.

To simulate the seiche, the event was divided in three parts. The first part was to simulate the collapse of the slope and its post failure flow simulating the erosion and entrainment to calculate flow depths, velocity and volume of the flow. The second part was made using simple mathematical calculations for the behavior of the lake and waves. The

third part was to model the run-out of the wave when it reached the shore with the FLO 2D program. The FLO 2D program is a simple volume conservation, two dimensional flood routing model that distributes a hydrograph or assign a time-stage hydraulic control on unconfined floodplain routing over a system of square grid elements.

The estimated volume (255,390 m^3), maximum velocity (16 m/s) and maximum depth (15 m) of the lahar triggered by the slope failure in the east part of the San Pedro Volcano by the computer model RAMMS, provided a range of values for calculating wave height and velocity. Empirical methods were used to calculate wave height and wave velocities. With these values, the run-out of the seiche when it reached the shore was calculated by FLO 2D.

The results of the simulation were reasonable when compared with the field observations. In conclusion, the proper use of the computer programs with adjusted parameters, reasonable assumptions and a good judgment by the user can be very useful for future simulations of similar events of tsunamis caused by landslides.

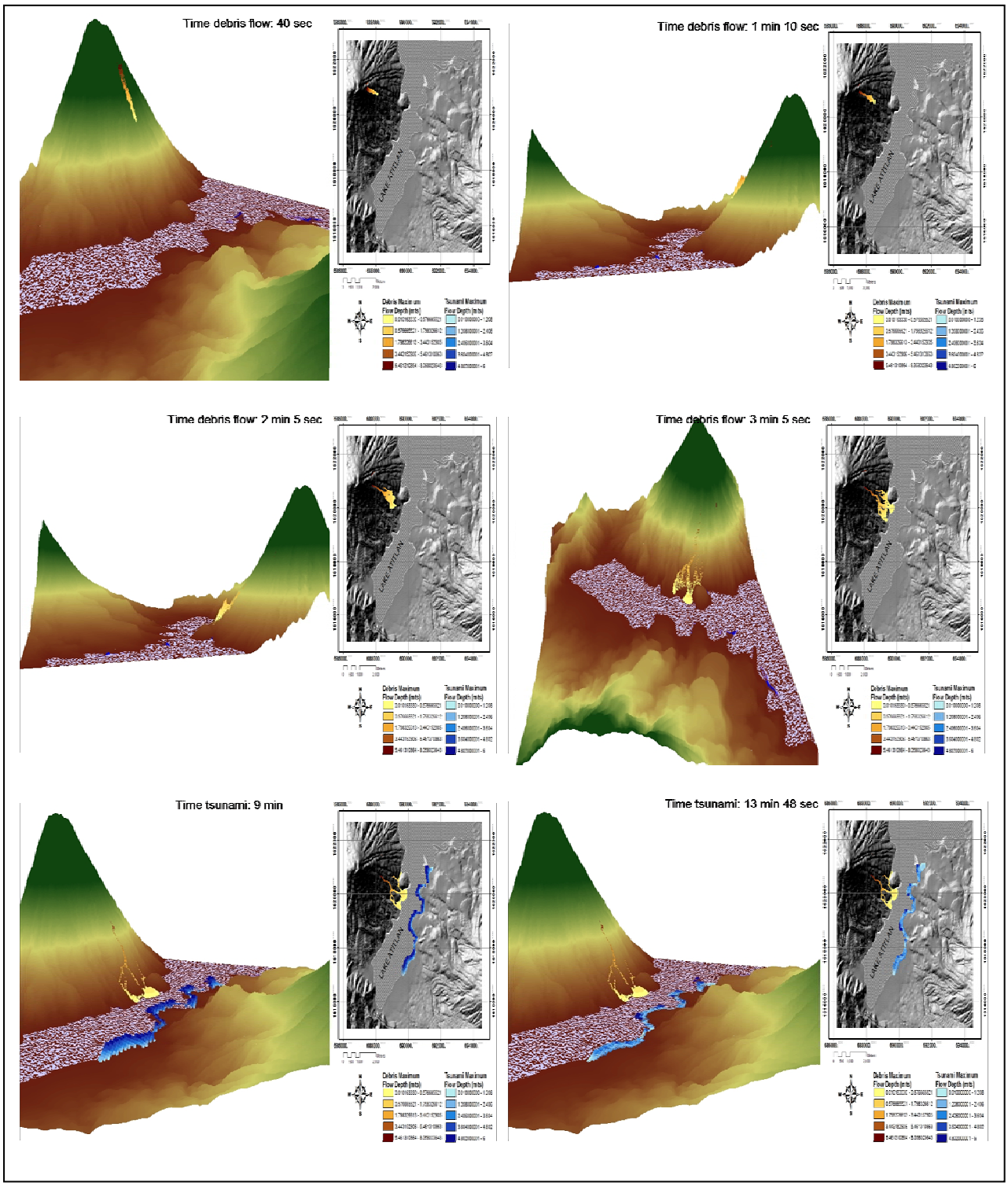

Fig.B.20. Pictures of the chronological order of the event

References to Appendix B

- Apel, J.R. 1987. **Principles of Ocean Physics**, 1987.

- Giron, J.; Matias, O.. 2006. **Small tsunami (seiche) in the Santiago Bay, Lake Atitlan, Solola Guatemala.** *INSIVUMEH (Institute of Seismology, Vulcanology, Meteorology and Hydrology of Guatemala) report for Hurricane Stan.*

- Huber, A. 1997. **Quantifying impulse wave effects in reservoirs**. *19 I COLD Congress Florence*, Q.74, R.35.

- Huber, A.; Hager, W.H. 1997. **Forecasting impulse waves in reservoirs**: *Commission Internationale des Grands Barrages, Dix-neuvieme Congres des Grands Barrages, Florence*. p. 993-1005.

- Miles, J. 1974. **Harbour seiching**, *Annu. Rev.Fluid Mech.*, 6:17–36.

- Noda, E. 1970. **Water waves generated by landslide: Proceedings of the American Society of Civil Engineers**. *Journal Waterways Harbors* Div. v. 96, n.4 p. 835-855.

- **The McGraw-Hill Encyclopedia of Science&Technology, 9th Edition**. Copyright_c 2003 by The McGraw-Hill Companies, Inc. All rights reserved.

- Wieczorek, G.F.; Jakob, M.; Motyka, R.; Zirnheld, S.; Craw, P.. 2003. **Preliminary assessment of landslide-induced wave hazards: Tidal Inlet, Glacier Bay National Park, Alaska.** *U. S. Geological Survey Open-File Report 03-100.*